IAEA TECDOC SERIES

IAEA-TECDOC-1988

Technical Insights from Benchmarking Different Methods for Predicting Pipe Failure Rates in Water Cooled Reactors

Final Report of a Coordinated Research Project

IAEA
International Atomic Energy Agency

TECHNICAL INSIGHTS FROM BENCHMARKING DIFFERENT METHODS FOR PREDICTING PIPE FAILURE RATES IN WATER COOLED REACTORS

The following States are Members of the International Atomic Energy Agency:

AFGHANISTAN
ALBANIA
ALGERIA
ANGOLA
ANTIGUA AND BARBUDA
ARGENTINA
ARMENIA
AUSTRALIA
AUSTRIA
AZERBAIJAN
BAHAMAS
BAHRAIN
BANGLADESH
BARBADOS
BELARUS
BELGIUM
BELIZE
BENIN
BOLIVIA, PLURINATIONAL STATE OF
BOSNIA AND HERZEGOVINA
BOTSWANA
BRAZIL
BRUNEI DARUSSALAM
BULGARIA
BURKINA FASO
BURUNDI
CAMBODIA
CAMEROON
CANADA
CENTRAL AFRICAN REPUBLIC
CHAD
CHILE
CHINA
COLOMBIA
COMOROS
CONGO
COSTA RICA
CÔTE D'IVOIRE
CROATIA
CUBA
CYPRUS
CZECH REPUBLIC
DEMOCRATIC REPUBLIC OF THE CONGO
DENMARK
DJIBOUTI
DOMINICA
DOMINICAN REPUBLIC
ECUADOR
EGYPT
EL SALVADOR
ERITREA
ESTONIA
ESWATINI
ETHIOPIA
FIJI
FINLAND
FRANCE
GABON
GEORGIA
GERMANY
GHANA
GREECE
GRENADA
GUATEMALA
GUYANA
HAITI
HOLY SEE
HONDURAS
HUNGARY
ICELAND
INDIA
INDONESIA
IRAN, ISLAMIC REPUBLIC OF
IRAQ
IRELAND
ISRAEL
ITALY
JAMAICA
JAPAN
JORDAN
KAZAKHSTAN
KENYA
KOREA, REPUBLIC OF
KUWAIT
KYRGYZSTAN
LAO PEOPLE'S DEMOCRATIC REPUBLIC
LATVIA
LEBANON
LESOTHO
LIBERIA
LIBYA
LIECHTENSTEIN
LITHUANIA
LUXEMBOURG
MADAGASCAR
MALAWI
MALAYSIA
MALI
MALTA
MARSHALL ISLANDS
MAURITANIA
MAURITIUS
MEXICO
MONACO
MONGOLIA
MONTENEGRO
MOROCCO
MOZAMBIQUE
MYANMAR
NAMIBIA
NEPAL
NETHERLANDS
NEW ZEALAND
NICARAGUA
NIGER
NIGERIA
NORTH MACEDONIA
NORWAY
OMAN
PAKISTAN
PALAU
PANAMA
PAPUA NEW GUINEA
PARAGUAY
PERU
PHILIPPINES
POLAND
PORTUGAL
QATAR
REPUBLIC OF MOLDOVA
ROMANIA
RUSSIAN FEDERATION
RWANDA
SAINT LUCIA
SAINT VINCENT AND THE GRENADINES
SAMOA
SAN MARINO
SAUDI ARABIA
SENEGAL
SERBIA
SEYCHELLES
SIERRA LEONE
SINGAPORE
SLOVAKIA
SLOVENIA
SOUTH AFRICA
SPAIN
SRI LANKA
SUDAN
SWEDEN
SWITZERLAND
SYRIAN ARAB REPUBLIC
TAJIKISTAN
THAILAND
TOGO
TRINIDAD AND TOBAGO
TUNISIA
TURKEY
TURKMENISTAN
UGANDA
UKRAINE
UNITED ARAB EMIRATES
UNITED KINGDOM OF GREAT BRITAIN AND NORTHERN IRELAND
UNITED REPUBLIC OF TANZANIA
UNITED STATES OF AMERICA
URUGUAY
UZBEKISTAN
VANUATU
VENEZUELA, BOLIVARIAN REPUBLIC OF
VIET NAM
YEMEN
ZAMBIA
ZIMBABWE

The Agency's Statute was approved on 23 October 1956 by the Conference on the Statute of the IAEA held at United Nations Headquarters, New York; it entered into force on 29 July 1957. The Headquarters of the Agency are situated in Vienna. Its principal objective is "to accelerate and enlarge the contribution of atomic energy to peace, health and prosperity throughout the world''.

IAEA-TECDOC-1988

TECHNICAL INSIGHTS FROM BENCHMARKING DIFFERENT METHODS FOR PREDICTING PIPE FAILURE RATES IN WATER COOLED REACTORS

FINAL REPORT OF A COORDINATED RESEARCH PROJECT

INTERNATIONAL ATOMIC ENERGY AGENCY
VIENNA, 2021

COPYRIGHT NOTICE

For further information on this publication, please contact:

Nuclear Power Technology Development Section
International Atomic Energy Agency
Vienna International Centre
PO Box 100
1400 Vienna, Austria
Email: Official.Mail@iaea.org

Printed by the IAEA in Austria
December 2021

IAEA Library Cataloguing in Publication Data

Names: International Atomic Energy Agency.
Title: Technical insights from benchmarking different methods for predicting pipe failure rates in water cooled reactors / International Atomic Energy Agency.
Description: Vienna : International Atomic Energy Agency, 2021. | Series: IAEA TECDOC series, ISSN 1011–4289 ; no. 1988 | Includes bibliographical references.
Identifiers: IAEAL 21-01467 | ISBN 978-92-0-141121-1 (paperback : alk. paper) | ISBN 978-92-0-141021-4 (pdf)
Subjects: LCSH: Water cooled reactors. | Pipeline failures. | Benchmarking (Management).

FOREWORD

The IAEA launched the coordinated research project entitled Methodologies for Assessing Pipe Failure Rates in Advanced Water Cooled Reactors in 2018. The primary objective of the coordinated research project was to provide Member States a strong technical basis to develop piping reliability parameters consistent with required standards and relevant to deployable advanced water cooled reactors. To meet this objective two interrelated activities were carried out. The participating Member State organizations first completed a set of benchmark case studies, which were specifically developed to compare different methodologies when applied to a common set of problems. The results of the benchmark case studies were compared and the reasons for differences were evaluated. The benchmark results, which are presented in this publication, provided input to the second activity of the coordinated research project, during which the participating Member State organizations developed an analysis framework on piping reliability good practices. The results of this activity are documented in a forthcoming IAEA publication on methodologies for assessing pipe failure rates in advanced water cooled reactors, which provides information on how to perform and document an advanced water cooled reactor centric piping reliability analysis.

The IAEA acknowledges the efforts and assistance provided by the contributors listed at the end of this publication. The IAEA officer responsible for this publication was T. Jevremovic of the Division of Nuclear Power.

EDITORIAL NOTE

This publication has been prepared from the original material as submitted by the contributors and has not been edited by the editorial staff of the IAEA. The views expressed remain the responsibility of the contributors and do not necessarily represent the views of the IAEA or its Member States.

Neither the IAEA nor its Member States assume any responsibility for consequences which may arise from the use of this publication. This publication does not address questions of responsibility, legal or otherwise, for acts or omissions on the part of any person.

The use of particular designations of countries or territories does not imply any judgement by the publisher, the IAEA, as to the legal status of such countries or territories, of their authorities and institutions or of the delimitation of their boundaries.

The mention of names of specific companies or products (whether or not indicated as registered) does not imply any intention to infringe proprietary rights, nor should it be construed as an endorsement or recommendation on the part of the IAEA.

The authors are responsible for having obtained the necessary permission for the IAEA to reproduce, translate or use material from sources already protected by copyrights.

The IAEA has no responsibility for the persistence or accuracy of URLs for external or third party Internet web sites referred to in this publication and does not guarantee that any content on such web sites is, or will remain, accurate or appropriate.

CONTENTS

1. INTRODUCTION

1.1 BACKGROUND

The International Atomic Energy Agency (IAEA) Coordinated Research Project (CRP) on Methodologies for Assessing Pipe Failure Rates in Advanced Water Cooled Reactors was launched in 2018. The goal of this CRP was to provide Member States with an open access to a strong technical basis for establishing nuclear power plant piping reliability parameters. To meet this goal two parallel and interrelated activities were carried out. In a first CRP activity, the participating institutions performed a series of benchmark studies. These studies were formulated for the purpose of evaluating different methodologies when applied to a common problem. The results were compared and contrasted, and the reasons for differences were identified. The technical insights that were gained from the benchmarks were input to a second activity of the CRP to develop a good practice piping reliability analysis framework.

1.2 OBJECTIVE

The topic of piping reliability analysis has remained an integral part of the evolution of nuclear power plant (NPP) safety and reliability. Different methodologies for the estimation of piping reliability parameters have been proposed, and their relevance to different types of problems have been the subject to research and development. Over the years, numerous benchmark studies have been performed in order to gain insights into the strengths and possible limitations of different methodologies, tools and techniques when applied to a common problem.

A unique aspect of the CRP benchmark was its interrelationship with a CRP activity to develop a good practices framework for piping reliability analysis. The objective of the benchmark was to compare and contrast three different methodologies for calculating piping reliability parameters: a) data-driven methods (DDM), b) probabilistic fracture mechanics methods (PFM), and c) integrated probabilistic physics of failure methods (I-PPoF). The specific objectives were developed to:

- Review different methodologies and associated software in terms of main features, capabilities and limitations;
- Benchmark the methodologies and associated software when applied to the analysis of thermal fatigue and primary water stress corrosion cracking (SCC);
- Investigate the reasons for differences in the results from the benchmark studies and to identify strengths and potential limitations of the methodologies and associated computational tools.

1.3 SCOPE

Two benchmarks were developed and specifics of each defined. A motivation behind the first benchmark was to address the possibilities for reconciling the results of PFM with operating experience (OPEX) data. The motivation behind the second benchmark was to address the ability of different methods to address an evaluation boundary for which no failure data exists beyond results from laboratory testing, and for which knowledge gaps exist regarding crack initiation times and crack propagation phenomena. The participants of the benchmarks applied three different methodologies and the results were evaluated as follows:

— *Intra-comparison of results*: the results obtained within respective methodology grouping were reviewed based on the input and output parameters, results presentation, and the treatment of uncertainties;
— *Inter-comparison of results*: the results obtained from the application of the three different methodologies were reviewed on the basis of input and output parameters, results presentation, and treatment of uncertainties;
— *Development of a synthesis on the strengths and limitations of respective methodology*: this step in the evaluation process also addressed the applicability of respective methodology to specific analytical contexts with clearly defined end-user requirements.

The contrast and comparison portion of the benchmark was performed in three steps as shown in Fig. 1. Firstly, an intra-comparison of methods and results was completed. Secondly, an inter-comparison of methods and results was performed in order to synthesize the insights gained by the seven participating institutions as summarized in Table 1. Finally, the conclusions and recommendations were developed on the basis of these technical insights.

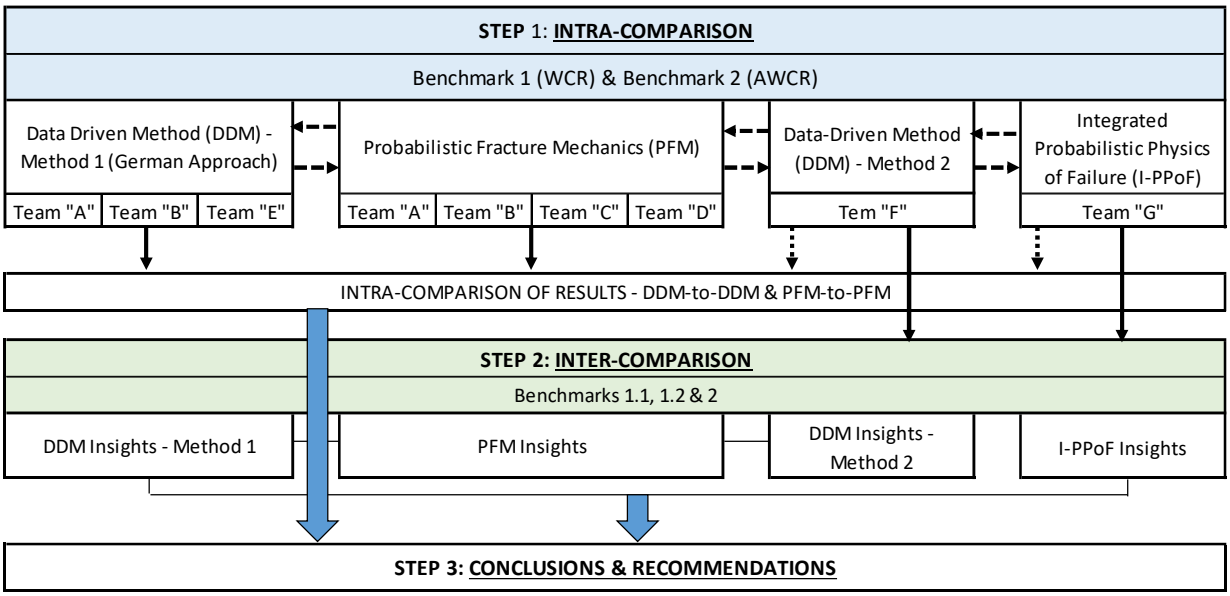

FIG. 1. The CRP benchmark contrast and comparison process.

TABLE 1. LIST OF BENCHMARK PARTICIPANTS

Country	**Method(s)**	**Institution**
Canada	DDM, PFM	CANDU Energy Inc. (CEI)
Germany	DDM, PFM	Gesellschaft für Anlagen- und Reaktorsicherheit (GRS)
Korea (Republic of)	PFM	Korea Atomic Energy Research Institute (KAERI)
Lithuania	PFM	Lithuanian Energy Institute (LEI)
Tunisia	DDM	Alternative Energies Project (PEA) of the Tunisian Electricity and Gas Company (STEG),
United States of America	DDM	Sigma-Phase Inc. (SPI)
	I-PPoF	University of Illinois, Urbana-Champaign (UIUC)

1.3 STRUCTURE

The main body of this publication is divided into five Sections, including the Introduction in Section 1. The benchmark evaluation boundaries are presented in Section 2. The results are described in Section 3, which also includes details on the reasons for differences in the obtained results. The lessons learned from the benchmark are summarized in Section 4. The conclusions and recommendations are given in Section 5.

Supporting information is provided in Annexes I through VII. These Annexes document the methods, techniques and computer implementations as developed by respective teams, as follows:

- Annex I. CANDU Energy Inc. (CEI), PFM using the computer code PRAISE-CANDU Version 2.1;
- Annex II. Global Research for Safety (GRS), PFM using the computer code PROST;
- Annex III. Korea Atomic Energy Research Institute (KAERI), PFM using the computer coded PROFAS-PIPE;
- Annex IV. Lithuanian Energy Institute (LEI), PFM using the computer code PIFRAP.
- Annex V. Sigma-Phase Inc. (SPI), Microsoft® Excel with add-in programs for pipe failure data, Bayesian reliability analysis and uncertainty propagation;
- Annex VI. Tunisian Electricity and Gas Company (STEG), DDM based on the German Probabilistic Safety Assessment (PSA) Leitfaden (PSA guidelines);
- Annex VII. University of Illinois at Urbana-Champaign (UIUC), integrated physics of failure models using I-PPoF.

2. COORDINATED RESEARCH PROJECTS BENCHMARKS

2.1 EVALUATION BOUNDARIES

The benchmark evaluation boundaries were defined in order to facilitate an inter- and intra-comparison of different methods. The first benchmark was performed in two phases; Phase 1.1 and Phase 1.2 as follows:

- *Benchmark 1.1.* Calculation of piping reliability parameters for evaluation boundaries within a chemical and volume control (CVC) piping system and the reactor coolant system (RCS) of a pressurized water reactor (PWR). Five analysis teams calculated piping reliability parameters and for an evaluation boundary chosen by respective teams as shown in Fig. 2. An objective of this benchmark was to highlight critical issues in comparing and contrasting results given allowances in respective analysis teams' interpretation of the evaluation boundary specification.
- *Benchmark 1.2.* Calculation of piping reliability parameters for a pre-defined, specific evaluation boundary within the primary pressure boundary of a CVC piping system of a PWR. A schematic of the intent of Benchmark 1.2 is illustrated in Fig. 3. Additional technical details of this evaluation boundary are provided in Section 2.1.

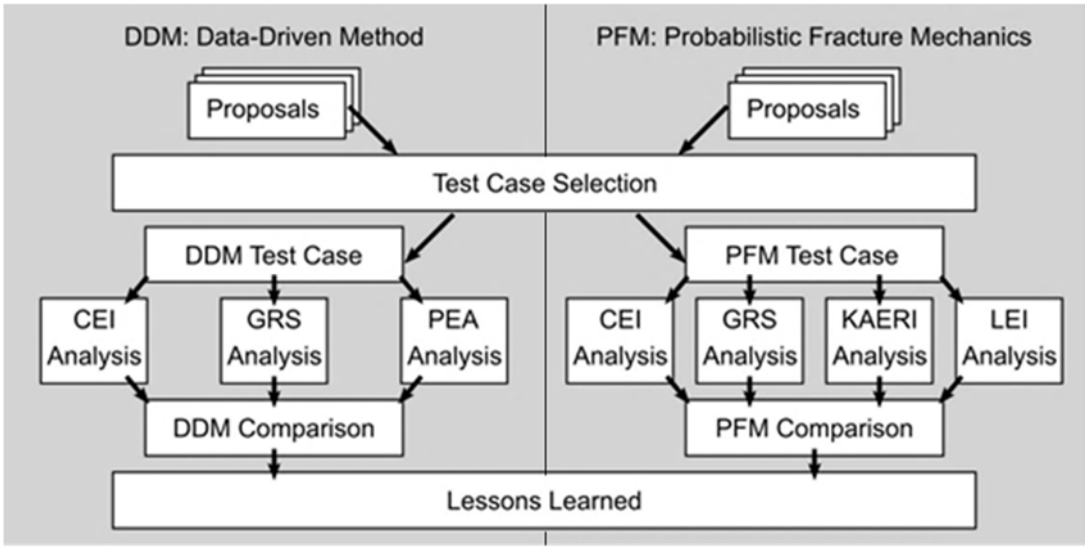

FIG. 2. Intra-comparison of methodologies in benchmark 1.1.

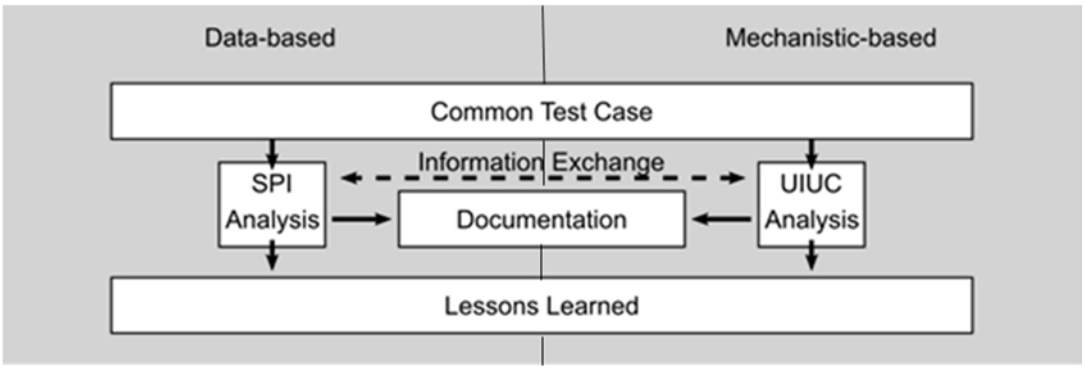

FIG. 3. Inter-comparison of methodologies in benchmark 1.2.

The second benchmark addressed an evaluation boundary within the primary pressure boundary of an advanced water cooled reactor (WCR). The technical details of this evaluation boundary are found in Section 2.3. The objective of this benchmark was to support an inter-comparison of different methodologies that were applied to a common evaluation boundary for which no failure data exists. A schematic of the intent of the second benchmark is shown in Fig. 4.

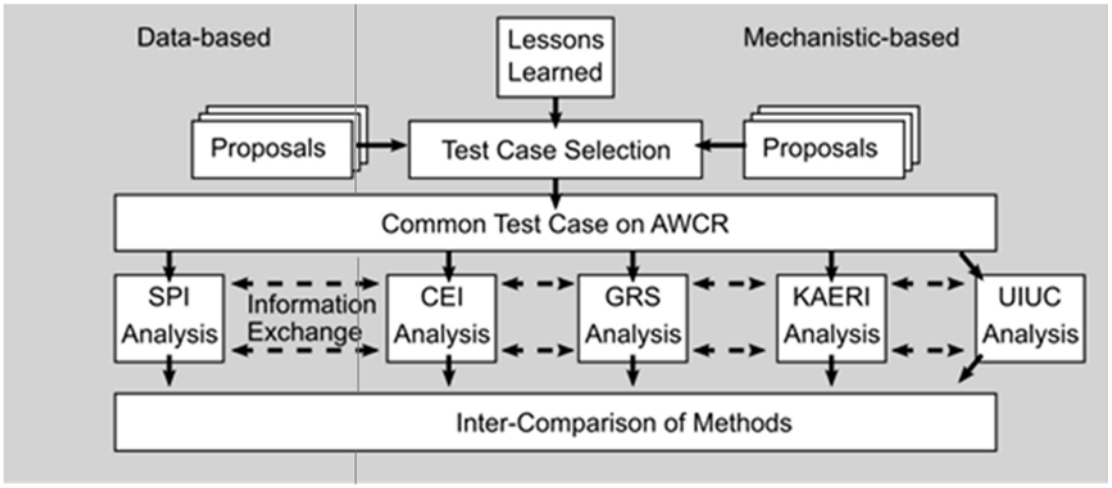

FIG. 4. Second benchmark on an advanced WCR evaluation boundary.

2.2 CHEMICAL AND VOLUME CONTROL PIPING SYSTEM

The first CRP benchmark was concerned with the calculation of CVC and RCS piping reliability parameters. In a first phase of the first benchmark, respective analysis team defined the evaluation boundary of interest, whereas in the second phase the participating teams considered a specific evaluation boundary within the primary pressure boundary (Safety Class 1), of a CVC piping system; Subsection 2.2.1 gives the details of this evaluation boundary. Figure 5 depicts a schematic of this system [1].

The primary purpose of the CVC system in a PWR are to regulate reactor coolant chemistry for reactivity and corrosion control, and to maintain the water level in the pressurizer of the RCS. The system also maintains seal-water injection flow to the reactor coolant pump seals; provides a means of filling, draining and pressure testing of the RCS; and assists in emergency core cooling following actuation of the safety injection system. In terms of number of welds and pipe spools, this system is quite large. In a typical four loop PWR there can be upwards of 200 welds within the CVC Safety Class 1 system boundary and about the same amount within the Safety Class 2 system boundary. The plant to plant variability in weld populations is significant.

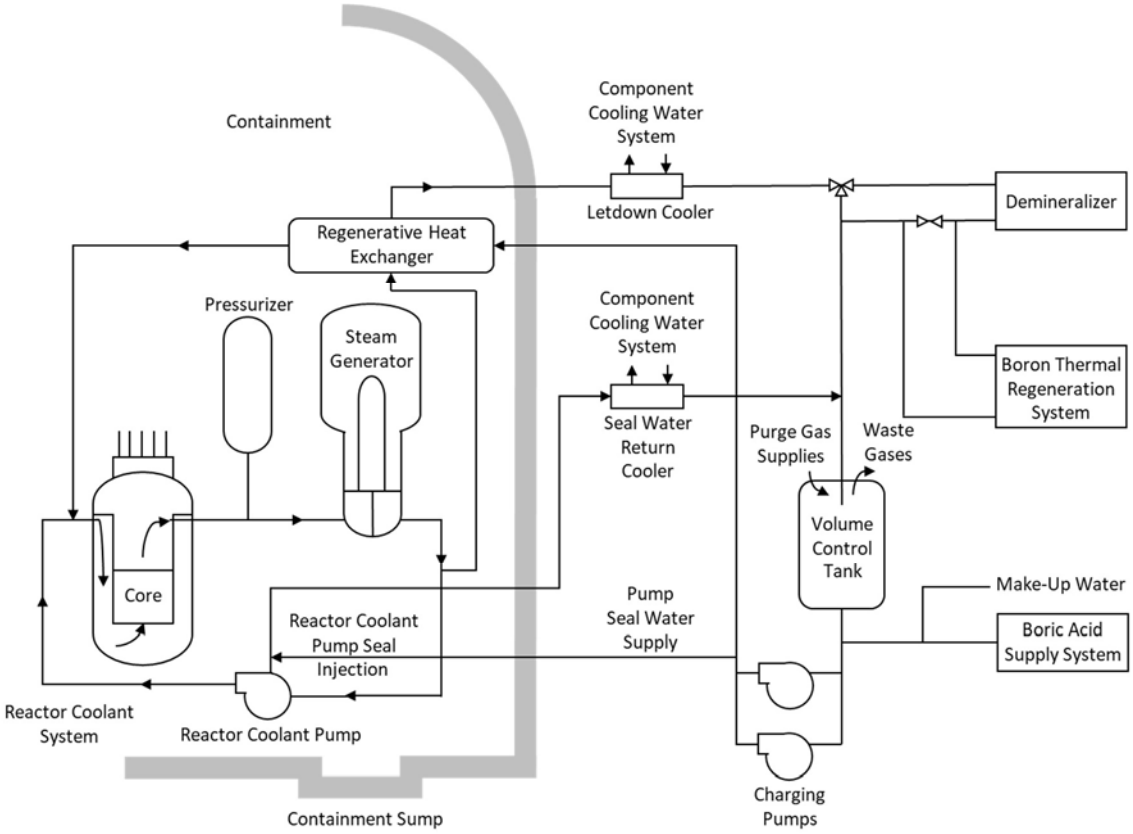

FIG. 5. Schematic of a typical CVC system [1].

The primary pressure boundary of the CVC system piping consists of all piping connecting the CVC system to the RCS cold legs; i.e. the piping between the reactor coolant pump and the reactor pressure vessel (RPV). This piping includes the normal letdown, excess letdown, charging, and alternate charging lines. The piping also includes the pressurizer auxiliary spray line, as well as the reactor coolant pump seal injection lines. Table 2 lists typical materials, operating conditions and design

parameters. The CVC pipe failure experience is extensive. However, most of these failures have occurred in sections of piping outside the primary pressure boundary. Since 1970, more than 500 CVC pipe failures have been reported, and with varying safety significance and operational impact. The majority of these failures have been located outside the primary pressure boundary.

TABLE 2. TYPICAL CVC PIPING MATERIAL AND DESIGN PARAMETERS

Safety Class 1 CVC Line Description	Nominal Diameter [mm]	Pipe Wall Thickness [mm]	Pipe Material	Design Pressure [MPa]	Design Temperature [°C]
Letdown Line	100	13.49	AISI Type 316 Stainless Steel (DIN 1.4401)	17.13	343
Makeup Line	100	13.49		17.13	343
Auxiliary Pressurizer Spray	50	8.74		17.13	343
Reactor Coolant Pump Seal Injection	50	8.74		19.43	93
Excess Letdown	50	8.74		17.13	343

2.2.1 Evaluation boundaries of benchmark 1.1

Benchmark 1.1 considered two different evaluation boundaries. The teams that applied the DDM approach analyzed unspecified locations within the primary pressure boundary of the CVC system. The unspecified locations referred to locations considered to be susceptible to material degradation. The teams that applied PFM approach analyzed an unspecified location in the pressurizer spray piping, which is part of the RCS.

The pressurizer provides a means of controlling the primary system pressure. Pressure is controlled by the use of electrical heaters, pressurizer spray, power operated relief valves, and safety valves. If pressure starts to increase above the desired setpoint, the spray line will allow relatively cold water from the discharge of the reactor coolant pump to be sprayed into the steam space. The cold water will condense the steam into water, which will reduce pressure (due to the fact that steam takes up about six times more space than the same mass of water). If pressure continues to increase, the pressurizer relief valves will open and dump steam to the pressurizer relief tank. If this does not relieve pressure, the safety valves will lift, also discharging to the pressurizer relief tank. A typical pressurizer spray line is a DN100 Schedule 160 (13.5 mm wall thickness) pipe size.

The function of the auxiliary spray line of the CVC system is to provide the operator with an auxiliary pressurizer spray to control the RCS pressure during the final stages of reactor shutdown by allowing cooling of the pressurizer. This line is located between the charging line and the pressurizer. Typically, it is a DN50 Schedule 160 (8.7 mm wall thickness) pipe size. The upstream end branches off the charge line that connects to the outlet of the regenerative heat exchanger outlet. The downstream end connects to the DN100 pressurizer line, which connects to the pressurizer inlet nozzle.

2.2.2 Evaluation boundary of benchmark 1.2

Benchmark 1.2 considered the CVC excess let-down branch connection off of the RCS cold leg. A failure of this portion of the CVC piping system constitutes a primary pressure boundary breach, and therefore is a precursor to a small or medium size loss of coolant accident (LOCA) depending on the size of the breach. The benchmark considered a piping configuration corresponding to that of the

Japanese PWR plant Mihama Unit 2 in which a thermal fatigue failure occurred on 30 April 1999; Fig. 6 depicts the geometry.

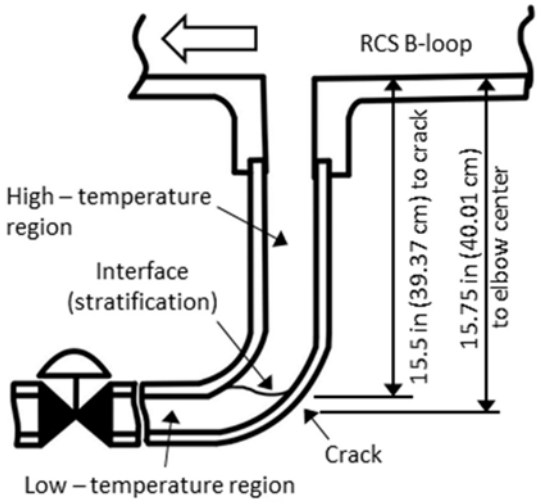

FIG. 6. CVC piping evaluation boundary of benchmark 1.2 [adopted after 3].

At the time of the event, the reactor unit was operating at reduced power when it was determined that the drain flow to the containment sump increased. A containment entry revealed a small leakage from the excess letdown piping off reactor coolant loop B (RCS cold leg). The leak had developed on the excess letdown line. It was subsequently found that there was a through-wall crack of about 7 mm length on the outside and of about 24 mm length on the inner surface near the elbow of the excess letdown system piping. The cracked pipe surface showed the features of fatigue damage. It became clear that, at the relevant elbow, in addition to the residual stress generated in the bending process, the repeated thermal stress was generated due to the change of the temperature boundary surface (thermal stratification) between the reactor coolant from the RCS cold leg and the stagnant water in the excess letdown system piping. The corrective action for this event was to shorten the vertical run to about 6 pipe diameters, such that the turbulence penetration boundary was well into the horizontal run, away from the elbow. This avoided thermal cycling at the elbow and assured that the horizontal run would have a continuous source of heat, eliminating stratification cycling. An elbow with reduced residual stress was used in the replacement.

2.2.3 Chemical and volume control piping operating experience

The international WCR OPEX with CVC piping is well documented, and a corresponding summary is given in Fig. 7. Limited to CVC piping within the primary pressure boundary, the OPEX in Fig. 8 is organized by system function and piping degradation mechanism. The following degradation mechanisms have been observed:

- Erosion-cavitation, 2 failures;
- High-cycle fatigue, 28 failures;
- Thermal fatigue, 14 failures.

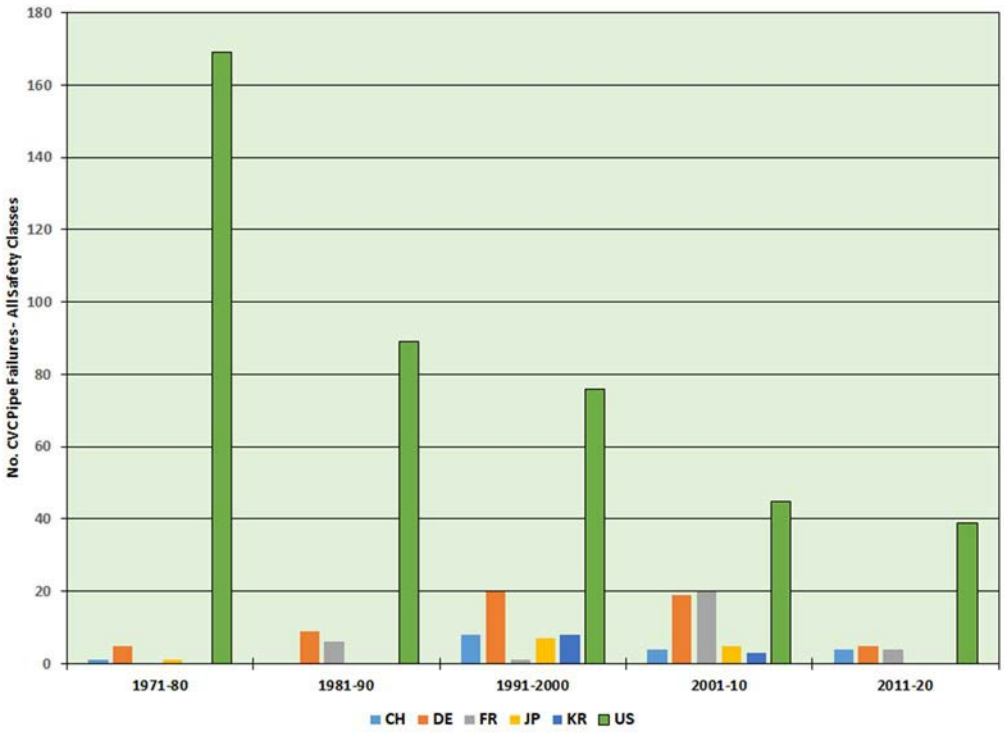

FIG. 7. CVC piping OPEX by country (WCR OPEX based on PIPEexp database[1]).

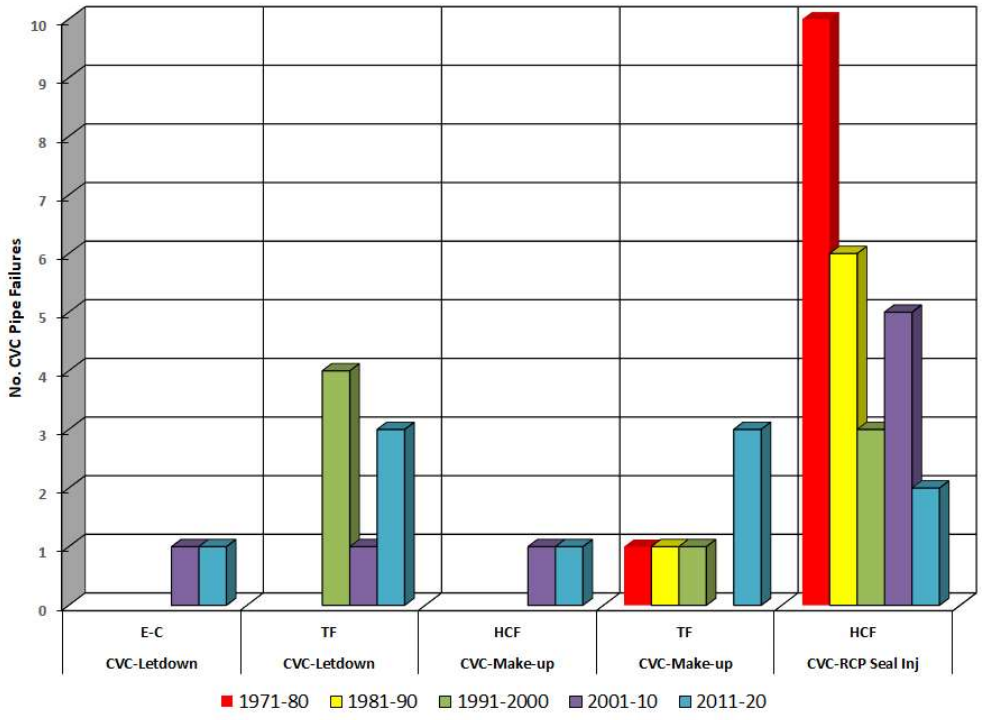

FIG. 8. The international OPEX with safety class 1 CVC piping (WCR OPEX based on PIPEexp database).

In Fig. 7 and Fig. 8, a pipe failure is equal to a through-wall leakage; from minor perceptible leakage to a more significant leakage that requires a controlled plant shutdown. Not included in the charts are two

[1] Proprietary database

significant CVC pipe failures. These events occurred at VVER plants in 1994 and 2003 and were attributed to corrosion fatigue and flow influenced vibration, respectively.

2.3 ADVANCED WATER COOLED REACTOR PIPING SYSTEM

The principal WCR piping materials are austenitic stainless steels, cast austenitic stainless steels, nickel-based alloys, low alloy steels and carbon steels. The same basic material types are being used in advanced WCRs. Some new materials have been developed by the steel producers and subsequently applied as replacement for the original as installed piping material. Examples includes Alloys 690/152/52 and super-austenitic (or high alloy) stainless steels. Both types were originally developed in the 1970s but with relatively limited application in the commercial nuclear industry until the 1980s. In defining the specification for the second benchmark a location within a primary pressure boundary for which there no failure data was selected.

2.3.1 Evaluation boundary of benchmark 2

The selected evaluation boundary for benchmark 2 corresponds to that of an AP-1000 (advanced passive PWR) dissimilar metal weld (DMW) between the RPV outlet nozzle (stainless steel clad carbon steel) and the RCS hot leg pipe (austenitic stainless steel) as shown in Fig. 9 and with the dimensional data summarized in Table 3.

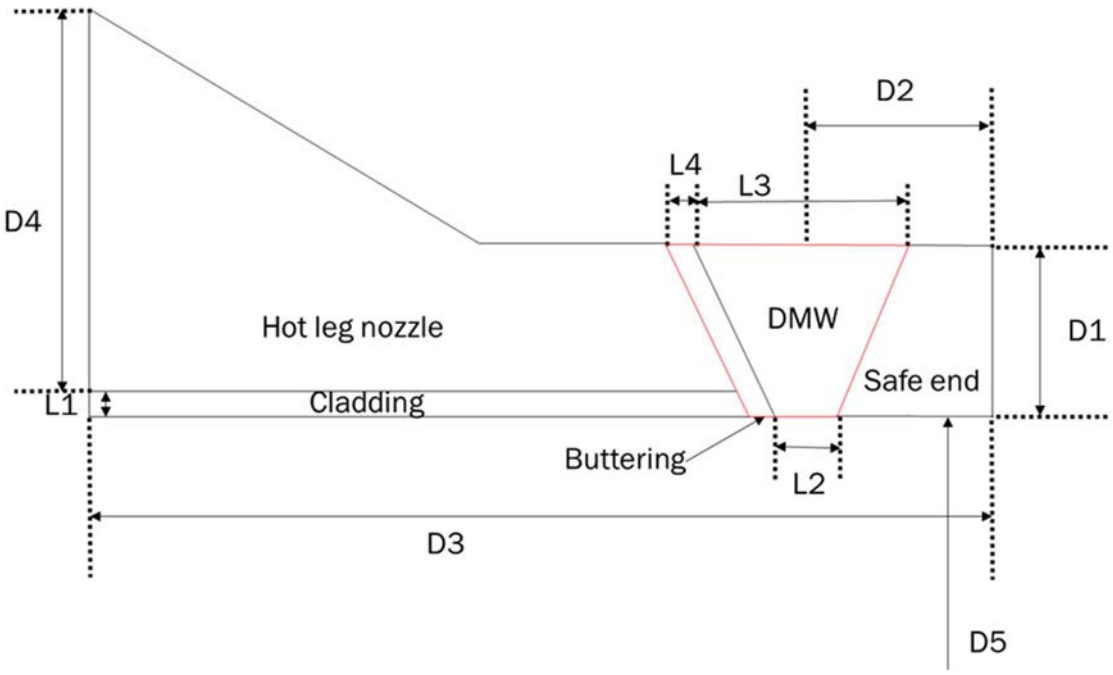

FIG. 9. Location and dimensions of the evaluation boundary.

The dimensional data are based on [4], [5]. The weld between the RPV outlet nozzle and the hot leg consists of nickel-based materials of type Alloy 152 buttering and Alloy 52 weld metal. The buttering is the weld metal which is deposited on RPV nozzle surface to provide a metallurgically compatible weld metal for the subsequent completion of the weld. For this evaluation boundary the analytical task was to determine the frequency of a DMW failure.

TABLE 3. EVALUATION BOUNDARY FOR BENCHMARK 2

Evaluation Boundary			
Reactor Design	AP1000 (PWR)		
System Name	RCS		
Evaluation Scope Type	Weld between pressure vessel outlet nozzle and RCS hot leg		
Evaluation Scope	DMW under an assumption of high-to-extremely high primary water stress corrosion cracking (PWSCC) resistance		
Pipe Dimensions			
Inside Diameter (ID)	RCS hot leg ID 787 mm D5 in Fig. 9		
Nominal Wall Thickness	RCS hot leg: 82.55 mm D1 in Fig. 9		
L1 = 6.4 mm	L2 = 27.6 mm	L3 = 57.1 mm	L4 = 10.0 mm

2.3.2 Operating experience with nickel-based materials

Nickel-based materials, such as Alloy 600, have been used extensively in WCRs. Already in the 1960s the material science community determined that this alloy was susceptible to SCC in certain high temperature environments. The first PWSCC events in commercial PWR plants were reported in the mid-1980s. The majority of the PWSCC incidents in the RPV inlet and outlet nozzles have occurred in the Alloy 82/182 nozzle-to-safe-end weld region of the outlet nozzle. These nozzles typically operate at 320°C–327°C. The relevant international OPEX is summarized in Fig. 10.

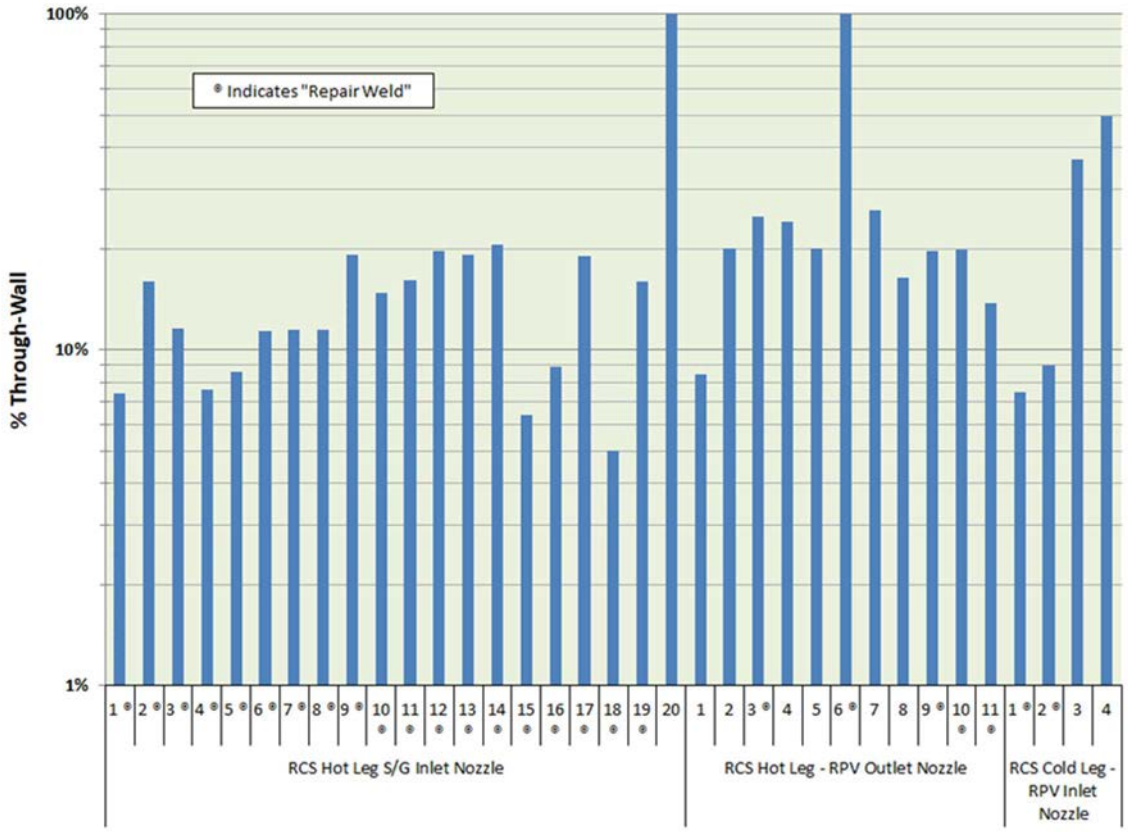

FIG. 10. OPEX involving PWSCC of large diameter piping (WCR OPEX based on PIPEexp database).[2]

[2] The numbers on the *x*-axis refer to specific events for which detailed flaw size data exists. As an example, there have been eleven (11) recorded incidents involving RPV outlet nozzle to hot leg piping, etc. Superscript "R" indicates a "repair welded" area with high stress concentration.

The majority of the events have involved relatively shallow cracks. In the year 2000 the first incidents involving RPV outlet nozzles occurred in Ringhals Units 3 and 4 in Sweden, and in V.C. Summer in the USA. No additional surface indications were reported until 2008, when indications were identified in the outlet nozzles of two different reactor vessels. The first was at Ohi-3 in Japan. This indication was detected prior to the application of water-jet peening to mitigate PWSCC. The indication was measured by ultrasonic testing as being 10 mm in length and 5 mm in depth. When the indication was actually removed by progressive grinding, it was measured to have a length of 13.5mm and a depth of 20.3 mm. The second indication was detected at Salem-1 in the United States as a result of ultrasonic testing inspection, prior to the application of the mechanical stress improvement process. This indication was determined to have a depth of about 15 mm. Finally, in 2009, an indication was found in the Seabrook reactor vessel outlet nozzle. This indication was axially oriented with a depth of ca. 6 mm and a length of ca. 24 mm. Since 2009 no RCS hot leg PWSCC incidents have been reported.

Significant improvements in the resistance of nickel-base alloys were made by increasing the chromium content from 14%−17% (Alloy 600) to 27%−31% (Alloy 690 and its weld metals Alloy 52/152). Laboratory crack growth rate data support factor of improvements (FOI) much greater than 10 in PWSCC resistance for Alloy 690 relative to that of Alloy 600. Alloy 690 and its weld metals have been used by the commercial WCR industry since the late 1980s and with no PWSCC incidents reported.

3. BENCHMARK RESULTS

3.1 BENCHMARK SPECIFICATIONS

Each Team performed the analyses based on benchmark specifications:

- *Benchmark 1.1* (Table 4) defines a broad scope with significant allowances in how respective Team interpreted the evaluation boundary for which piping reliability parameters were sought;
- In contrast, *Benchmark 1.2* (Table 5) and Benchmark 2 (Table 6) consist of more narrow scopes.

TABLE 4. BENCHMARK 1.1 SPECIFICATIONS

Evaluation Boundary		**Comment**
System	CVC of a PWR	Respective Team to define specifics of the evaluation boundary. Based on information provided by GRS, to be assumed that there is total of 43 susceptible locations within the CVC piping system of which 20 locations are Safety Class 1, and 23 locations are Safety Class 2.
Scope	Locations susceptible to material degradation.	
Pipe Diameter	DN50	
Material Type	Stainless steel	
Process Medium	Primary water	
OPEX	German experience (1968-2017): 7 failures for DN50, 24 failures for the range DN50 to DN100 over 441 ROYs	Source of the data is the GRS database KomPass. The participating teams used the same OPEX data.
PFM Parameters		
Material Mechanical Properties	Young's Modulus Poisson Ratio Yield Stress Ultimate Stress Fracture Toughness	The values of these parameters were defined by respective analysis team.

TABLE 4. BENCHMARK 1.1 SPECIFICATIONS (CONT)

Evaluation Boundary		Comment
Design and Operating Conditions	Pressure	15.41 MPa
	Temperature	345°C
	Process Medium Chemistry	PWR primary water chemistry
	Pipe Stresses	Membrane stress: 61.3 MPa Bending stress: 33.7 MPa Weld residual stress (WRS): refer to Fig. 11
	Reactor Operating Year (ROY)	8000 hours are assumed
Inspection	Probability of Detection (POD)	$POD(a) = \frac{\exp(\beta_0 + \beta_1 \ln a)}{1 + \exp(\beta_0 + \beta_1 \ln a)}$ β_0=0.8256, β_1=0.8711, α = *flaw depth*
	Inspection interval	Every 1 year, 5 years or 10 years
Leak Detection	Detectable leak rate	0.3 kg/s
Initial Crack Size	Crack length	9.38 mm
	Depth	1.00 mm
Crack Initiation Rate	4.08×10^{-4} ROY^{-1}	
Crack Growth Rate	$\frac{da}{dt} = \begin{cases} C_{SCC}K_I^{nscc} & K_I \le K_{thr} \\ C_{sat} & K_I > K_{thr} \end{cases}$ C_{SCC} =1.05×10^{-14} (MPa m$^{1/2}$)$^{-5.76}$ mm/s n_{SCC} =5.76 C_{sat} = 1.74×10^{-6} mm/s K_{thr} = 26.7 MPa m$^{1/2}$	
Analysis Objectives		
Reliability Parameters	Annual frequency of a leak and rupture	Leak is defined as formation of through-wall crack, and rupture is equivalent to a double ended guillotine break (DEGB)
Reliability and integrity management (RIM) Strategy	Leak detection and in-service inspection (ISI)	Each team to address impact of RIM on the probabilistic failure metrics

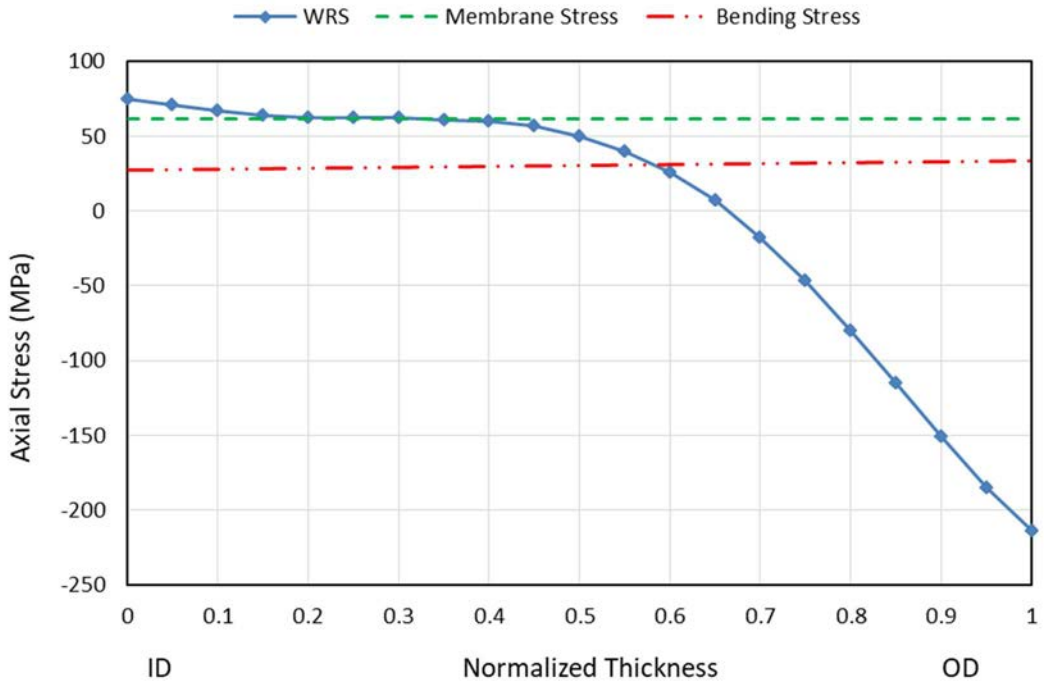

FIG. 11. Axial stresses used in PFM portion of benchmark 1.1.

TABLE 5. BENCHMARK 1.2 SPECIFICATIONS

Evaluation Boundary		Comment
System	CVC	This evaluation boundary corresponds to the 1999 primary pressure boundary leak in Mihama-2. The through-wall thermal fatigue crack was located 220 mm from the reactor coolant loop inside surface. The crack was in the center extrados of the elbow, oriented 45° from the pipe centerline. It measured 25 mm long on the inside surface, and 6 mm long. The peak leak rate was about 0.095 kg/s.
Scope	Letdown line; first elbow below RCS cold leg.	
Pipe Diameter	DN50	
Wall Thickness	8.71 mm (Schedule 160)	
Material Type	Stainless steel, AISI Type 316	
Process Medium	Primary water	
PFM Parameters		
Material Mechanical Properties	Young's Modulus	The values of these parameters were defined by respective analysis team.
	Poisson Ratio	
	Yield Stress	
	Ultimate Stress	
	Fracture Toughness	
Design and Operating Conditions	Pressure	
	Temperature	
	Process Medium Chemistry	
	Pipe Stresses	
Analysis Objective		
Piping Reliability Parameters	Frequency of a "leak"	The meaning of "leak" and "rupture" was defined by respective analysis team
	Frequency of a "rupture"	
	Conditional failure probability	

TABLE 6. BENCHMARK 2 SPECIFICATIONS

Evaluation Boundary		Comment
Reactor Type	Advanced WCR, Type AP-1000	The weld material is Alloy 52/152 which has high resistance to PWSCC. The RCS hot leg is made of austenitic stainless steel, and the weld between the hot leg and the ferritic pressure vessel nozzle is made of Ni-base material.
System	RCS	
Scope	DMW between RPV outlet and RCS hot leg	
RCS hot leg inside diameter	787 mm	
Wall Thickness	82.55 mm	
Material Type	Alloy 52/152	
Process Medium	Primary water	
Flow rate	11,250 kg/s	
Degradation Mechanism		
Degradation Mechanism	PWSCC	The crack initiation and crack growth models were defined by respective team.
	Crack initiation model	
	Crack growth model	
PFM Parameters		
Material Mechanical Properties and Loading Conditions	Young's Modulus	The values of these parameters were defined by respective analysis team.
	Poisson Ratio	
	Yield Stress	
	Ultimate Stress	
	Fracture Toughness	
	WRS	
	Pipe Stresses	
Design and Operating Conditions	Pressure	15.5 MPa
	Temperature	321.1°C
	Process Medium Chemistry	Not specified
Leak Detection	Detectable leak rate	<0.0631 kg/s

TABLE 6. BENCHMARK 2 SPECIFICATIONS (CONT)

Evaluation Boundary		Comment
Analysis Objective		
Piping Reliability Parameters	Frequency of a leak	The exact meaning of "leak" and "rupture" was defined by respective analysis team. Also, respective analysis team defined the relevant ISI intervals and POD curves (POD as a function of crack depth).
	Frequency of a rupture	
	Conditional failure probability	
Failure Mode(s)	Through-wall leak	
	Rupture	
	Non-through-wall crack	
ISI	ISI interval	
	POD	

3.2 RESULTS OF BENCHMARK 1.1

3.2.1 DDM results

Three teams applied a DDM, which is based on a German approach, [6]–[8]. The basic elements of this approach are summarized in Table 8 and as follows:

$$F_{Pipe\ Failure} = \lambda_L \times CFP \tag{1}$$

where $F_{Pipe\ Failure}$ is pipe failure frequency, given a pre-existing degraded condition, which can be a crack or a small leakage. Three types of uncertainties were considered: uncertainty in the failure count (the numerator in the equation for C_x, Table 7), uncertainty in the exposure term (the denominator in the equation for C_x), and uncertainty in the conditional failure probability (CFP) (Table 7).

The approaches to uncertainty analysis are found in Table 8. The results are presented in Fig. 12.

TABLE 7. BENCHMARK 1.1 METHODOLOGY FOR DDM

Pipe Diameter	Formula	Parameters
DN ≤ 50	Parameter λ_L (the pipe failure rate) is estimated from failure data DN = Nominal diameter [mm]	λ_L = frequency of leak [1/CB.ROY]. CB is component boundary e.g. weld
50 < DN ≤ 150	$\lambda_L = C_x(L_D \times DN)/t_D^x$	Parameters C_x, L_D, t_D, and x are obtained from the paper by R.M. Thomas; Reference [8]. $C_x = \frac{\sum_{50}^{150} N_{L,D}}{\sum_{50}^{150} L_D \times DN/t_D^x \times T}$ L_D = Number of susceptible locations t_D = Pipe wall thickness [mm] x = a dimensionless parameter; Reference [8] N = number of leaks T = ROY
25 < DN ≤ 150	$CFP = \lambda_B / \lambda_L = 2.5/DN$ if no relevant failure data is available	λ_B = pipe break frequency. CFP = conditional failure probability given a through-wall flaw

TABLE 8. TREATMENT OF UNCERTAINTIES IN BENCHMARK 1.1

Parameter	Symbol	GRS and PEA	CEI
Number of events	$N_{L,D}$	χ^2 distribution	Log-normal (LN) distribution
Number of leak relevant locations	N_i	LN distribution	LN distribution
Conditional failure probability	*CFP*	β-distribution	β-distribution

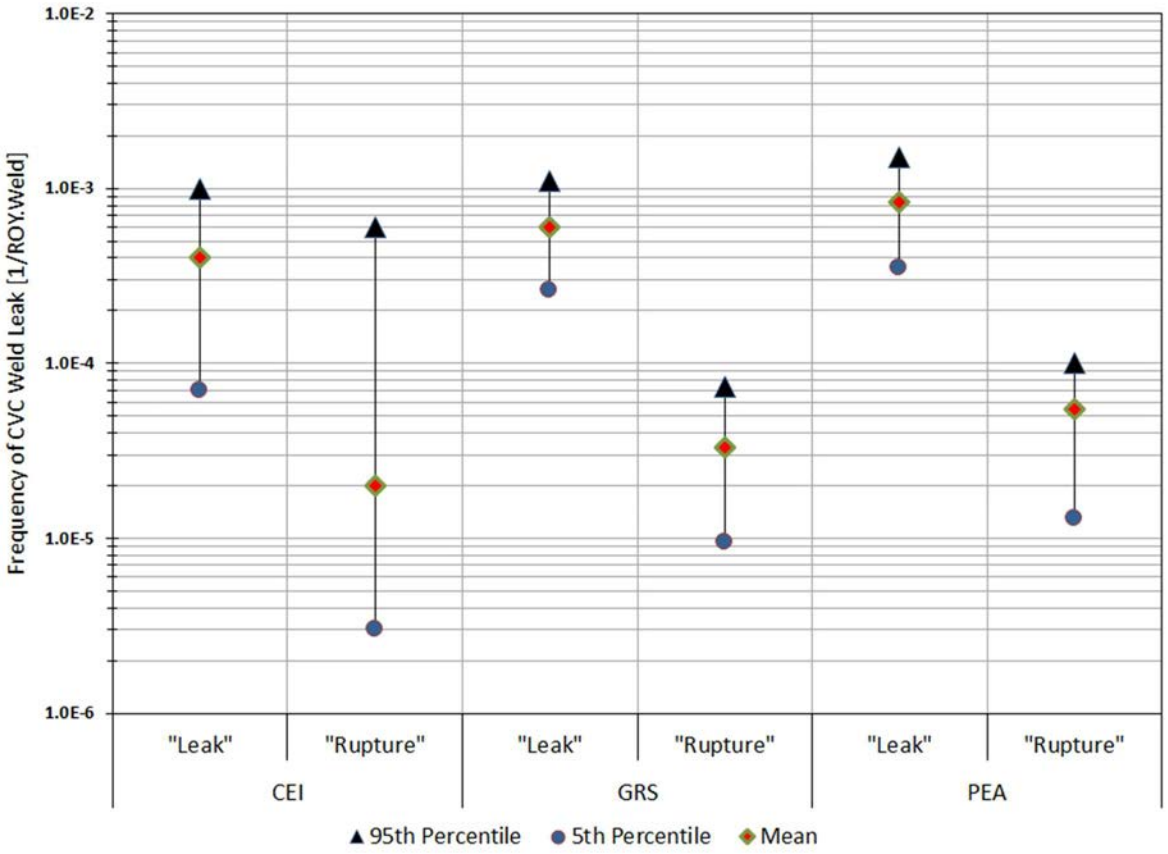

FIG. 12. Benchmark 1.1 DDM results.

3.2.1 PFM results

3.2.1.1 Computer codes

Four teams applied four different computer code implementations of PFM. Detailed descriptions are available in the annexes. The following computer codes were used:

- PROST: This code consists of models for crack initiation and growth, for specific leakage and rupture criteria, [9], [10]. The computer code models corrosion, fatigue, and ductile crack growth mechanisms;
- PIFRAP: This code models crack initiation and crack growth attributed to high cycle fatigue and intergranular SCC, [11]–[13];
- PRAISE-CANDU: This computer code establishes the threshold break size beyond which a large break LOCA (LB-LOCA) can be reclassified as a beyond design basis accident for CANDU plants, [14]–[16];

— PROFAS-PIPE: Developed especially for the CRP, this code consists of modules that generate probabilistic variables based on assigned distributions and calculates the stress intensity values of circumferential through-wall and partial through-wall defects, and the crack growth rate;

3.2.1.2 Definition of failure frequency and failure rate

Benchmark 1.1 is a time-variant reliability problem. Before comparing and contrasting the results among the teams, it is necessary to define the measures of reliability parameters: annual frequency and failure rate. In accordance with [17], the failure probability density at a given time is defined as the temporal derivative, $p(t)$. Often, it is convenient to define the failure frequency f_{t_a,t_b} with respect to a finite interval $[t_a, t_b]$ instead of an infinitesimal time; the annual failure frequency is an example:

$$f_{t_a,t_b} = \frac{1}{t_b - t_a} \int_{[t_a,t_b]} \dot{p}(t)\, dt = \frac{p(t_b) - p(t_a)}{t_b - t_a} \tag{2}$$

Since Eq. (2) is a numerical evaluation of the probability density over the time interval [t_a, t_b], the failure rate can be evaluated by introducing the survival function in the denominator as follows:

$$\lambda_{t_a,t_b} = \frac{p(t_b) - p(t_a)}{(t_b - t_a)[1 - p(t_a)]} \tag{3}$$

When the time interval t_b–t_a is one year, the numerical evaluation of the annual frequency and annual failure rate are simplified as:

$$f_{t_a,t_a+1} = \frac{1}{year}[p(t_a + 1) - p(t_a)];\ \lambda_{t_a,t_a+1} = \frac{1}{year}\frac{p(t_a+1) - p(t_a)}{[1 - p(t_a)]} \tag{4}$$

In the limit of small probabilities ($p(t) \ll 1$), these two expressions in Eq. (4) are closely related, i.e. $f_{t_a,t_a+1} \approx \lambda_{t_a,t_a+1}$.

3.2.1.3 Comparison of deterministic results

The PFM codes that were used in this benchmark adopt vastly different analytical solutions on the calculation of stress intensity factors (SIF), crack initiation and crack growth, leak rate, and crack stability. For these reasons, extensive deterministic studies were performed during this phase of benchmark to better understand the differences among the codes. Table 9 shows a comparison of different SIF, and as indicated in table three of the teams obtained their SIF solutions based on three different standards. The ratio between the maximum K_a and the minimum K_a is 1.338, the ratio between the maximum K_b and the minimum K_b is 1.363. Per the definition of crack growth rate in Table 4, when the SIF (K_I) is less than the threshold SIF (K_{thr}), crack growth rate is an exponential function of SIF with a power of 5.76. Therefore, a factor of 1.338 in K_a would result in 5.35 ($1.338^{5.76}$) times the difference in the crack growth rate in depth direction. Similarly, a factor of 1.363 in K_b would result in 5.95 ($1.363^{5.76}$) times difference in the crack growth rate in surface direction.

Such a difference on part-through wall crack size is then propagated through the through-wall crack growth, leak rate calculation, and stability evaluation; refer to Table 10 for the comparison on the critical crack size and the corresponding leak rate. The critical crack sizes calculated by CEI and GRS are almost identical whilst KAERI result is substantially lower. The corresponding leak rate shows an even larger difference. The leak detection limit was assumed to be 0.3 kg/s. Based on such a definition, any

leakage will not be detected in the GRS simulations because the leak rate at critical crack size is only 0.15 kg/s. Leak detection appears to be more feasible in the CEI simulations. Note leak rate calculation is also heavily affected by the different crack opening displacement (COD) solutions.

TABLE 9. COMPARISON OF STRESS INTENSITY FACTORS

Parameter	SIF Solution for Part-Through-Wall Crack			
	CEI	GRS		KAERI
	ASME FFS-1[3]	IWM[4]	R6[5]	RCC-MRx[6]
SIF at deepest point (MPa $m^{1/2}$), K_a	10.33	7.85	7.72	10.30
SIF at surface point (MPa $m^{1/2}$), K_b	4.44	3.50	3.42	4.66

TABLE 10. COMPARISON OF CRITICAL CRACK SIZE AND LEAK RATE

Parameter	CEI	GRS	KAERI
Critical crack size, mm	121	124	56
Leak rate, kg/s	7.33	0.15	0.66

3.2.1.4 Comparison of probabilistic results

The differences in the underlying deterministic calculations strongly influence the probabilistic failure metrics. Figure 13 compares the annual frequency of leak without consideration of ISI. Note that leak detection has no impact on the calculated annual frequency of leak because leak is defined as the formation of through-wall crack.

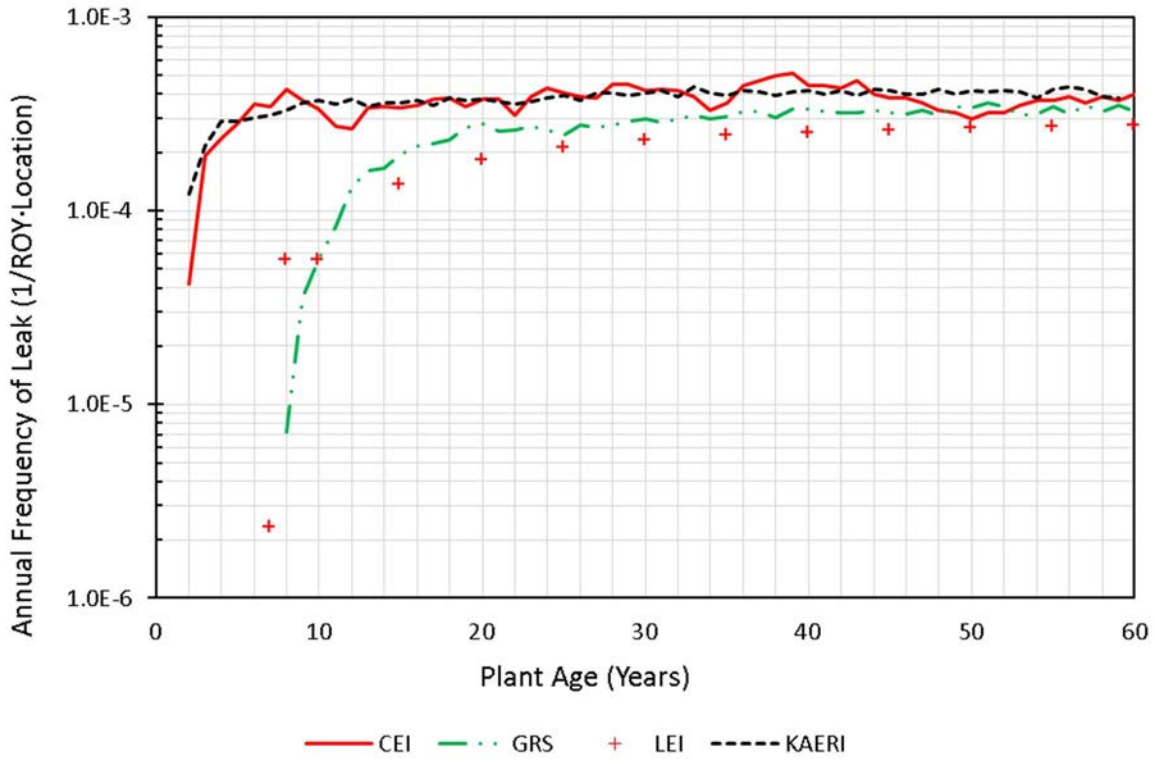

FIG. 13. Benchmark 1.1 PFM results without ISI.

[3] ASME (American Society of Mechanical Engineers) standard for fitness-for-service (FFS) assessment.
[4] Frauenhofer Institute for Mechanics of Materials, IWM.
[5] Stress intensity factors included in the R6 computer code.
[6] RCC-MRx is the French national standard for pressure retaining nuclear components.

After approximately 30 years, the leak frequency calculated by all teams is close to the prescribed crack initiation frequency of 4.08×10^{-4} per ROY. CEI and KAERI results are very close to each other; this is reflected in the calculated SIF values in Table 10. Since GRS' SIF values are substantially lower than those by CEI and KAERI, it is not surprising to see a lower leak frequency and it takes much longer time to form a through-wall crack. This is also consistent with OPEX. The effect of ISI on the leak frequency is shown in Fig. 14. The inspections are assumed to be performed once every ten years and with a POD according to the benchmark specification. The drop in leak frequency immediately after an inspection confirms the benefit of RIM.

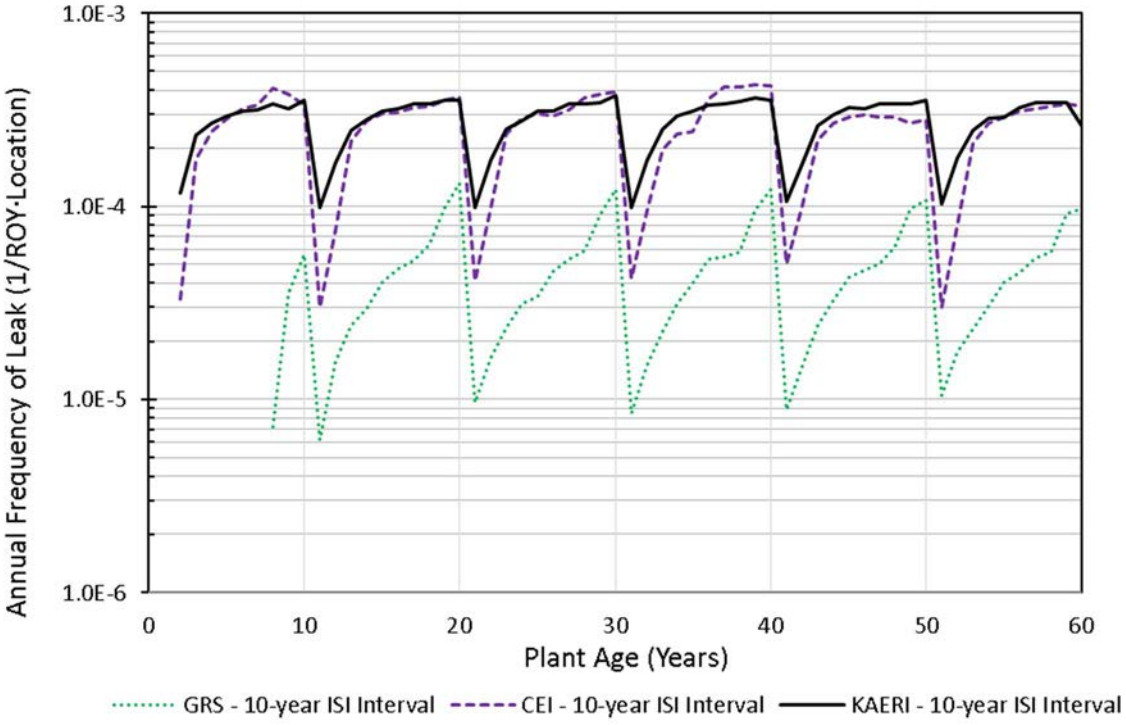

FIG. 14. Benchmark 1.1 PFM results with ISI.

Figure 15 shows a comparison of the effect of different ISI interval on the leak frequency. As expected, more frequent inspections would reduce the leak frequency. GRS's one-year ISI interval results appear to over-estimate the effect of ISI or underestimate the leak frequency. This is primarily attributed to the slower crack growth so that there is more chance for a part-through wall crack picked up by inspections. To study the effect of leak detection, the failure mode of interest is changed from leak to rupture, which in this benchmark is defined as a DEGB. Only the CEI results are provided. Figure 16 shows the results for the following RIM strategies:

- No ISI and no leak detection;
- No ISI but with leak detection;
- ISI every 10 years and no leak detection;
- ISI every 10 years and with leak detection;
- ISI every 5 years and no leak detection;
- ISI every 5 years and with leak detection;
- Annual ISI but no leak detection;
- Annual ISI and with leak detection.

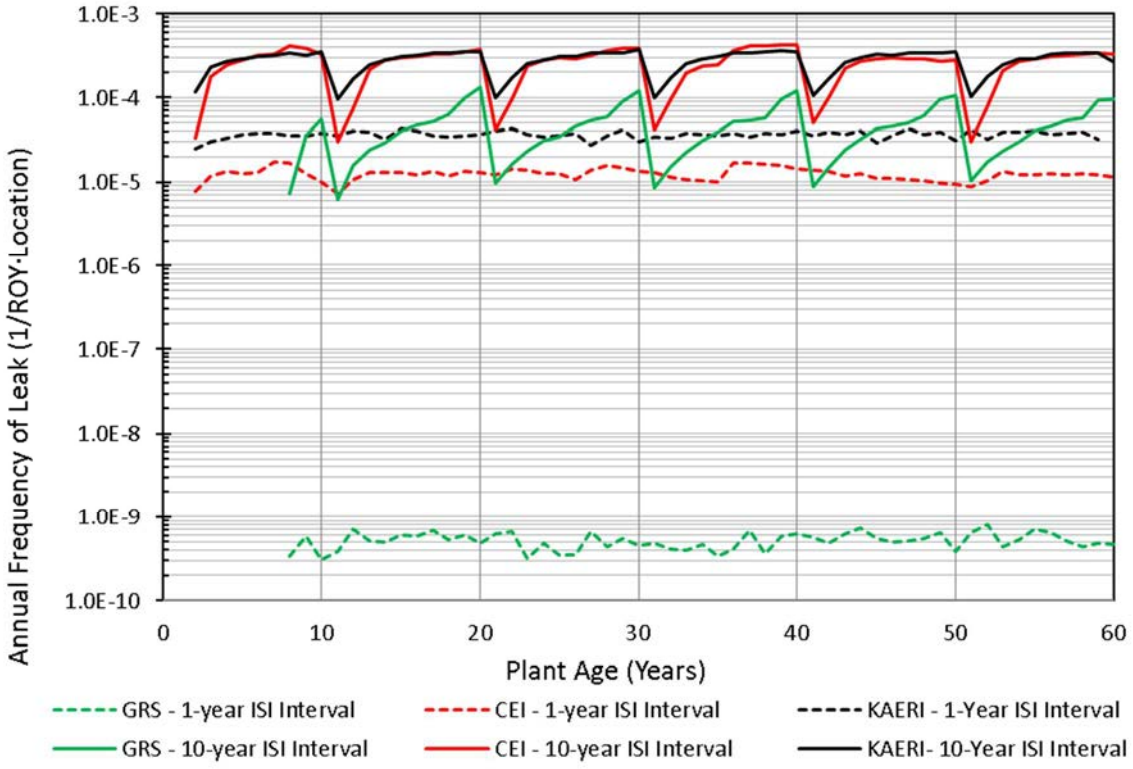

FIG. 15. Benchmark 1.1 results given different ISI intervals.

The results are summarized in Table 11 from which it can be concluded that leak detection is more effective in reducing the frequency of a DEGB than is the case for ISI only. For a typical PWR plant, the leak detection limit is on the order of 0.0631 kg/s and ISI is performed every 10 years.

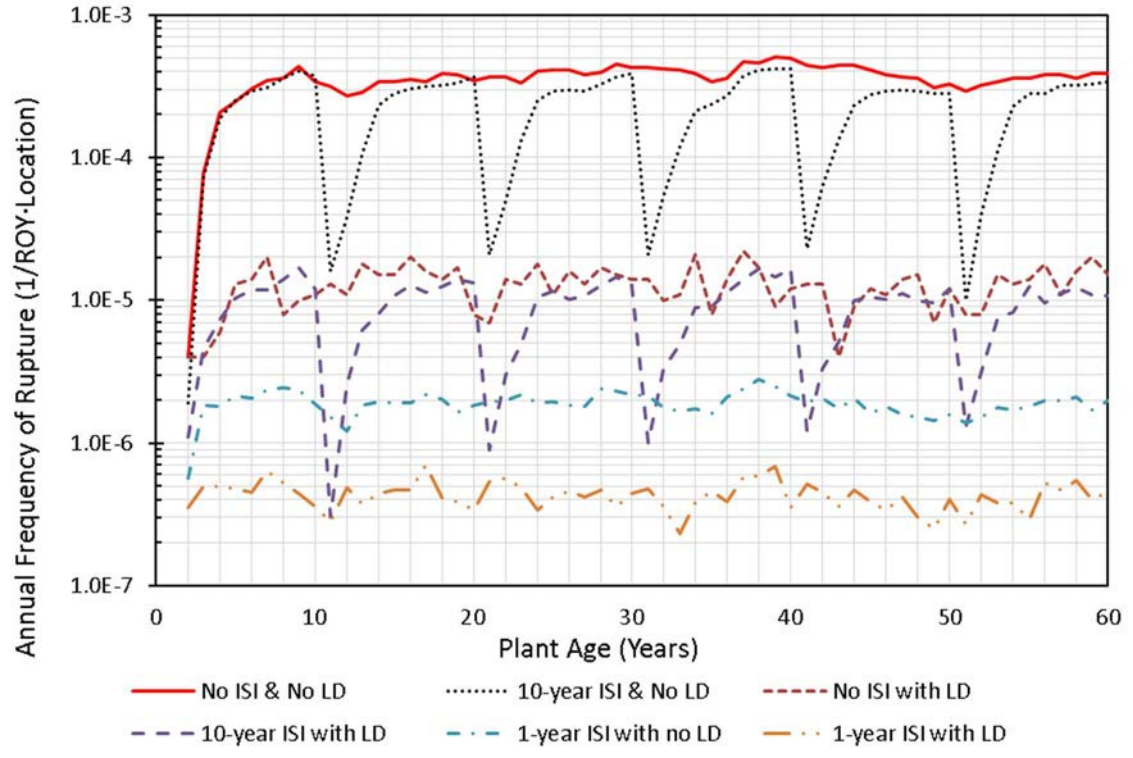

FIG. 16. Benchmark 1.1 results for different RIM strategies.

TABLE 11. ANNUAL RUPTURE FREQUENCY FOR DIFFERENT RIM STRATEGIES

RIM Strategy	Rupture Frequency (1/ROY.Location)
No ISI and no leak detection	3.9×10^{-4}
ISI every 10 years but no leak detection	3.4×10^{-4}
ISI every 5 years but no leak detection	2.7×10^{-4}
No ISI but with leak detection	1.5×10^{-5}
ISI every 10 years and leak detection	1.1×10^{-5}
ISI every 5 years and leak detection	1.0×10^{-5}
ISI every year but no leak detection	2.0×10^{-6}
ISI every year and leak detection	4.5×10^{-7}

3.3 RESULTS OF BENCHMARK 1.2

Two analysis teams participated in Benchmark 1.2 and applied two different methodologies. One team used a data-driven method in which the rate of flaw initiation up to a through-wall leak was based on OPEX data and the conditional failure probability was based on a combination of OPEX data, expert elicitation and fracture mechanics. The results were in the form of a cumulative frequency of pipe failure as a function of the through-wall flow rate. A Bayesian technique in combination with Monte Carlo simulation performed the propagation of uncertainties through the pipe failure frequency equation, [18]–[20]. The DDM results are shown in Fig. 17.

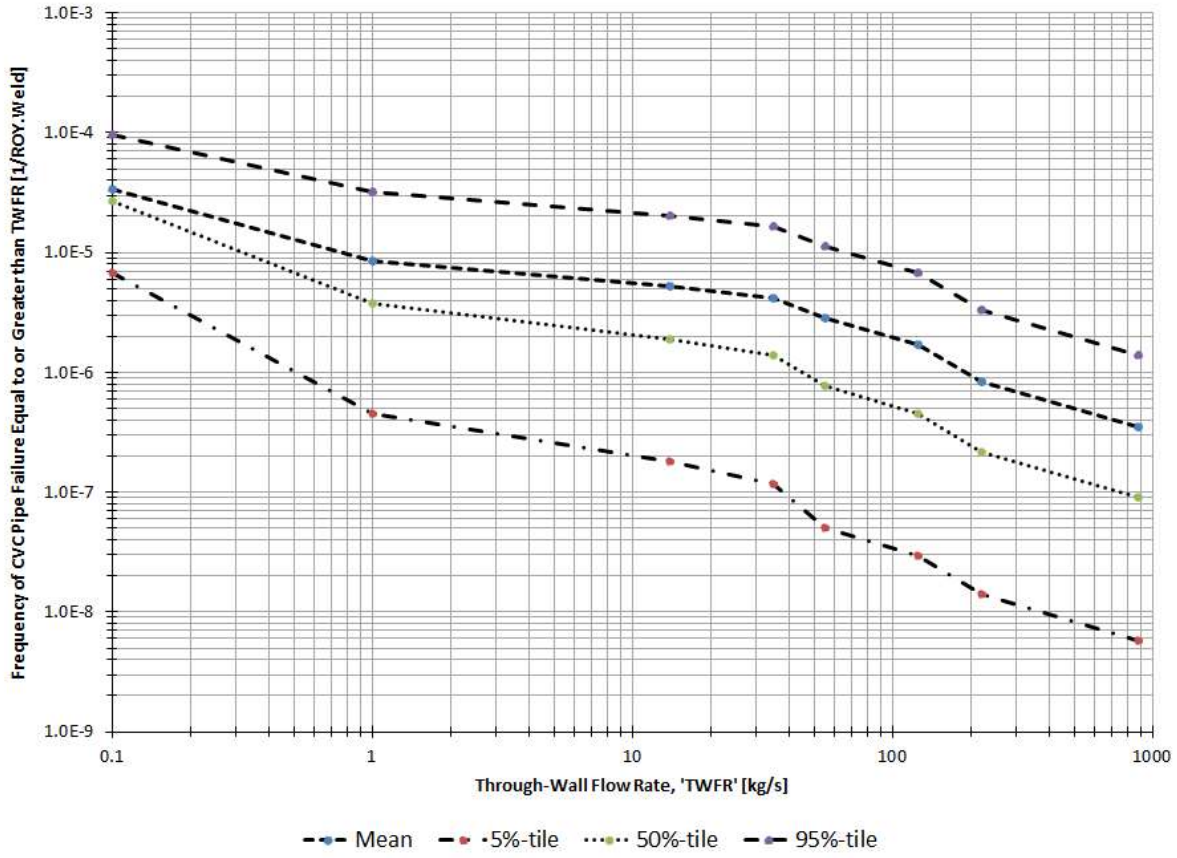

FIG. 17. Benchmark 1.2 DDM results.

TABLE 12. BENCHMARK 1.2 DDM AND I-PPOF RESULTS

Methodology	Failure Mode	Pipe Failure Frequency [1/ROY.EB]		
		Mean	5%-tile	95%-tile
DDM	Perceptible leakage, at or below detection limit	2.81×10^{-4}	1.28×10^{-4}	5.16×10^{-4}
	Rupture – through-wall flow Rate ≥ 15 kg/s (medium LOCA)	5.18×10^{-6}	1.79×10^{-7}	2.02×10^{-5}
IPPoF	Through-wall crack	1.01×10^{-4}	1.53×10^{-6}	3.41×10^{-2}
	Rupture	5.33×10^{-6}	1.51×10^{-8}	3.43×10^{-4}

EB = Evaluation Boundary

The second team used a physics based approach to model crack initiation due to thermal fatigue and a renewal process model to analyze the interactions between crack growth, leak detection, and ISI. The analysis produced results for the frequency of a leak (equal to a through-wall crack) and the frequency of rupture; Table 12, which also includes the DDM results. The details of the integrated physics of failure methodology are found in [21], [22].

3.4. RESULTS OF BENCHMARK 2

The format for the results presentation is as follows. Firstly, a comparison is made of the results obtained by the teams that applied a DDM and a physics of failure methodology. Second, the results of the PFM analyses are presented. Three teams applied three different PFM computer codes.

3.4.1 DDM and I-PPoF results

A sample of the calculated pipe failure frequencies is found in Table 13.

TABLE 13. SELECTED DDM AND I-PPoF RESULTS

FOI	Analysis Case	5%-tile	50%-tile	95%-tile
DDM Results by SPI – Mitigated Alloy 82/182 in Lieu of Alloy 52/152				
14 Calculated	Frequency of Detectable Flaw	3.41×10^{-6}	1.89×10^{-5}	1.10×10^{-4}
	Frequency of Leak - ≤ Leak Detection Limit (“perceptible leakage”)	1.21×10^{-6}	1.16×10^{-5}	1.09×10^{-4}
	Frequency of Rupture - DEGB	2.88×10^{-13}	1.70×10^{-11}	8.95×10^{-10}
DDM Results by CEI				
Refer to Annex I	Frequency of Leak	5.62×10^{-7}	3.89×10^{-6}	3.29×10^{-5}
	Frequency of Rupture - DEGB	3.59×10^{-14}	1.58×10^{-10}	8.21×10^{-9}
I-PPoF Results				
6 1%-tile	Frequency of Detectable Flaw	5.96×10^{-2}	5.99×10^{-2}	6.04×10^{-2}
	Frequency of Leak	4.89×10^{-3}	4.95×10^{-3}	5.04×10^{-3}
	Frequency of Rupture	5.48×10^{-8}	1.07×10^{-7}	2.58×10^{-7}
497 50%-tile[7]	Frequency of Detectable Flaw	6.43×10^{-10}	1.63×10^{-7}	6.28×10^{-7}
	Frequency of Leak	1.70×10^{-18}	1.09×10^{-13}	1.62×10^{-12}
	Frequency of Rupture	5.65×10^{-19}	3.63×10^{-14}	5.39×10^{-13}

[7] This value is to be contrasted with the EPRI MRP-386 (2017) recommended FOI = 324 for the Alloy 52/152 crack growth rate, [25].

In the DDM analysis a prior failure rate distribution was developed on the basis of the existing OPEX with Alloy 82/182. Next the prior failure rate distribution was updated under an assumption of having a full structural weld overlay applied to all operating WCR plants, Fig. 18. The experience with full structural weld overlay is very extensive, providing high confidence in the effectiveness of this technique for arresting crack growth given a preexisting weld flaw.

In the IPPoF analysis the potential crack initiation and crack growth of Alloys 52/152 was modeled explicitly. The effect of using a material that is considered highly resistant to PWSCC is expressed by the FOI, [23], [24]. Using test data from MRP-386 [25], a gamma distribution was used to characterize the uncertainty in the FOI for Alloy 52/152 crack initiation and crack growth relative to Alloy 82/182.

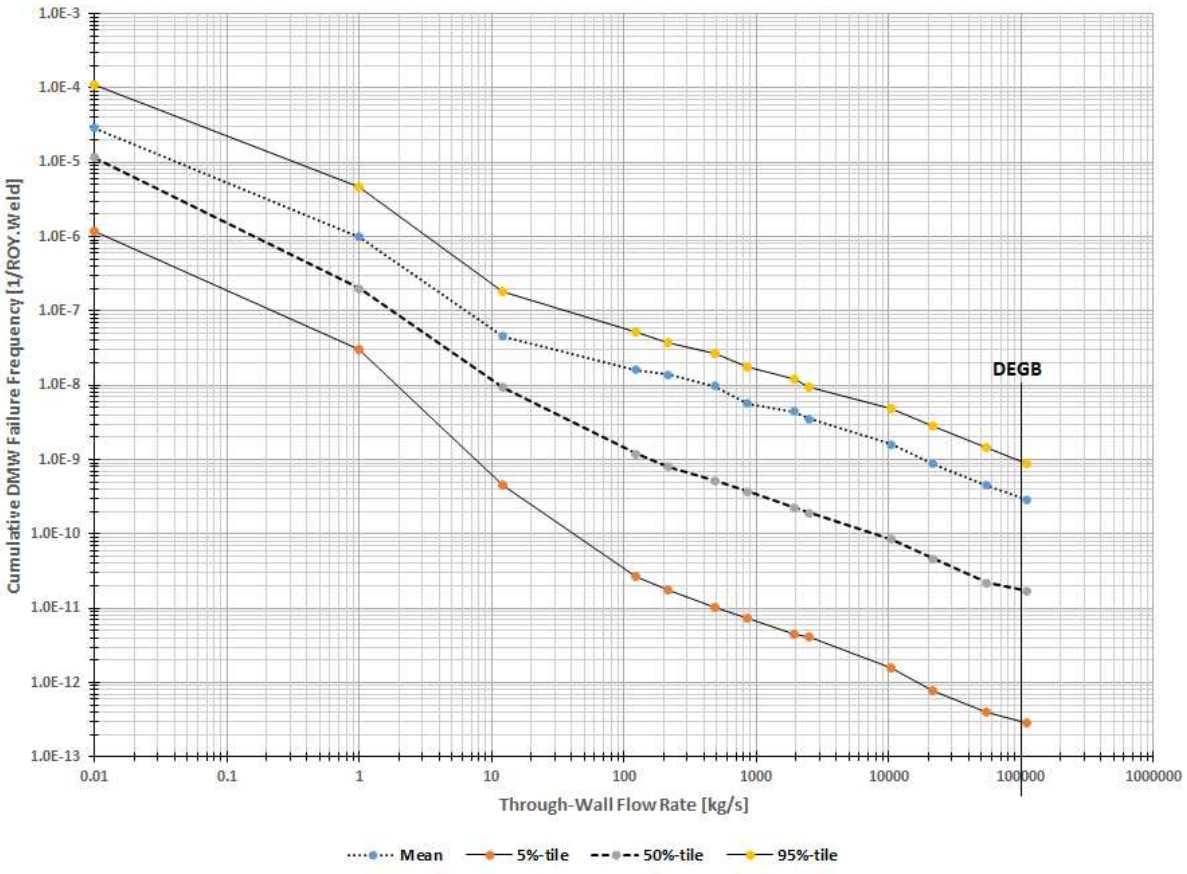

FIG. 18. Cumulative frequency of a DMW failure.

3.4.2 PFM results

Three teams (CEI, GRS and KAERI) participated in the Benchmark 2 PFM activity.

Unlike Benchmark 1.1, only the basic geometry, operating conditions and leak detection capability are specified in Table 14. The remaining parameters such as operating loading stress, weld residual stress, crack initiation frequency or time, crack growth rate, inspection capability, inspection interval, and mechanical properties are determined by each team based on their knowledge of the piping design and operation.

TABLE 14. PROBABILITY OF DETECTION

Depth (mm)	0.0	0.41	0.81	1.63	2.44	4.06	8.13	20.31	81.25	100
POD	0.0	0.05	0.1	0.2	0.3	0.5	0.522	0.572	0.666	1.0

The following common parameters are assumed by each team:

- Operating life, 40 year for WCR and 60 years advanced WCR;
- POD as per Table 14;
- Inspection interval, every 10 years. However, the exact year for the inspection is not the same. CEI assumes ISI is performed at the following years: 6th, 16th, 26th, 36th, 46th and 56th;
- Since none of the recorded Alloy 600/82/182 failures were attributed to severe loading conditions, safe shutdown earthquake loads were not considered in the analyses; and
- References [26] and [27] document the basis for the Alloy 600/82/182 modeling parameters although some parameters were adjusted per the description in Section 3.4.2.1.

3.4.2.1 Calibrating the PFM modeling parameters against Alloy 600/182/82 OPEX

A two-step procedure was applied to adjust the PFM model parameters to match the PFM predictions with the DDM results for Alloy 600/82/182, and to apply different FOIs on crack initiation frequency and crack growth rate between Alloy 600/82/182 and Alloy 690/52/152. The first step was to adjust PFM modeling parameters to match the failure frequency of Alloy 600/82/182. Failure is defined as through-wall flow rate in the unit of kg/s. Values in Fig. 19 were derived by SPI using DDM analysis of OPEX data described in Section 2.3.1. These values were then used by each PFM participant to adjust their modeling parameters to match the DDM results. Because of the different PFM code implementations, there is no generally accepted approach for how to decide which parameters to be adjusted.

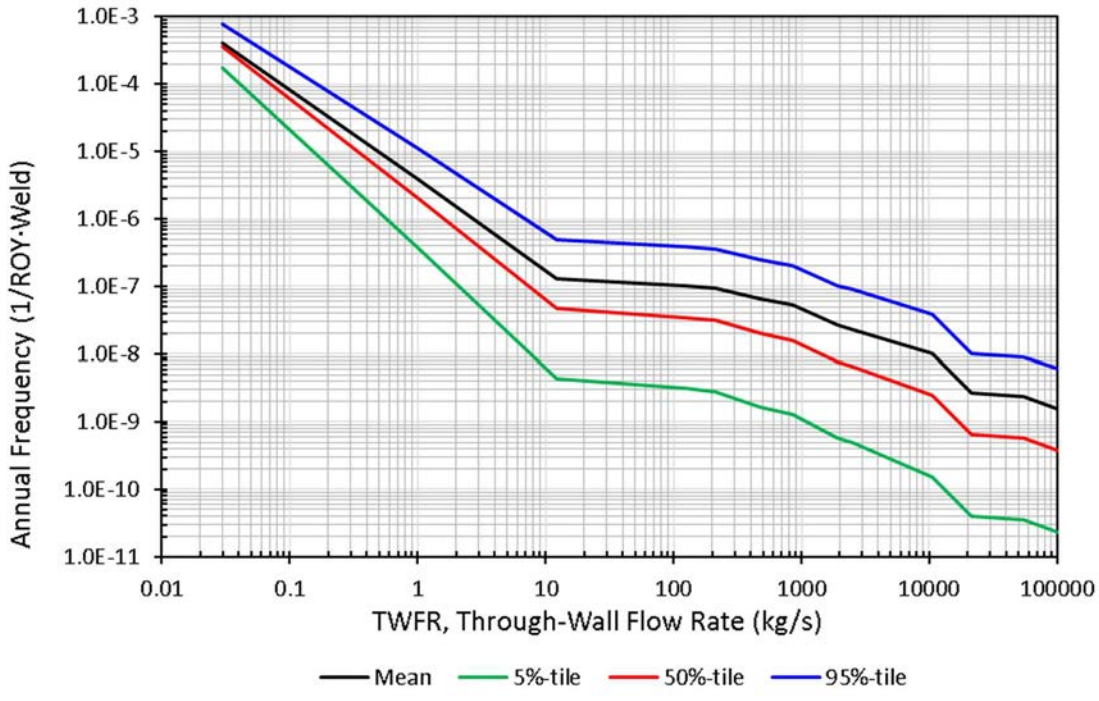

FIG. 19. Annual frequency of failure of Alloy 600/82/182 DMW.

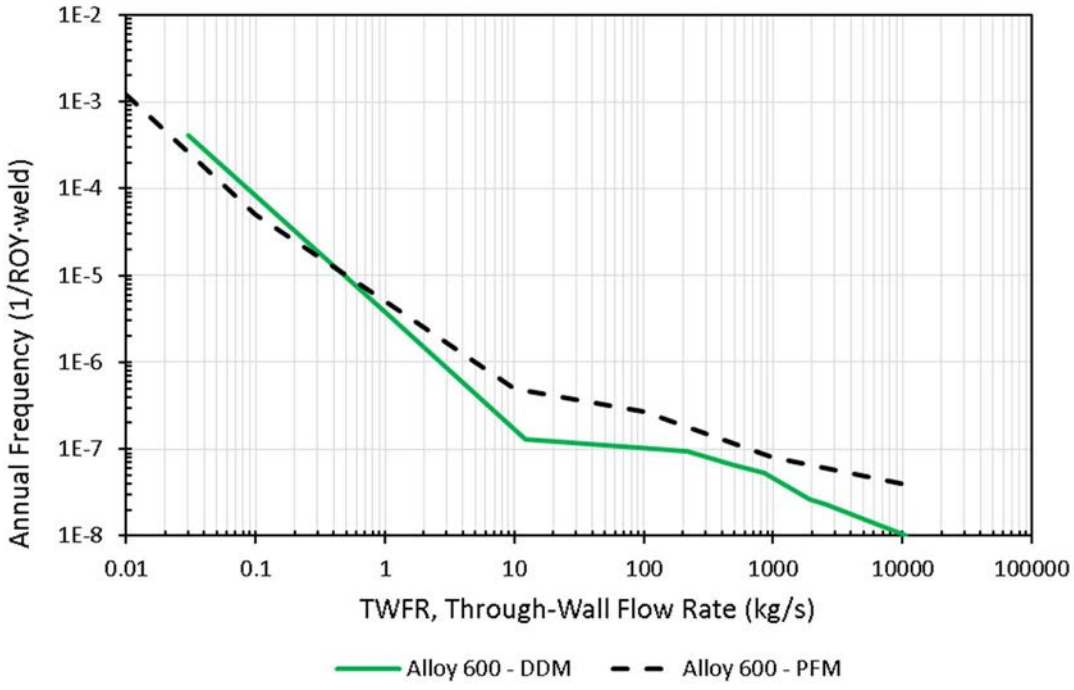

FIG. 20. Comparison of failure frequency according to DDM and PFM for Alloy 600/82/182.

Using an iterative process, CEI adjusted the bending stress and the weld residual stress to match the predicted failure frequency with the DDM mean curve in Fig. 19. In Fig. 20 DDM and PFM predictions are compared.

GRS adjusted the crack initiation frequency and crack growth rate to match three OPEX data observations: (1) the leak frequency of 4×10^{-4} per weld year, (2) the total number of two leaks or two through-wall cracks, and (3) the total number of 33 surface flaws. KAERI took the same approach adopted by GRS for adjusting the PFM modeling parameters. The comparison between PFM and DDM is discussed in Subsection 3.4.2.5.

3.4.2.2 Factor of improvement approach

Covering multiple decades of experimental work, extensive published information on the Alloy 690 to Alloy 600 FOI determination exists. The published work covers the different methods for FOI determination, a wide array of test methods, test specimens and test variables. Active research remains ongoing and is conditioned by: (a) as of yet (year 2021) no evidence of Alloy 690/52/152 failures, and (b) an increasing number of nuclear power plants entering into periods of long-term operation (> 40 years).

Adjusting the Alloy 600/82/182 PFM models to reflect the Alloy 690/52/152 DMW state-of-knowledge involves using two types of FOIs:

- FOI on crack initiation time or frequency. Compared to Alloy 600/82/182, an FOI=5 means that it takes 5 times the operating life for Alloy 690/52/152 to initiate a crack;
- FOI on crack growth rate. Compared to Alloy 600/82/182, an FOI=38 means that Alloy 690/52/152 growth rate is 1/38 of that of Alloy 600/82/182.

In the implementation of the FOI approach, GRS and KAERI applied a constant FOI=10 to both crack initiation frequency and crack growth rate. CEI applied different FOI to crack initiation time and crack growth rate.

Detailed descriptions of the crack initiation and crack growth models adopted by each PFM code are provided in the annexes. For these reasons, the predicted failure frequency is expected to show large difference. Figure 21 illustrates CEI's study on the effect of FOI on crack initiation time and crack growth rate, an FOI=5 is assumed. For the same FOI, the FOI on crack initiation time has more pronounced effect in reducing the annual failure frequency. This is expected because there is no crack growth without crack initiation.

3.4.2.3 Quantitative results for Alloy 690/152/52

Only the CEIs results are provided in Figs. 22 and 23. The results by GRS and KAERI show a similar trend and are therefore not included.

In Fig. 22, the cumulative probability for through-wall flow rate greater than 0.1 kg/s does not increase with time, this is attributed to the assumed leak detection limit of 0.0631 kg/s. In Fig. 23, the annual frequency of through-wall crack and through-wall flow rate of 0.1 kg/s drops immediately after the 6th, 16th, 26th, 36th, 46th and 56th year, this is attributed to the effect of ISI.

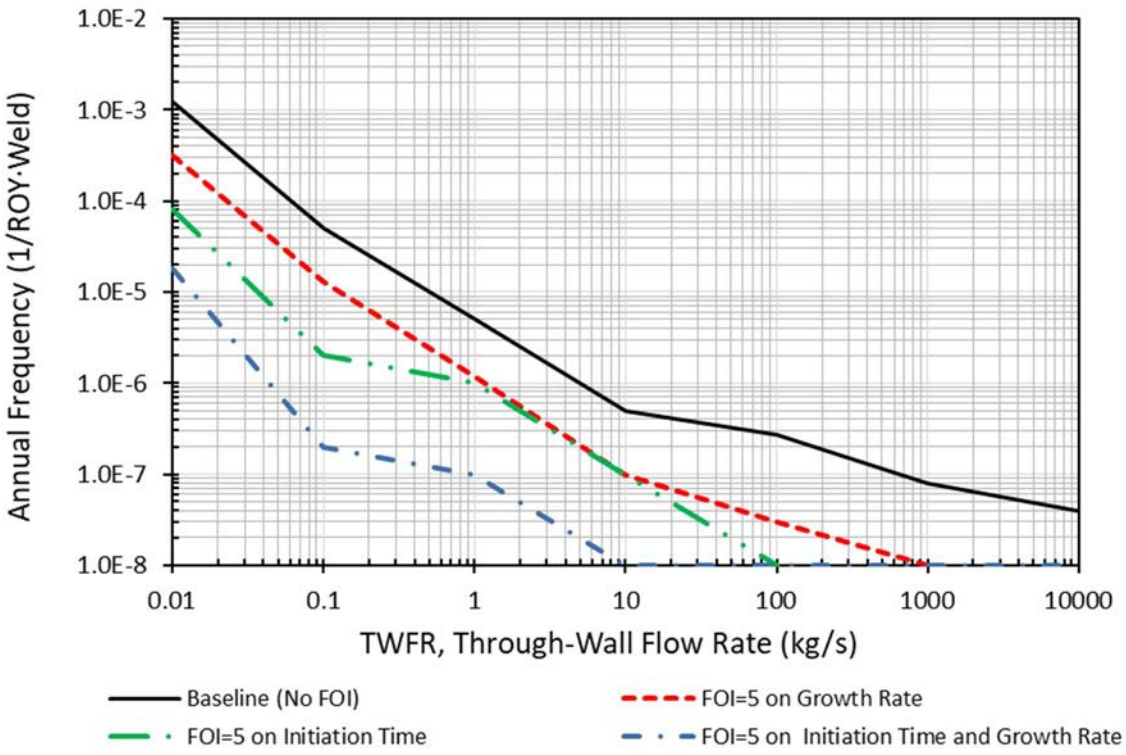

FIG. 21. Effect of FOI on crack initiation time and crack growth rate.

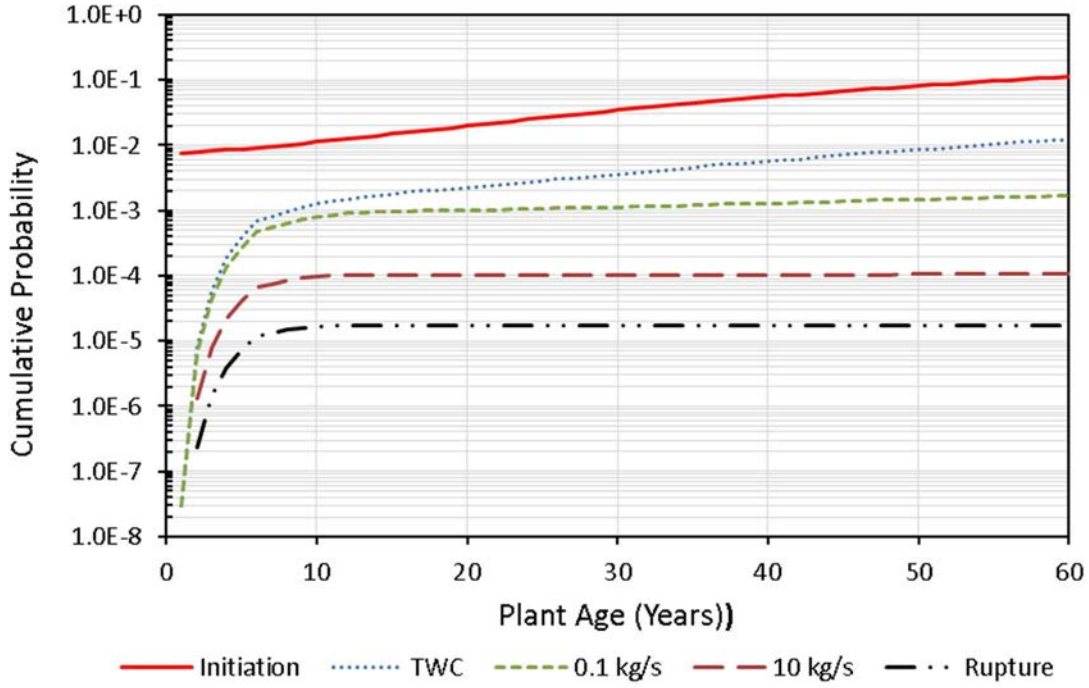

FIG. 22. Cumulative probability of failure of Alloy 690/52/152 with FOI=5 on crack growth rate.

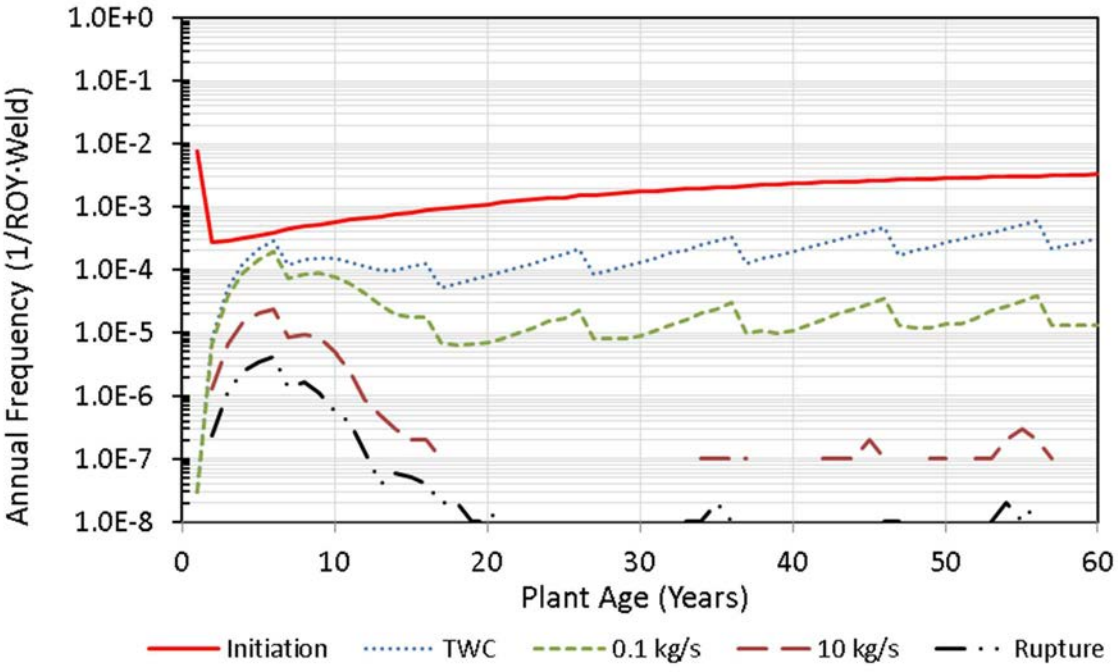

FIG. 23. Annual failure frequency of Alloy 690/52/152 with FOI=5 on crack growth rate.

3.4.2.4 Intra-comparison of PFM results

An intra-comparison on the annual failure frequency for Alloy 600/82/182 DMW is shown in Fig. 24. Also included is the mean DDM curve. Not surprisingly, there is a very large scatter across the PFM results. These differences are not only reflected in the range of through-wall flow rate (e.g. GRS only provided the leak rate between 0.01 kg/s to 1 kg/s) but also in the magnitude of the annual failure frequency.

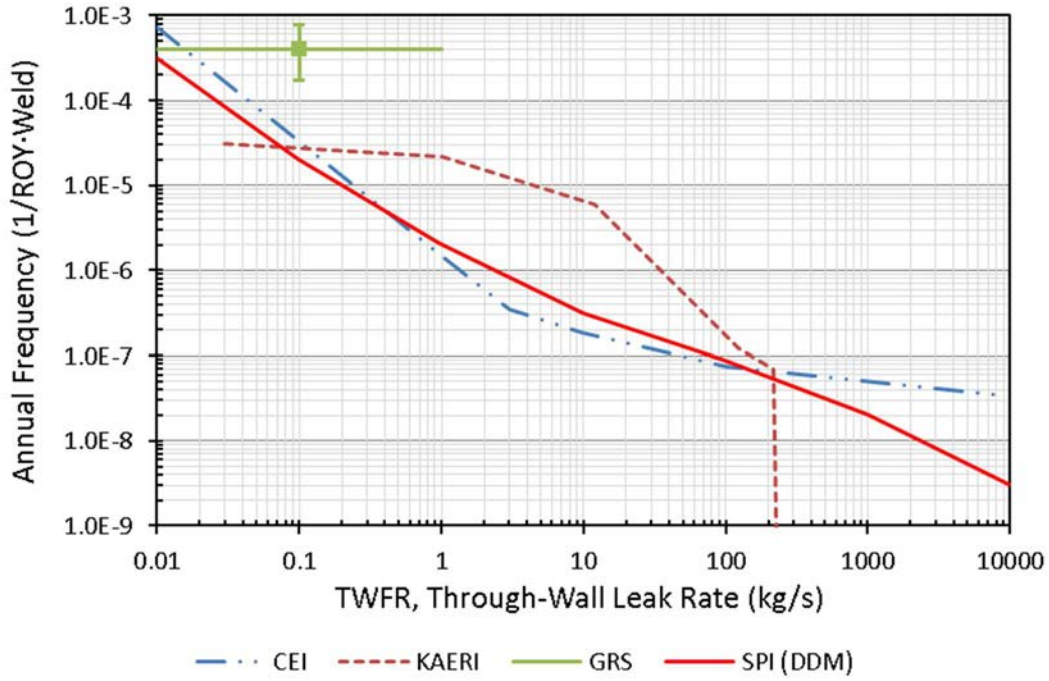

FIG. 24. Intra-comparison of results for Alloy 600/82/182.

An intra-comparison on the annual failure frequency for Alloy 690/52/152 is shown in Fig. 25. Also included is the mean DDM curve. Noticeably the scatter increases substantially. For the leak rate of 0.1 kg/s, the annual frequency varies from ca. 1×10^{-14} to ca, 1×10^{-5}; i.e. nine (9) orders of magnitude. Note that the CEI's results are based on an FOI=5 on crack growth rate.

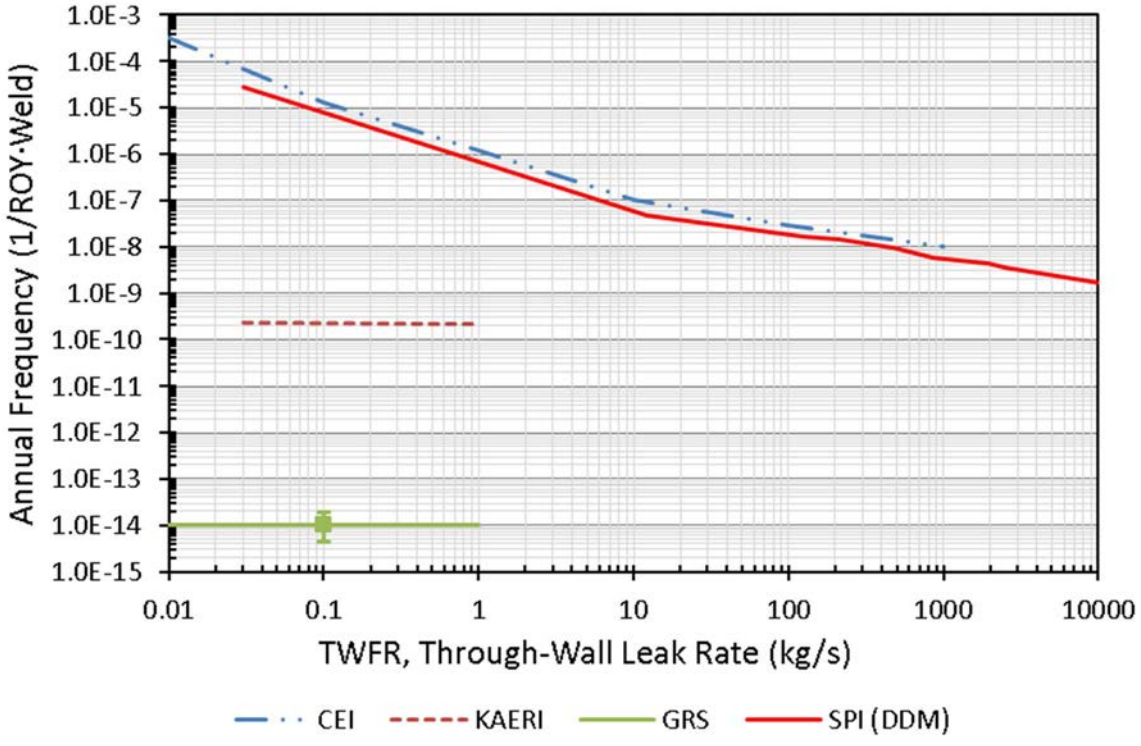

FIG. 25. Intra-comparison of results for Alloy 690/52/152.

3.4.2.5 Inter-comparison of DDM and PFM results

A limited inter-comparison of CEI's PFM results and the DDM results were performed. Various combinations of FOIs on crack initiation time and crack growth rate were investigated. Generally, the annual failure frequency decreases with increasing FOI. The PFM case "FOI=5 on Growth Rate" or "FOI=5 on Initiation Time" matches well the mean curve of the DDM analysis. The PFM case "FOI=38 on Growth Rate" agrees reasonably well with the 5th percentile of the DDM results. It is noted that [25] conservatively recommends: (1) FOI=38 for Alloy 690 compared to Alloy 600, and (2) FOI=324 for Alloy 52/152 compared to Alloy 182. Failure frequencies less than 10^{-10} per weld year were not calculated because it requires extremely long computing times. This is also consistent with the following:

> "*… there is no generally accepted lowest plausible failure frequency for individual welds, for instance individual pipe welds. As a general guide, claims for pipework weld failure rates for gross failure (e.g. guillotine failure) much better than 10^{-8} to 10^{-9} per weld year should not be considered plausible*." [28]

3.4.2.6 Uncertainty analysis

An interesting observation could be made from comparing Figs. 25 and 26. The scatter across the PFM results is up to nine (9) orders of magnitude in Fig. 25. In contrast, the scatter across the DDM to PFM results is less than five (5) orders of magnitude in Fig. 26. This contrast illustrates the importance of the assumptions that were adopted in the analyses. DDM and PFM handle the epistemic uncertainties differently.

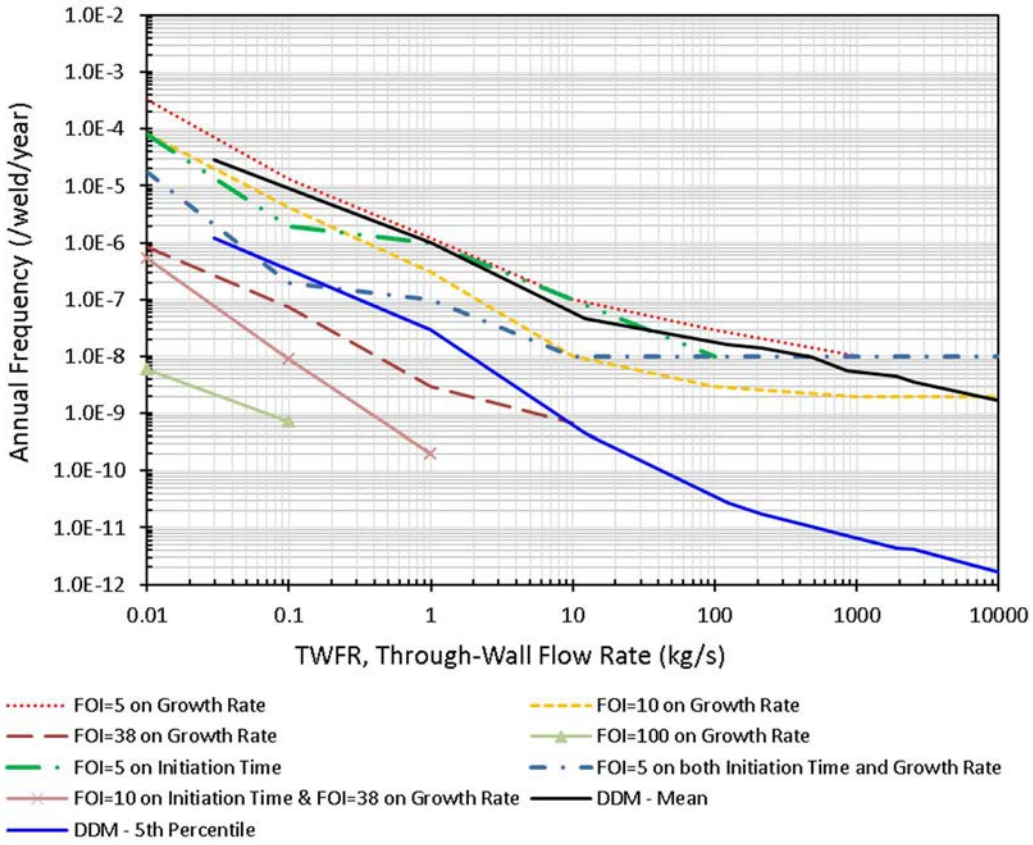

FIG. 26. Intra-comparison of results for Alloy 690/52/152.

Figure 27 compares the DDM and PFM means and 95%-percentiles. In the PFM modeling, the inner diameter WRS, the WRS zero-crossing, the heat-to-heat initiation model variable B, and Ramberg-Osgood Parameter D are treated as epistemic random variables. These four random variables are the most influencing parameters on the through-flaw flow rate of 1 kg/s by the use of amplification ratio method, refer to Section 4.4 for the detailed discussion.

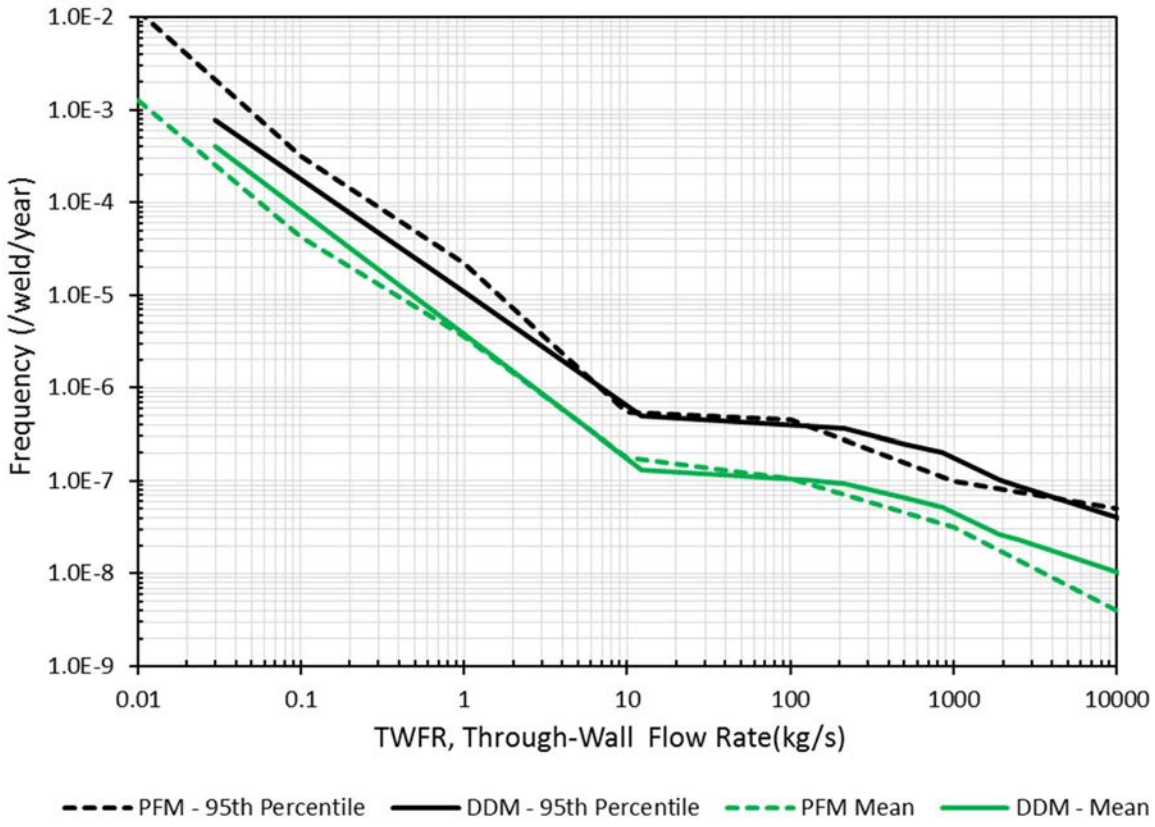

FIG. 27. Inter-comparison of DDM and PFM uncertainty analysis for Alloy 600/82/182.

4. LESSONS LEARNED

4.1 BENCHMARK OBJECTIVES

The integrated research plan of the CRP consisted of two main activities: 1) benchmarking, and 2) development of a good practices framework for piping reliability analysis. The latter activity benefitted from the first activity in which the capabilities of different methodologies were assessed. Summarized in this section are the principal observations from the benchmarking activity.

4.2 INTRA-COMPARISON OF RESULTS

4.2.1 Benchmark 1.1 of data-driven methods

Using a common set of input parameters, the three participating teams calculated the frequency of leak and rupture for a generic CVC system. A formal degradation mechanism analysis was not performed.

However, the benchmark specification included a statement about the number of locations within the CVC system that could be susceptible to material degradation; e.g. fatigue failure. The assumptions used by respective team and the quantitative results are summarized in Tables 15 and 16, respectively.

TABLE 15. ASSUMPTIONS IN BENCHMARK 1.1 ON DDM

Assumption / Comment	GRS	STEG	CEI
Employed data base filtering	The 14 German PWR plants in the database were sorted into 3 classes, according to the commissioning year.		
Evaluation boundary	The technical details were provided by GRS.		
Assumptions for computation of failure frequency distributions	Ratio of rupture to leak frequency: Beta-distribution (p=5.5, q=95.5); Number of leak relevant positions: Log-Normal distributions (=3.65, =0.233, mean=43, sigma=43/2); Number of leaks: Non-central chi-square distribution (=(7+0.5)/441, =2(7+0.5))	Same as GRS.	Ratio of rupture to leak frequency: Beta-distribution (p=5.5, q=95.5); Number of leak relevant positions: Log-Normal distributions (=3.65, =0.472, mean=43, sigma=43/2); Number of leaks: lognormal distribution(-4.55, 0.65, mean=0.015, STD = 0.015)
Meaning of the term "rupture"	Assumed to correspond to DEGB		
Comments	The assumption of similar volume control systems for all the plants of the same class (see a) is a very rough classification.	STEG questioned several of the assumptions in the benchmark specification: Is the CVC piping system design the same for all PWR plants? Is Thomas formula sensitive to the length of the operation period? Is this formula be modified to also account for the number of ROYs?	The assumption of similar volume control systems for all the plants of the same nuclear steam supply system design is a very rough approximation

TABLE 16. QUANTITATIVE RESULTS OF BENCHMARK 1.1 ON DDM

Parameter	GRS	STEG	CEI
Frequency of a Leak (Events per ROY and Weld)			
Expected value	6.1×10^{-4}	8.3×10^{-4}	4×10^{-4}
Median	5.7×10^{-4}	7.7×10^{-4}	3×10^{-4}
5% quantile	2.6×10^{-4}	3.5×10^{-4}	7×10^{-5}
95% quantile	1.1×10^{-3}	1.5×10^{-3}	1×10^{-3}
Frequency of a Rupture (Events per ROY and Weld)			
Expected value	3.3×10^{-5}	4.5×10^{-5}	2×10^{-5}
Median	2.9×10^{-5}	3.9×10^{-5}	1×10^{-5}
5% quantile	9.5×10^{-6}	1.3×10^{-5}	3×10^{-6}
95% quantile	7.3×10^{-5}	1.0×10^{-4}	6×10^{-4}

The three teams applied the same general modeling concept and the same set of input parameters. The quantitative results are somewhat similar. The differences are attributed to how respective team treated the uncertainties in the failure rate exposure term; i.e. variability in the number of susceptible locations as well as variability in the susceptibility to degradation across this population.

4.2.2 Benchmark 1.1 on probabilistic fracture mechanics

The PFM codes that were used in this benchmark adopted very different analytical solutions on the calculation of SIF, crack initiation, crack growth, leak rate, and crack stability. For these reasons, extensive deterministic studies were performed to better understand the differences among four different computer codes. The differences in the underlying deterministic calculations strongly influenced the calculated probabilistic failure metrics.

4.2.3 Benchmark 2 on probabilistic fracture mechanics

The second benchmark focused on the modeling of crack initiation and crack growth in Alloys 690/52/152, a material which is highly resistant to PWSCC. The crack growth rate module of respective PFM code was not developed for this material, however. In preparing for the computations of probabilistic failure metrics, each team (CEI, GRS and KAERI) determined the necessary input parameters such as operating loading stress, weld residual stress, crack initiation frequency or time, crack growth rate, inspection capability (defined by the POD), inspection interval, and mechanical properties.

Adjusting the PFM models to handle Alloys 690/52/152 focused on the FOI concept. There are two types of FOI, one on crack initiation time and another crack growth rate. In the implementation of the FOI concept in the PFM modeling, GRS and KAERI applied the same FOI=10 for the crack initiation and crack growth. CEI applied different FOIs for the crack initiation time and the crack growth rate. For these reasons, significant differences were noted in the calculated failure frequencies. An important, and expected, outcome of this benchmark was the pronounced effect of the crack initiation FOI in reducing the calculated annual failure frequency.

4.3 INTER-COMPARISON OF RESULTS

4.3.1 Benchmark 1.2 on data-driven methods and physics-of-failure methods

In Benchmark 1.2 the chosen evaluation boundary was carefully defined. Associated with the evaluation boundary was the well documented OPEX data on real failures. The two teams (SPI and UIUC) produced similar results. SPI quantified probabilistic failure metrics for a through-wall flaw producing a perceptible leakage (i.e. $<< 6.3\times10^{-2}$ kg/s). UIUC calculated probabilistic failure metrics for a “leak”. Results of both teams were approximately a factor of two (2) apart; (2.8×10^{-4} per ROY vs. 1.1×10^{-4} per ROY) but with significantly different uncertainty distributions.

When calculating probabilistic failure metrics for rupture the probabilistic failure metrics were remarkably similar (central values as well as upper and lower bounds). One of the teams interpreted rupture to correspond to a through-wall flow rate > 15 kg/s; i.e. in excess of the normal make-up capability of a CVC system. The other team used the term “rupture” in lieu of a DEGB.

4.3.2 Benchmark 2 on data-driven methods, physics-of-failure methods, and PFM

Six teams responded to the Benchmark 2 challenge. That is to calculate probabilistic failure metrics for a very well defined advanced WCR piping evaluation boundary consisting of a DMW between a RPV outlet nozzle and an RCS hot leg. This DMW consists of an Alloy 152 buttering and an Alloy 52 weld.

Although three fundamentally different methodologies were applied, a FOI approach was used by all teams to account for the improvement in the resistance to PWSCC. The team that used DDM, estimated the expected minimum achievable FOI from OPEX with PWSCC mitigation techniques. The physics of failure approach used different assumptions about the FOI based on reviews of published results of experimental work. Two of the PFM teams applied a fixed FOI, and a third PFM team applied different FOIs for the crack initiation time and crack growth rate.

All teams generated annual frequencies of an Alloy 152/52 weld failure. Significant variability in results was observed, spanning about nine (9) orders of magnitude. However, this variability was due to the FOI assumptions and other assumptions made by respective team.

4.4 SENSITIVITY AND UNCERTAINTY ANALYSIS

As part of Benchmark 1.1 PFM benchmark studies, CEI, GRS and LEI explored the following six (6) methods for the ranking of relevant influence parameters on the cumulative rupture probability [17]:

- *Amplification ratio*. The amplification is useful for identifying basic variables that have a strong effect on the resulting estimate of failure probability;
- *Direction cosine method*. This method is based on the position of the most probable failure point, and it provides a measure of the sensitivity or importance of the failure probability to the corresponding random variable;
- *Most probable failure point analysis*. The position of the most probable failure point with respect to the median of each basic variable is the opportunity to measure the influence of each parameter. A basic variable with high influence will differ much from the median at the most probable failure point, while a parameter with low influence will differ little (or not) from the median value at the most probable failure point;
- *Degree of separation*. The mean value (μ_i) and the standard deviation (σ_i) are estimated from all realizations sampled in the simulation rather than those of user-defined input distributions;
- *Separation of uncertainty method*. A two-loop PFM code architecture for the treatment of the uncertainties allows for separate treatment of the aleatory and epistemic uncertainties;
- *Sample-based uncertainty method*. Based on the anticipated variations and uncertainties, three levels (at least) are considered for each parameter: Low/Baseline/High, where baseline represents the original parameter set, Low numerically smaller, and High numerically higher values – alternatively, the Low/High nomenclature can refer to the expected structural performance or risk.

The ranking of the random variables on the rupture probability are summarized in Table 17. All methods gave consistent ranking for this simple demonstration problem: high sensitivity (initiation time), medium sensitivity (initial flaw width), and low sensitivity (material properties). Although Benchmark 1.1 successfully validated the six (6) sensitivity analysis methods, a number of opportunities for making improvement were also identified. For example, to treat WRS, crack initiation parameters and crack growth parameters as distributed random variables.

The CEI team studied the Benchmark 2 problem with the adjusted PFM models for Alloy 600/82/182 using PRAISE-CANDU 2.1; the description of the various physics-based models is presented in Annex I. Two of these six methods (amplification ratio and separation of uncertainty) were selected to rank the contribution of random variables to the cumulative probability of through-wall flow rate of 1 kg/s.

Eleven (11) random variables were studied; the description of each random variable and its ranking is summarized in Table 18. As expected, the inner diameter WRS value is the most influencing parameter. This also explains why CEI adjusted WRS to match PFM predictions with the DDM results in Fig. 20. The next important influencing parameters are the coefficient of Ramberg-Osgood formula and the zero-crossing of WRS. The least important parameter is the initial crack size, it does not matter whether the assumed mean initial crack depth is 1 mm or 3 mm. In this study, the leak detection capability is assumed as constant of 0.0631 kg/s (or 1 gpm). Additional case studies showed that leak detection limit of 0.095 kg/s (1.5 gpm) has no impact on the ranking. For advanced WCR plants the leak detection limit is less than 1 gpm.

TABLE 17. COMPARISON OF PARAMETER RANKING FOR BENCHMARK 1.1

Method	**Performing Organization**	**High Influence**	**Medium Influence**	**Low Influence**
Amplification ratio	GRS	Initial time	Initial flaw length, fracture toughness	Yield stress, Ultimate stress
Direction Cosine	GRS	Initial time	Initial flaw length	Yield stress, Ultimate stress, Fracture toughness
Degree of Separation	CEI	Initial time	Initial flaw length	Yield stress, Ultimate stress, Fracture toughness
Most probable failure point Analysis	GRS	Initial time	-	Yield stress, Ultimate stress, Fracture toughness, Initial flaw length
Separation of Uncertainty	CEI	Initial time	Initial flaw length	Yield stress, Ultimate stress, Fracture toughness
Sample-Based Uncertainty	LEI	Initial time	Initial flaw length	Yield stress, Ultimate stress, Fracture toughness

TABLE 18. BENCHMARK 2 PARAMETER RANKING

Random Variable	**Statistical Distribution**	**Amplification Ratio Method**	**Separation of Uncertainties**
Initiation Model Parameter B, Heat-to-Heat, see Eq. (I-1) of Annex I	Lognormal	4	6
Initiation Model Parameter B, Within-Heat, see Eq. (I-1) of Annex I	Lognormal	6	4
Growth Model C_g, Heat-to-Heat, see Eq. (I-3) of Annex I	Lognormal	5	3
Growth Model C_g, Within-Heat see Eq. (I-3) of Annex I	Lognormal	7	7
Initial Crack Depth	Normal	8	8
Initial Crack Length	Normal	9	9
Flow Strength	Normal	10	2 (no separation of these 3 variables)
Yield Strength	Normal	11	
Ramberg-Osgood Coefficient D see Eq. (I-14) of Annex I	Normal	2	
Inner Diameter WRS, see Fig. I–4 of Annex I	Normal	1	1
WRS Zero-Crossing see Fig. I–4 of Annex I	Normal	3	5

Each random variable in Table 19 is assumed to be independent. However, some models involve with two or three related parameters such as the within-heat and heat-to-heat variability. Table 20 presents the ranking of PFM models. Both sensitivity analysis methods result in the same ranking.

TABLE 19. BENCHMARK 2 MODEL RANKING

PFM Model	Random Variables	Ranking by Amplification Ratio Method	Ranking by Separation of Uncertainties
WRS Model see Eq. (I-12) of Annex I	Inner diameter WRS and zero-crossing	1	1
Material Properties see Eq. (I-14) of Annex I	Flow strength, yield strength and Ramberg-Osgood coefficient D	2	2
Growth Model see Eq. (I-3) of Annex I	Heat-to-Heat and Within-Heat parameter Cg	3	3
Initiation Model see Eq. (I-1) of Annex I	Heat-to-Heat and Within-Heat parameter B	4	4

5. CONCLUSIONS

5.1 MAIN INSIGHTS FROM THE BENCHMARKS

The CRP benchmark was performed during 18 months period with participants from seven Member States' institutions. It involved the application of different methodologies to a common set of problems. A first benchmark was for three different WCR primary piping system evaluation boundaries for which there are well-documented OPEX histories. A second benchmark was concerned with a single advanced WCR primary piping system evaluation boundary for which no known material degradation has been recorded as of yet.

5.1.1 Insights concerning methods selection

Three different methodologies were applied by the benchmark participants. Two different implementations of the data-driven methodology were used. Four teams used four different PFM computer codes. One of these teams applied a new computer code developed especially for the benchmark. One team used a physics-of-failure methodology. The main conclusions were:

- All implementations required extensive input data preparation, and some form of computer code implementation to facilitate the quantification processes, including the uncertainty analyses;
- Implementations of the three methods tended to be computationally intense necessitating pre-planning of the computations and the post-processing of results;
- Regardless of the selected methodology, a successful implementation depended on the experiences that had been obtained by the analysts from previously performed practical applications;
- The value and importance of OPEX data could not be understated. All methods benefited from and required information on material performance and pipe failures.

5.1.2 Insights from inter- and intra-comparisons

The first phase of the benchmark demonstrated the shortcomings of applying an overly simplistic data-driven methodology. As one example, in this methodology the model of the conditional failure probability did not account for different material degradation mechanisms, nor did it account for any relevant OPEX data.

PFM suffers from the tail sensitivity problem, which means that the computed probabilistic failure metrics are sensitive to very uncertain input parameters. This was clearly demonstrated in the benchmark. When comparing the DDM and PFM results, it became obvious that it is not a foregone conclusion that the DDM can be applied to any problem especially defined to be solved on a fracture mechanics premise, or vice versa. In other words, the objectives of an analysis are conditioned on the context of an analysis; i.e., whether an analysis is risk-informed and is an input to a PSA task, or a fitness for service analysis context.

The second benchmark on the prediction of probabilistic failure metrics for an evaluation boundary within an advanced WCR primary pressure boundary highlighted most of the anticipated obstacles. The lack of operational experience necessitated the interpretation and analysis of laboratory test data. A crucial point for the mechanistic approaches was the compilation of relevant references with respect to crack initiation and crack growth rates in Alloys 690/52/152. This demonstrated that the value of using a collaborative approach to the up-front information gathering concerning corrosion resistance of these materials.

An important aspect of the benchmark was the comparative analysis of respective contribution. One objective was to check the consistency of model assumptions, and especially of the uncertainties in the model assumptions. This analysis stressed the importance of a multi-disciplinary approach to benchmark definitions and input data preparation. Mechanistic models can be key to the transfer of operational experience from WCRs to other reactor concepts, such as an advanced WCR. The level of mechanistic modelling to represent the relevant phenomenology can, in principle, vary from micro-mechanical (or beyond) to empirical relations, but the approaches clearly showed that the notion of cracks (i.e. crack initiation and crack growth) is an adequate starting point. A computational approach is expected to be consistent with the available knowledgebase about material degradation and piping system performance.

5.1.3 Insights concerning advanced Water Cooled Reactor applications

In the area of advanced WCR piping reliability analysis there are two different potential analytical challenges facing an analyst: 1) an analysis boundary consisting of a material or combinations of materials for which extensive OPEX exists including experience with different types of RIM strategies, and 2) an analysis boundary for which there is no known failure history.

The first of these challenges can be addressed using any of the three methodologies and given that these methods explicitly account for the effect of a RIM strategy that has been approved for advanced WCR use. As demonstrated by the CRP benchmark, the second challenge can also be addressed using any of the different methodologies. The effort needed to develop necessary input parameters is significant, however. The integrated modeling of the many uncertain input parameters requires a carefully crafted implementation of the uncertainty analysis. The five teams that responded to the advanced WCR analytical challenge applied a common philosophy to how to handle the knowledge gaps concerning

material degradation of Alloys 690/52/152. While the DDM and I-PPoF approaches produced quantitative results that were largely consistent, the PFM teams produced results spanning many orders of magnitude.

5.2 CONCLUDING REMARKS

The nine (9) orders scatter in the PFM results of Benchmark 2 demonstrates that there is a strong need to develop the documentation guidelines to ensure that the information and data are scrutable, i.e. that the assumptions, input/output data, models selected, etc. are clearly stated. In a formal submission of an analysis, the following items are the considerations for a sound probabilistic assessment:

- All credible degradation mechanisms are to be identified;
- The supporting technical and QA documents for the PFM code is expected to be available for the regulatory authority for examination. It is important that new information or better modelling assumptions are continuously incorporated into the PFM code and the associated software so that the generated results may reflect the best current knowledge;
- All sources of uncertainties are expected to be specified. The assigned statistical distribution of each basic random variable is to be justified and documented. Use of interpolation, extrapolation and truncation and curve fitting to be discussed;
- Each model to be described in sufficient detail to allow an independent review. Model uncertainties/bias to be documented;
- Sensitivity studies to be performed to rank important parameters;
- Uncertainties of the calculated results to be discussed with respect to the conservative treatment of inputs and models; and
- Temporal (for time dependent problems), spatial (flaw initiation at different segments of the cross section) and computational (for sampling algorithm) convergence studies to be performed.

Piping reliability analysis is a relatively complex undertaking, involving multiple disciplines and requiring intensive input data preparation including engineering analyses, and some level of engineering judgment. Taking PFM as an example, a qualified user is assumed to possess the following qualifications:

- Proper training to know the capabilities and limitations of the PFM code;
- Good knowledge on fracture mechanics, piping design and analysis, life cycle management (inspection included), material science (degradation mechanisms and the associated important parameters), and statistics; and
- Familiarity with the national regulatory requirements; more specifically how the PFM results are used in a risk-informed decision making process.

REFERENCES

[1] GROVE, E.J., Travis, R.J., "Effect of Aging on PWR Chemical and Volume Control System", NUREG/CR-5954, US Nuclear Regulatory Commission, Washington, DC, 1995.

[2] HIRSCHBERG, T., Operating Experience Regarding Thermal Fatigue of Unisolable Piping Connected to the PWR Reactor Coolant Systems (MRP-25), 1001006, Electric Power Research Institute, Palo Alto, CA, 2000.

[3] KAMAYA, M., "Assessment of Thermal Fatigue Damage Caused by Local Fluid Temperature Fluctuations. Part I: Characteristics of Constraint and Stress Caused by Thermal Striation and Stratification," Nuclear Engineering and Design, 268:121-138, 2014.

[4] ZHAO, L., XUE, H., YANG, F., SUO, Y, "Numerical Investigation on Stress Corrosion Cracking Behavior of Dissimilar Weld Joints in Pressurized Water Reactor Plants," Frattura ed Integrità Strutturale, **Vol.** 8, No. 29, pp. 410-418, 2014.

[5] SOUTHERN NUCLEAR COMPANY, Vogtle Unit 3 and 4 Updated Safety Analysis Report, Chapter 5, Reactor Coolant System and Connected Systems, Rev. 7, Birmingham, AL, 2018.

[6] GERSINSKA, G., GREBNER, H., SIEVERS, J., WEIL, L., "Estimation of Leak and Break Frequencies for Probabilistic Safety Assessment of Piping Systems," Paper 2529, Proc. 20th Int. Conf. Structural Mechanics in Reactor Technology (SMiRT 20), Espoo, Finland, 2009.

[7] BERG, H.-P., GERSINSKA, G., SIEVERS, J., "Procedure for Probabilistic Safety Assessment of Leaks and Breaks of Piping Systems," Int. Journal of Pressure Vessels and Piping, 87:94-99, 2010.

[8] THOMAS, R.M., "Pipe and Vessel Failure Probability," Reliability Engineering, 2:82-124, 1981.

[9] HECKMANN, K., SIEVERS, J., "Code Development for Piping Integrity Assessment with Respect to New German Safety Standard," Paper 148, Transactions SMiRT-23, Manchester, United Kingdom, 2015.

[10] HECKMANN, K., SIEVERS, J., "Integrity Assessment of Piping with the PROST Code," Proc. EHPG 2017 – The 40th Enlarged Halden Program Group Meeting, Lillehammer, Norway, September 2017

[11] BERGMAN, M., BRICKSTAD, B., NILSSON, F., A procedure for Estimation of Pipe Break Probabilities due to Intergranular SCC, SAQ/FoU-Report 97/06, SAQ Kontroll AB, Stockholm, Sweden, 1997.

[12] ALZBUTAS, R., "Approaches of Risk Measures Minimization and Application to Inspection," Proc. 13th Int. Conf. on Probabilistic Safety Assessment and Management (PSAM 13), Seoul, Korea (Republic of), 2016.

[13] DUNDULIS, G., ALZBUTAS, R., "Pipe Rupture and Inspection Sensitivity Analysis," Proc. 52th ESReDA Seminar, Kaunas, Lithuania, 2017.

[14] DUAN, X., WANG, M., KOZLUK, M.J., "Benchmarking PRAISE-CANDU 1.0 with Nuclear Risk Based Inspection Methodology Project Fatigue Cases," PVT-13-1217, Journal of Pressure Vessel Technology, **Vol**. 137, No. 2, 2015

[15] WANG, M., DUAN, X., KOZLUK, M.J., "Benchmarking PRAISE-CANDU 1.0 with xLPR 1.0," Paper Number: PVP2013-98010, Proc. PVP2013, American Society of Mechanical Engineers, New York, NY, 2013.

[16] SOMASUNDARAM, D., WANG, M., HUANG, Y., DUAN, X., "Probabilistic Fracture Mechanics Code – PRAISE-CANDU2.1", Proceedings of the 40th Annual Conference of the Canadian Nuclear Society and 45th Annual CNS/CNA Student Conference Virtual Conference, June 6 – June 9, 2021.

[17] HECKMANN, K., ALZBUTAS, R., WANG, M., JEVREMOVIC, T., Lydell, B.O.Y., SIEVERS, J., DUAN, X., “Comparison of Sensitivity Measures in Probabilistic Fracture Mechanics”, International Journal of Pressure Vessels and Piping, **Vol.** 192, 2021 104388.

[18] FLEMING, K., LYDELL, B., “Database Development and Uncertainty Treatment for Estimating Pipe Failure Rates and Rupture Frequencies,” Reliability Engineering and System Safety, **86**:227-246, 2004.

[19] LYDELL, B., “The Probability of Pipe Failure on the Basis of Operating Experience,” PVP-26281, Proc. ASME Pressure Vessel & Piping Division Conference, American Society of Mechanical Engineers, New York, NY, 2007.

[20] FLEMING, K., LYDELL, B., “Insights into Location Dependent Loss-of-Coolant-Accident (LOCA) Frequency Assessment for GSI-191 Risk-Informed Applications,” Nuclear Engineering and Design, **305**:433-450, 2016.

[21] CHENG, W.-C., DING, C., O’SHEA, N., SAKURAHARA, T., SCHUMOCK, G., MOHAGHEGH, Z., REIHANI, S., KEE, E., "Global Sensitivity Analysis to Rank Parameters of Stress Corrosion Cracking in the Spatio-Temporal Probabilistic Model of Loss of Coolant Accident Frequencies," Proc. 2017 International Topical Meeting on Probabilistic Safety Assessment and Analysis (PSA2017), American Nuclear Society, LaGrange Park, IL, 2017.

[22] SAKURAHARA, T., O'SHEA, N., CHENG, W.-C., ZHANG, S., REIHANI, S., KEE, E., and MOHAGHEGH, Z., Integrating Renewal Process Modeling with Probabilistic Physics-Of-Failure: Application to Loss of Coolant Accident (LOCA) Frequency Estimations in Nuclear Power Plants, Reliability Engineering & System Safety, **Vol**. 190 (October), 2019.

[23] HICKLING, J., Resistance of Alloys 690, 52 and 152 to Primary Water Stress Corrosion Cracking (MRP-237, Rev. 1): Summary of Findings from Completed and Ongoing Test Programs Since 2004, 1018130, Electric Power Research Institute, Palo Alto, CA, 2008.

[24] AKASHI, M., OHTOMO, A., “Evaluation of the Factor of Improvement for the Intergranular Stress Corrosion Cracking Life of Sensitized Stainless Alloys in High-Temperature, High-Purity Water Environment,” J. Society of Materials Science, Japan, **Vol.** 40, Issue 400, pp 59-64, 1987.

[25] EPRI, Recommended Factors of Improvement for Evaluating Primary Water Stress Corrosion Cracking Growth Rates of Thick- Wall Alloy 690 Materials and Alloy 52, 152, and Variants Welds (MRP 386), 3002010756, 2017.

[26] ERICKSON, M. et al, Models and Inputs Developed for Use in the xLPR Pilot Study, 1022528, Electric Power Research Institute, Palo Alto, CA, 2011.

[27] EPRI, “Review of Stress Corrosion Cracking of Alloys 182 and 82 in PWR Primary Water Service (MRP-220)”, 1015427, 2007 October.

[28] ONR, Safety Assessment Principles for Nuclear Facilities, 2014 Edition Revision 0.

ANNEX I
METHODOLOGY AND IMPLEMENTATION OF COMPUTER CODE (CEI)

I−1. INTRODUCTION TO PRAISE-CANDU PFM CODE

Piping Reliability Analysis Including Seismic Events for CANDU reactors (PRAISE-CANDU), is a Monte Carlo based PFM software that was developed in 2013 and compliant with the Canadian Standard CSA N286.7-99 "Quality Assurance of Analytical, Scientific and Design Computer Programs for Nuclear Power Plants." The software has the capability to model crack initiation and crack growth due to fatigue and SCC. Version 1.0 solely focused on circumferential crack and has the following features:

- The capability to perform both probabilistic and deterministic analyses;
- Separation of aleatory and epistemic uncertainties;
- Modular construction for ease of future changes;
- Consideration of service bending and tension loads (rather than all tension);
- Time-dependent material properties;
- Inspection model that includes sizing uncertainty and repair;
- Time-dependent wall thinning from inside surface.

PRAISE-CANDU separates the randomness due to inherent randomness (aleatory) and lack of knowledge (epistemic) by implementing two-loop system as shown in Fig. I−1(a). The inner loop is a conventional Monte Carlo simulation using the aleatory random variables that defines one (time-dependent) result, while the epistemic random variables are sampled in outer loop. For each epistemic sampling, a set of aleatory Monte Carlo simulation is performed. Each Monte Carlo simulation follows the deterministic modules as shown in Fig. I−1(b).

I−2. PRAISE-CANDU 2.1

Since the development of the first version in 2013 [I–1], [I–2], significant technical advancements in fracture mechanics has been achieved, especially in crack opening area, crack transitioning and SIF solutions for circumferential cracks. In addition, there is growing importance of considering axial cracks in the bend/elbow for leak-before-break application. Moreover, international benchmark projects have allowed cross-verification of the software and identified areas for improvements. The above led to the development of PRAISE-CANDU 2.1 [I–3], which includes the following features:

- Axial crack with crack transitioning;
- Crack transitioning for circumferential cracks;
- Updated SIF (K) solutions for part-through wall circumferential cracks;
- Updated COD module for circumferential cracks;
- Inergranular SCC crack growth mechanism;
- ASME Code Case N-643-2 fatigue crack growth law.

Following the same programming approach of modular construction, PRAISE-CANDU 2.1 was updated and deployed in Version 4.6 of Microsoft® .NET (C#) Framework. The software has the capability to run in both Windows 7 and Windows 10 and 32 bit and 64 bit platforms.

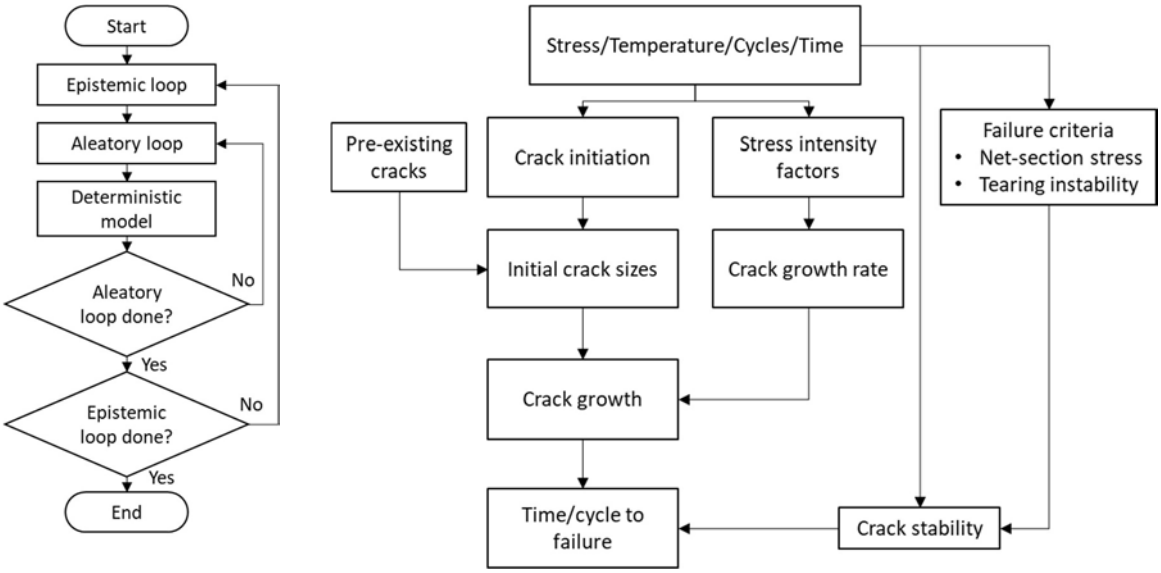

FIG. I–1. Analysis data flow: (a) two loop uncertainty analysis, (b) deterministic models.

I–3. MODULES IN PRAISE-CANDU 2.1

Only the modules related to PWSCC and used in the present benchmark studies are described in this section.

I–3.1. Crack initiation

Two relations for defining the initiation time are implemented in PRAISE-CANDU. The Garud relation [I–4] is used for the benchmark. A crack initiates with a random size, and its subsequent growth is treated by fracture mechanics. The initiation time is defined by the following set of relations:

$$t_I = BGe^{\frac{Q}{T}} ln\left[\frac{D-z}{\left(\frac{\sigma}{\sigma_{ys}}\right)-z}\right] \quad \text{(I–1)}$$

where:

$u = \frac{\sigma_{ult}}{\sigma_{ys}}$

$m = 10\left[\frac{\frac{\sigma_{ys}}{E}}{u(u-1)^3}\right]^{\frac{1}{4}}$

$z = 0.35 + \frac{1}{3}\ln(u)$

$D = 0.67e^{u/2}$

$$G = \frac{ln}{m^{\frac{3}{8}} ln\left(\frac{D-z}{1-z}\right)}$$

Equation (I–1) is the desired end result of initiation time. A threshold stress for crack initiation is built into the above relations. From Eq. (I–1), for the initiation time to be a real number, σ/σ_{ys} is to be greater than z. This leads to the following relation for the threshold stress.

$$\sigma_{th} = \sigma_{ys}\left[0.35 + \frac{1}{3} ln \frac{\sigma_{ult}}{\sigma_{ys}}\right] \quad \text{(I–2)}$$

The yield and ultimate strengths used here are the local ones at the initiation sites, which can differ from the values used in the more global analyses, such as the flow strength used in the critical net section stress criterion. The yield strength for the Garud model can be random variable, which results in a random threshold stress for crack initiation.

Scatter in the initiation time is described by considering B to be a random variable. The distribution of B can be estimated from initiation data or field experience. The distribution of B can change with environment, such as water chemistry. The value of Q, activation energy, is to be taken from measurement. SCC is time dependent, hence it is dominated by the long time spent at steady state (normal operating) load.

I–3.2. Crack growth

The stress corrosion crack growth relation employed in PRAISE-CANDU 2.1 is based on the relation that has been developed for Alloy 600 and related weld materials [I–5]. The basic equation is given with:

$$\frac{da}{dt} = C_g\, exp\left[-Q_g\left(\frac{1}{T} - \frac{1}{T_{ref}}\right)\right](K - K_{th})^{\beta} \times \left\{\frac{1}{P} + \frac{P-1}{P}\exp\left[-\frac{1}{2}\left(\frac{\Delta ECP_{\frac{Ni}{NiO}}}{c_w}\right)^2\right]\right\} \quad \text{(I–3)}$$

with P being the peak-to-valley ratio and c_w the characteristic width and the value of $\Delta ECP_{\frac{Ni}{NiO}}$ is calculated from the following expression

$$\Delta ECP_{\frac{Ni}{NiO}} = 29.58\left(\frac{T+273.15}{298.15}\right) log_{10}\left(\frac{[H_2]}{[H_2]_{\frac{Ni}{NiO}}}\right) \quad \text{(I–4)}$$

where $[H_2]$ is the concentration of the dissolved hydrogen in water (cc/kg at standard condition for temperature and pressure)

$$[H_2]_{\frac{Ni}{NiO}} = 10^{(0.0111T - 2.59)} \quad \text{(I–5)}$$

In Eqs. (I–3) and (I–4) the temperature is given in °C. The above hydrogen specific terms and the constants are specific to Alloy 182.

PRAISE-CANDU 2.1 uses the form of Eq. (I–3) with C_g being a random variable, heat-to-heat and within-heat scatter treated in the Monte Carlo simulation, and the term in { } beyond the multiplication symbol used as a multiplying factor.

I–3.3. Stress intensity factor

In ASME FFS-1 [I–6], for smaller values of R_i/t (<10), K solution coefficients are limited to larger crack depth to half-crack length (a/b) ratios. In PRAISE-CANDU 2.1, the K solution is updated to validated curve fits provided in ASME B&PV Code Appendix A (Article-3532) [I–7]. K solution for through-wall crack is based on Tahakshi's formulation [I–8].

I–3.4. Crack opening displacement

Significant development has been made in the COD solution based both on Finite Element Analysis (FEA) and experiments. For circumferential crack, the xLPR 2.0 COD estimation scheme [I–9] is implemented. This solution is empirically adjusted to account for large deformation theory, crack-tip plasticity and includes bending correction due to axial force. Additionally, the solution is applicable for various R_m/t and also provides COD at inner, mid and outer surface.

I–3.5. Crack transitioning

In PRAISE-CANDU 1.0, once the depth of the part-through wall (Fig. I–2(a)) circumferential crack exceeds 95% of the wall thickness, an idealized through-wall circumferential crack is considered (Fig. I–2(c)), i.e., the crack angle through the wall thickness is treated as constant.

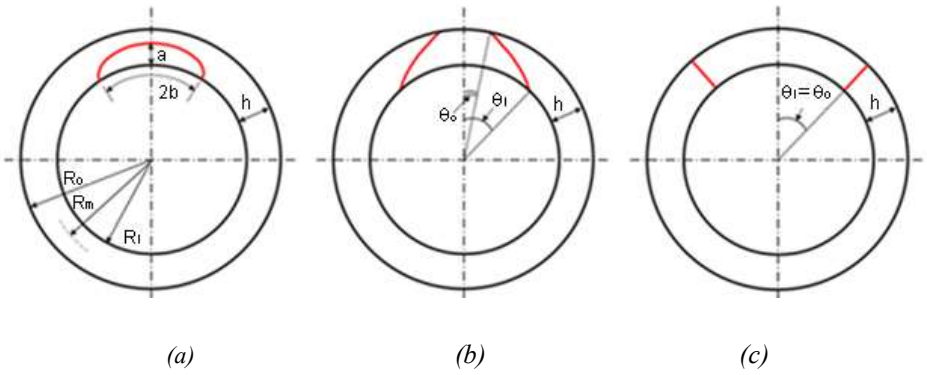

FIG. I–2. Circumferential cracks in cylinder: (a) circumferential PWT crack, (b) crack after transition, the angle at the inner diameter surface is larger than the crack angle at outer diameter surface, (c) idealized through-wall circumferential crack.

The approach of idealized through-wall crack transition does not accurately represent the actual behaviour. Use of idealized crack transitioning might provide less conservative results in terms of leak detection and up to the time instant when natural crack would become idealized. However, when rupture is considered, idealized crack transitioning method might provide more conservative results as the crack growth is faster. To overcome the above limitations, in PRAISE-CANDU 2.1, axial and circumferential crack transitioning models [I–10] are introduced.

$$K_{ID} = K^{Idealized} G_1 \quad \text{(I–6)}$$

$$K_{OD} = K^{Idealized} G_2 \quad \text{(I–7)}$$

$$COD_{ID} = COD_{ID}^{Idealized} H_1 \quad \text{(I–8)}$$

$$COD_{OD} = COD_{OD}^{Idealized} H_2 \quad \text{(I–9)}$$

where:

$K^{Idealized}$ is K solution for idealized circumferential crack

$COD_{ID}^{Idealized}$ is the inner diameter COD solution for idealized circumferential crack

$COD_{OD}^{Idealized}$ is the outer diameter COD solution for idealized circumferential crack

G_1, G_2 are the correction factors for K

H_1, H_2, are the correction factors for COD

I–3.6. Crack instability

PRAISE-CANDU has the capability to calculate instability by net section collapse or J-tearing instability or both. In the CRP benchmark, net section collapse was selected. The stresses considered in the net section stress calculation are from global loading (pressure, deadweight, constrained thermal expansion and seismic if considered). PRAISE-CANDU 2.1 can perform the net section collapse analysis using only the load-controlled stress (such as deadweight, pressure and seismic inertia) plus a user-defined portion of the displacement controlled portion of the normal operating stress. This factor is denoted as k_f, with a value of 0 resulting in only load-controlled portion of the normal operating stress being considered for the stability assessment, and a value of 1, results in all of the normal operating stress being considered for the stability assessment.

I–3.7. In-service inspection

The modeling of inspections in PRAISE-CANDU 2.1 is depicted in Fig. I–3. The inspection procedure consists of detecting, sizing and possible remedial action.

The detection probability as a function of crack size is the initial step. PRAISE-CANDU employs either a tabular input of detection probability as a function of crack depth, a, or one of the two functional forms of Eqs. (I–10) and (I–11):

$$P_D(a) = \frac{1}{2}(1-\varepsilon)\left[1 + erf\left(\nu ln\frac{a}{a^*}\right)\right] \quad \text{(I–10)}$$

where: $erf(x)$ is the error function, ε is the probability of not detecting a crack no matter how deep it is, a^* is the depth having an approximately 50% chance of being detected, and ν controls how rapidly the detection probability transitions from ε to 1.

As an alternative to the lognormal form of Eq. (I–10), the logistical form of Eq. (I–11) can be employed

$$P_D\left(\frac{a}{h}\right) = \frac{exp\left[\beta_1 + \beta_2 \frac{a}{h}\right]}{1 + exp\left[\beta_1 + \beta_2 \frac{a}{h}\right]} \quad \text{(I–11)}$$

The capability of defining non-detection probability, P_{ND} by a tabular input provides great flexibility and circumvents the need for a functional form such as Eq. (I–10) or Eq. (I–11). However, it is not apparent how uncertainty in P_{ND} (such as due to lack of data) can be expressed in a convenient tabular form. Hence, Eq. (I–10), with random ε, ν and a^* or Eq. (I–11) with random β_1 and β_2 to specify (epistemic) uncertainty in the detection probability is also included.

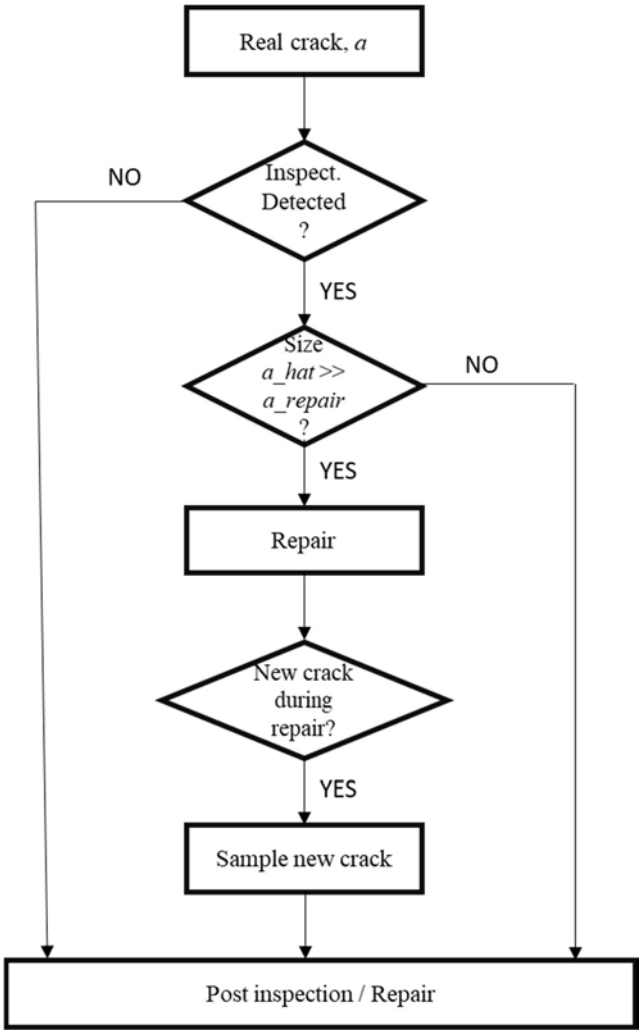

FIG. I–3. Inspection detection, sizing and repair in PRAISE-CANDU.

In a given Monte Carlo trial at a given time step, there is a crack of depth a. If an inspection is performed at this time step, a unit uniform random number, u, is sampled. If $P_{ND}(a)$ is less than u, the crack is considered to have been detected. The next step is then the sizing of the indication.

I–3.8. Leak detection

Leaks rates through cracks are not computed in PRAISE-CANDU 2.1. All leak-rate detection inputs are in terms of crack opening area. For instance, the area of a crack that will leak at the detectable rate is input to PRAISE-CANDU 2.1 as a detectable crack opening area. Similarly, the break sizes that are computed during a PRAISE-CANDU 2.1 run are specified in terms of a crack opening area. Crack opening areas are evaluated for normal operating conditions (loads).

I–3.9. Residual stress

Various distributions (spatial and statistical) of residual stresses can be defined for a PRAISE-CANDU 2.1 analysis. The most commonly used is a third order polynomial, as follows:

$$\sigma_{WRS}(\xi) = s_0 + s_1\xi + s_2\xi^2 + s_3\xi^3 \quad \text{(I–12)}$$

where $\xi = \frac{x}{h}$, x being the distance from the inner pipe wall. Figure I–4 depicts such a distribution.

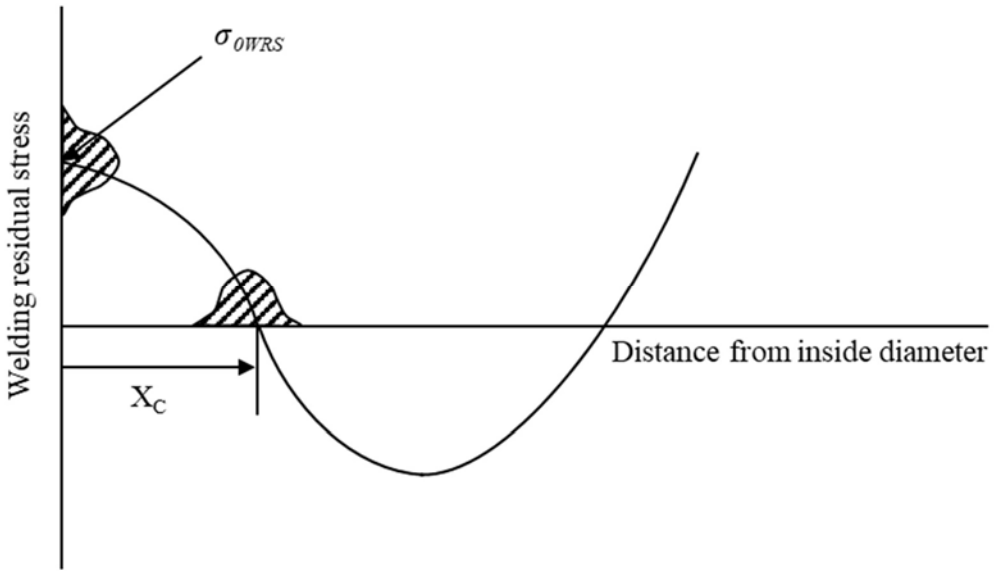

FIG.I–4. Through thickness residual stress distribution [I–11].

The randomness is described by three random variables:

- Residual stress at the inner surface ($\sigma_{0WRS} = s_0$);
- Location of zero crossing (X_c or ξ_c);
- Ratio of outer wall stress to inner wall stress.

These three random variables are sampled from their respective (normal) distributions, the parameters of which are user defined. These three values, along with the requirement of self equilibrium through the thickness, provide the four pieces of information required to solve for the four coefficients in Eq. (I–12).

I–3.10. Ramberg-Osgood relationship

Equation (I–13) shows generic form of Ramberg-Osgood stress-strain relation and Eq. (I–14) shows the form of Ramberg-Osgood stress-strain relation adopted for PRAISE-CANDU 2.1.

$$\frac{\varepsilon}{\varepsilon_0} = \frac{\sigma}{\sigma_0} + \alpha\left(\frac{\sigma}{\sigma_0}\right)^n \quad \text{(I–13)}$$

$$\varepsilon = \varepsilon^e + \varepsilon^p = \frac{\sigma}{E} + \left(\frac{\sigma}{D}\right)^n \quad \text{(I–14)}$$

where:

ε_0 and $\sigma_0$are reference strain and reference stress, respectively.

ε^e and ε^p are the elastic and plastic components of the strain, respectively.

E is the elastic modulus, $E = \sigma_o/\varepsilon_o$.

α, D and n are constants in Ramberg-Osgood stress-strain relation, $D^n = \sigma_o^n/\alpha\ \varepsilon_o$.

I–4. CEI DATA-DRIVEN METHODOLOGY

CEI participated both in Benchmark 1.1 and Benchmark 2 DDM exercise. A Monte Carlo simulation was used to evaluate pipe failure rate of leak and rupture.

I–4.1. Benchmark 1.1

I–4.1.1. Methodology

The failure rate of leak (λ_L) is calculated using:

$$\lambda_L = \frac{n}{f.N.T} \quad \text{(I–15)}$$

where:

λ_L: failure of leak
n: number of past leak events
N: number of leak-relevant positions
T: operational time
f: the fraction of the component exposure (=1)

The failure rate of rupture (λ_R) is calculated from the failure rate of leak obtained from Eq. (I–15) and the conditional probability of rupture:

$$\lambda_R = \rho_{L|R} \times \lambda_L \quad \text{(I–16)}$$

where:
λ_R: failure rate of rupture
$\rho_{L|R}$: conditional probability of rupture on leak

The parameters n/T, N and $\rho_{L|R}$ in Eqs. (I–15) and (I–16) are considered as random variables following specific distribution functions described in Table I–1.

Figure I–5 shows the histograms of one million random samples for each parameter in Monte Carlo simulation.

TABLE I–1. PROBABILITY DISTRIBUTIONS FOR RANDOM VARIABLES

Variable	Distribution Type	Parameters of the Distribution
n/T	Log-Normal	-4.95, 0.833
N	Log-Normal	3.65, 0.472
$\rho_{R\|L}$	Beta	5.5, 95.5

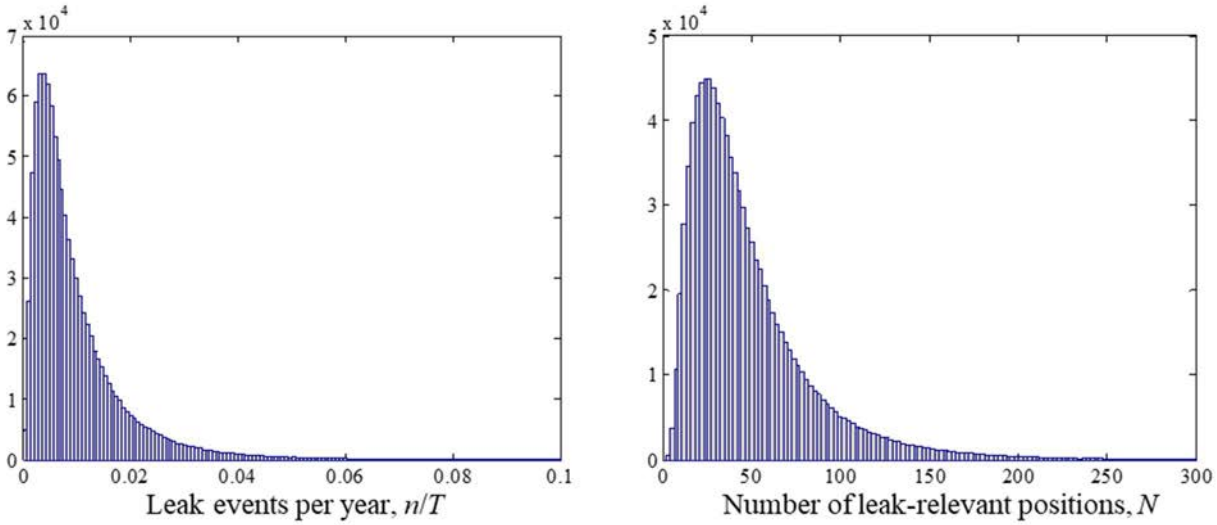

(a) *(b)*

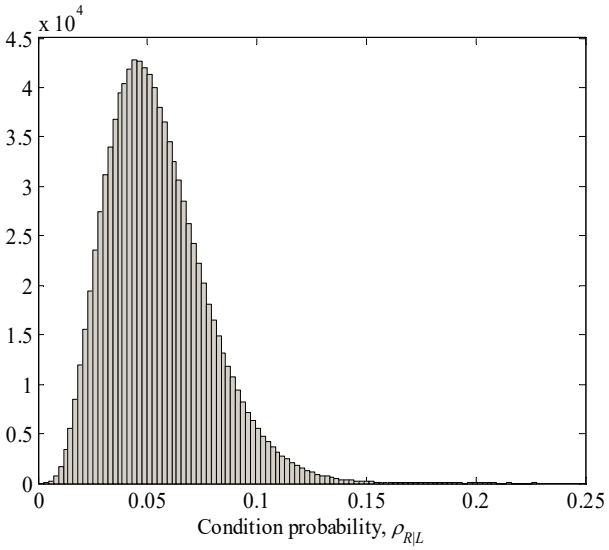

(c)

FIG.I–5. Histograms of random samples.

I–4.1.2. Evaluation

Figure I–6 presents the empirical distribution of leak frequency and rupture frequency.

The mean value, 5th, 50th and 95th percentiles are listed in Table I–2.

TABLE I–2. FAILURE RATE ESTIMATIONS FOR LEAK AND RUPTURE

Parameter	Failure Rate of Leak, λ_L	Failure Rate of Rupture, λ_R
Mean	3.30×10^{-4}	1.80×10^{-5}
5th percentile	3.12×10^{-5}	1.34×10^{-6}
50th percentile	1.84×10^{-4}	9.22×10^{-6}
95th percentile	1.09×10^{-3}	6.17×10^{-5}

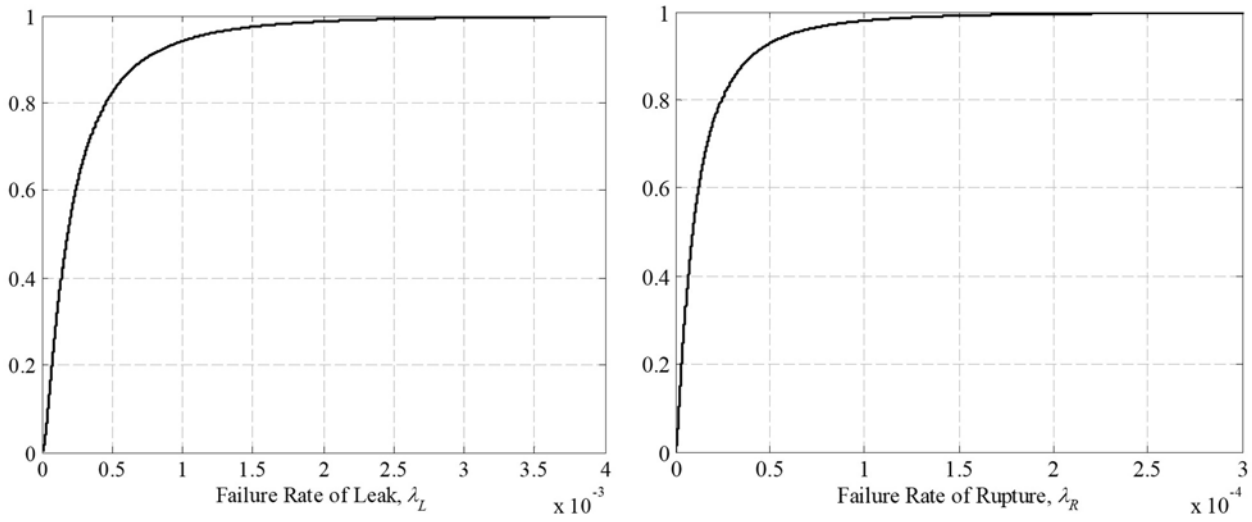

FIG.I–6. Empirical distributions.

I–4.2. Benchmark 2

I–4.2.1. Methodology

The failure rate of rupture (λ_R) of Alloy 690 DMW is calculated from that of Alloy 600 with an improvement factor (*IF*) as given in:

$$\lambda_R = IF \times \rho_{L|R} \times \lambda_L \tag{I–17}$$

When Eq. (I–17) is used to estimate failure rate of Alloy 600, *IF* equals to one. Note that $\rho_{L|R}$ and λ_L are treated as random variables and their distributions are updated using Bayes' theorem based on the recent OPEX of Alloy 600. The Bayesian updating of distribution parameter θ is given as follows:

$$f(\theta|x) \propto L(x|\theta) \times f(\theta) \tag{I–18}$$

where:
x: observation of random variable X
θ: vector of distribution parameters of X
$f(\theta|x)$: posterior joint distribution of θ given the observation of x
$L(x|\theta)$: likelihood of observation x given the distribution parameter θ
$f(\theta)$: prior joint distribution of θ.

For computational continence, conjugate prior distributions are usually selected for Bayesian updating, i.e., the posterior distribution and prior distribution are in the same family. In piping reliability analysis, if the failure events follow a Poisson distribution with failure rate λ, a Gamma (α′, β′) prior on λ is a conjugate prior. The posterior distribution of λ is also a Gamma distribution with parameters (α″, β″):

$$\alpha'' = \alpha' + \text{new failure evidences} \tag{I–19}$$

$$\beta'' = \beta' + \text{new exposure time} \tag{I–20}$$

Since a Beta distribution takes on values between 0 and 1, it is convenient to express the prior uncertainty distribution of the conditional failure probability in a Beta distribution with two parameters a' and b'. When the relevant OPEX are "failures" or "successes" data, the selected Bete distribution is also a conjugate prior, therefore the posterior distribution of ρ is also a Beta distribution with the following parameters:

$$a'' = a' + \text{new failure} \tag{I–21}$$

$$b'' = b' + \text{new success} \tag{I–22}$$

Once that $\rho_{L|R}$ and λ_L in Eq. (I–17) are updated using OPEX, Monte Carlo simulation is employed to evaluate the failure rate λ_R of Alloy 690.

I–4.2.2. Evaluation

The report NUREG-1829 [I–12] developed a generic PWR piping and non-piping passive system LOCA frequency estimates as a function of break size and operating time using an expert elicitation process. The results relevant to PWSCC are used to develop the prior distributions of $\rho_{L|R}$ and λ_L. Assuming λ_L follows a Gamma prior distribution with a mean value of 6×10^{-3} per year and shape parameter α′ of 0.5, the rate parameter β′ is calculated to be 83.3. Based on the OPEX that 10 cracks with depth greater than 10%tw were observed in the past 27,315 reactor years, the parameters of the posterior distribution were updated to be α″=10.5 and β″=27398. The prior and posterior distributions of λ_L are shown Fig. I–7. Assuming $\rho_{R|L}$ follows a Beta prior distribution and the 5th, 50th and 95th percentiles are 10^{-6}, 5×10^{-5} and 10^{-3}, the parameters of the prior distribution are estimated to be a' = 0.278 and b' = 1281 using the three-point estimate approximations [I–13]. Since no rupture observed from the 10 cracks occurred in the past OPEX, the parameters of the posterior distribution were updated to be a″=0.278 and β″=1291. The prior and posterior distributions of λ_L are shown in Fig. I–7. Since the OPEX is relatively small, the prior and posterior distributions of $\rho_{R|L}$ are almost identical. The improvement factor *IF* of Alloy 690 in Eq. (I–17) is assumed to be lognormally distributed with a

median value of 100 and 5th percentile of 10. The lower and upper limits of *IF* are 5 and 1000, respectively. Monte Carlo simulation with one million random samples was performed to evaluate the failure rate of rupture (λ_R) of Alloy 690 and Alloy 600. The results are summarized on Table I–3 and the mean failure rates are shown in Fig. I–8.

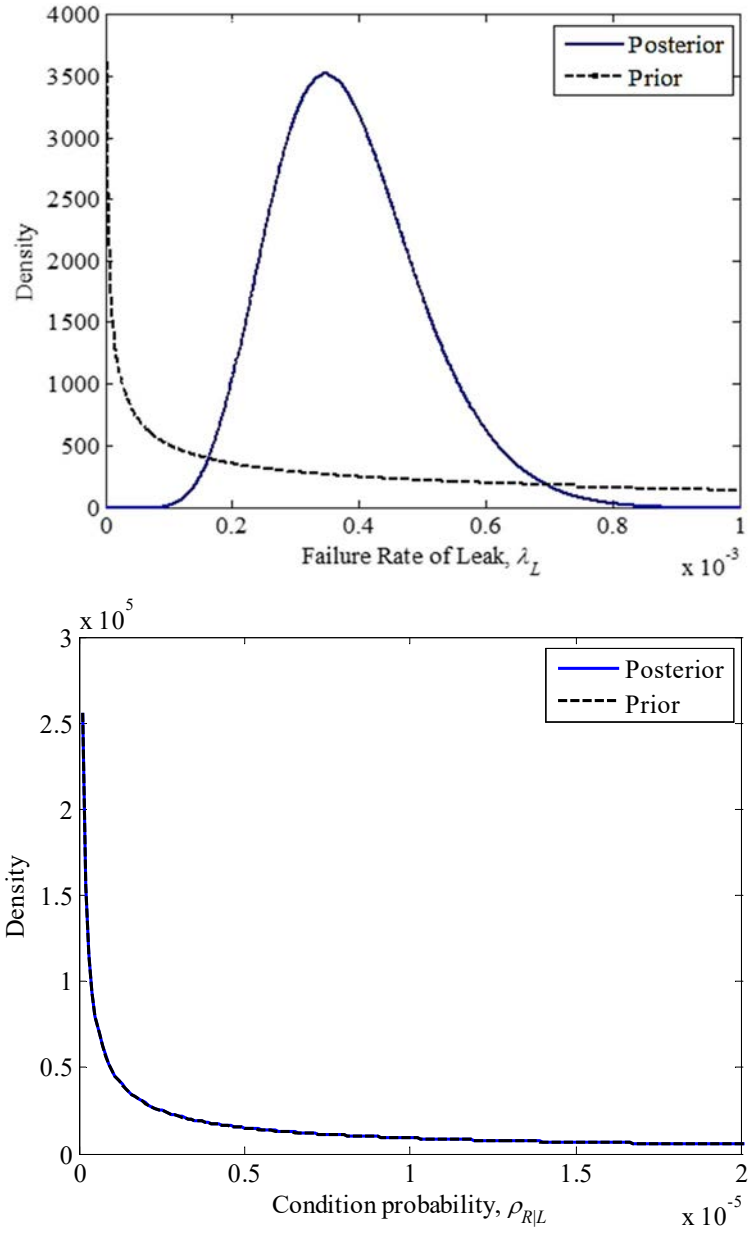

FIG. I–7. Prior and posterior distributions of λ_L and $\rho_{L|R}$.

TABLE I–3. FAILURE RATE ESTIMATIONS FOR ALLOY 600 AND ALLOY 690

Parameter	**Alloy 600**		**Alloy 690**	
	Leak	Rupture	Leak	Rupture
Mean	3.83×10^{-4}	8.20×10^{-8}	8.41×10^{-6}	1.80×10^{-9}
5th percentile	2.11×10^{-4}	3.98×10^{-12}	5.62×10^{-7}	3.59×10^{-14}
50th percentile	3.71×10^{-4}	1.65×10^{-8}	3.89×10^{-6}	1.58×10^{-10}
95th percentile	5.96×10^{-4}	3.86×10^{-7}	3.29×10^{-5}	8.21×10^{-9}

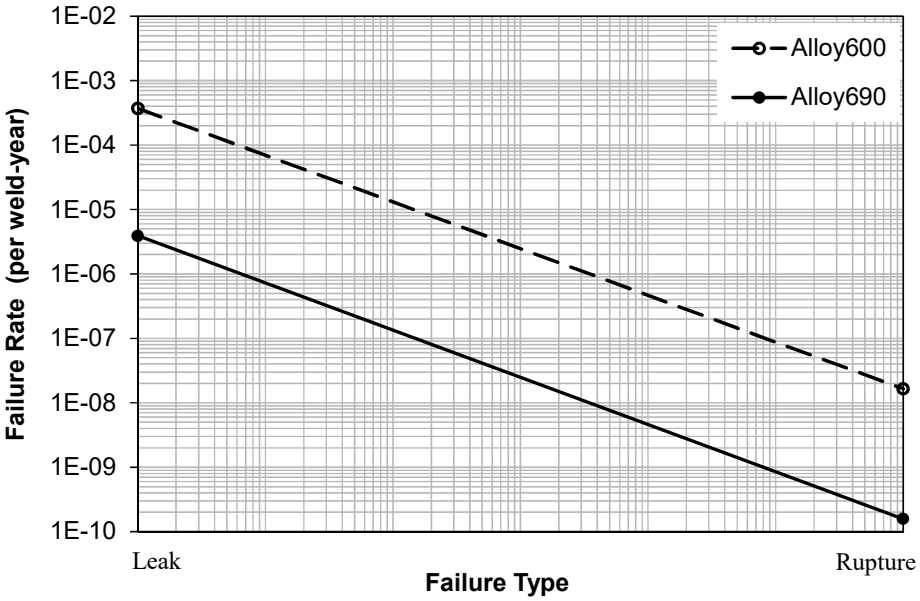

FIG.I–8. Failure rates of Alloy 600 and Alloy 690.

REFERENCES TO ANNEX I

[I–1] DUAN, X., WANG, M., KOZLUK, M.J., "Benchmarking PRAISE-CANDU 1.0 with Nuclear Risk Based Inspection Methodology Project Fatigue Cases," PVT-13-1217, Journal of Pressure Vessel Technology, **Vol.** 137, No. 2, 2015

[I–2] WANG, M., DUAN, X., KOZLUK, M.J., "Benchmarking PRAISE-CANDU 1.0 with xLPR 1.0," Paper Number: PVP2013-98010, Proc. PVP2013, American Society of Mechanical Engineers, New York, NY, 2013.

[I–3] SOMASUNDARAM, D., WANG, M., HUANG, Y., DUAN, X., "Probabilistic Fracture Mechanics Code – PRAISE-CANDU2.1", Proceedings of the 40th Annual Conference of the Canadian Nuclear Society and 45th Annual CNS/CNA Student Conference Virtual Conference, June 6 – June 9, 2021.

[I–4] GARUD, Y.S., "SCC Initiation Model and its Implementation for Probabilistic Assessment", Proceedings of the ASME 2010 Pressure Vessels and Piping Division, Paper PVP2010-25468, Bellevue, Washington, July 18-22, 2010.

[I–5] WHITE, G.A., HICKLING, J., MATHEWS, L.K., "Crack Growth Rates for Evaluating PWSCC of Thick-Wall Alloy 600 Material", Proceedings of the 11th International Conference on Environmental Degradation of Materials in Nuclear Systems, Stevenson, WA, Aug 2003, pp 166-179.

[I–6] AMERICAN SOCIETY OF MECHANICAL ENGINEERS, "Fitness-For-Service", ASME FFS-1, Second Edition, 2016 June.

[I–7] AMERICAN SOCIETY OF MECHANICAL ENGINEERS, "ASME Boiler and Pressure Vessel Code Section XI Rules for Inservice Inspection of Nuclear Power Plant Components", 2017 Edition, July 1, 2017.

[I–8] TAKAHASHI, Y., "Evaluation of Leak-Before-Break Assessment Methodology for Pipes with a Circumferential Through-wall Crack. Part I: Stress Intensity Factor and Limit Load Solutions", International Journal of Pressure Vessels and Piping, **Vol**. 79, 2002, pp. 385-392.

[I–9] YOUNG, B.A., OLSON, R.J., KERR, M., “Advances in COD Equations: Circumferential Through-Wall Cracks”, Proceedings of the ASME 2012 Pressure Vessels and Piping Conference (PVP2012), Paper No. PVP2012-78181, Toronto, Canada, July 15-19, 2012.

[I–10] SHIM, D.J., KURTH, R., RUDLAND, D., “Development of Non-Idealized Surface to Through-Wall Crack Transition Model”, Proceedings of ASME 2013 Pressure Vessels and Piping Conference (PVP2013), Paper No. PVP2013-97092, Paris, France, 2013 July 14–18, 2013.

[I–11] RUDLAN D.L., Harington, C., “xLPR Version 1.0 Report: Technical Basis and Pilot Study Problem”, ADAMS Access Number ML110660292, US Nuclear Regulatory Commission, Washington, DC, 2011.

[I–12] TREGONING, R., ABRAMSON, L., SCOTT, P., “Estimating Loss-of-Coolant Accident (LOCA) Frequencies through the Elicitation Process”, NUREG-1829, US Nuclear Regulatory Commission, Washington, DC, 2008.

[I–13] LYDELL, B., “A Review of the Progress with Statistical Models of Passive Component Reliability,” Nuclear Engineering and Technology, 49:349-359, 2017.

ANNEX II
METHODOLOGY AND IMPLEMENTATION OF COMPUTER CODE (GRS)

II−1. INTRODUCTION TO PROST

The computer software PROST (PRObabilistic STructure mechanics) is a mainly fracture mechanics assessment tool for integrity analysis of pipes and vessels. It is capable to perform deterministic fracture mechanical assessments as well as probabilistic fracture mechanical (PFM) computations by combining several deterministic simulations. For quality assurance in the software development process, the IAEA SSG-2 [II−1] together with the standards ISO-9001 [II–2] and ISO-27001 [II–3] are applied. Recent publications with an overview over PROST features are e.g. [II–4] and [II–5].

II−2. STRUCTURES, LOADS, AND DEFECTS

PROST is mainly designed for cylindrical pipes with defects. The standard internal crack geometries for straight pipes (or cylindrical vessel shells) are shown in Fig. II−1. Additional geometries involve cylindrical welds and massive round bars.

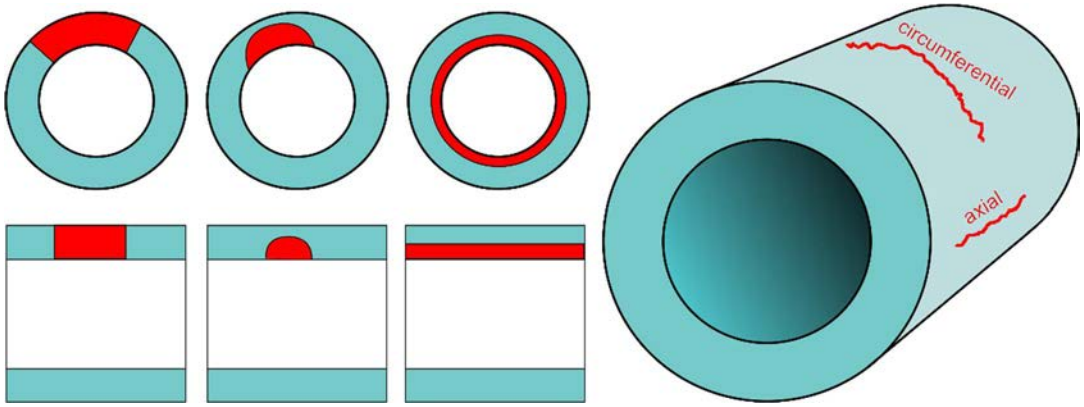

FIG. II–1. Crack configurations cylindrical structures.

PROST implements SIF solutions and limit load formulations for these crack configurations from various compendia. In most cases, more than one formulation per geometry is implemented, which allows a comparison of different approaches. Beside these analytical formulations, it is also possible to provide FEA-computed SIF as an input in PROST. Several types of loads can be defined and combined to simple or complex load-time functions. Beside interior pressure, tensile forces, and bending moments, it is possible to provide radial variating WRS, thermal gradients and in some cases also azimuthal or longitudinal stress variations. These load types can be combined in chronological series to simulate operational states, transients or singular events.

II−3. DAMAGE MECHANISMS

PROST considers two categories of damage mechanisms: Crack initiation mechanisms and crack growth mechanisms. The crack initiation models the transition from an intact component to a cracked

one, for which a fracture mechanical approach is required. An initiation model for corrosive damage is based on an initiation time, while models for fatigue damage are based on SN-curves and different damage accumulation hypotheses. Both models have in common that a damage parameter D evolves over the time.

$$\frac{dD}{dt} = F_D \tag{II–1}$$

A crack is formed when D reaches a critical value D_{crit}. F_D depends on the actual model; it is a constant for the initiation time approach, and a function dependent on the stress amplitudes and cycle frequency for the fatigue damage model.

Crack growth is considered by PROST due to SCC, fatigue crack growth, and ductile tearing. Combinations of different crack growth damage mechanisms are, in principle, possible. The crack growth is described by the change in the crack size parameters, such as crack depth or crack length (short−hand notation a is used as a crack size parameter in the following, but the statements generalize to vectors).

The evolution of the SCC crack growth rate is governed by a differential equation as a function of time, which depends on the SIF K at the given crack growth direction.

$$\frac{da}{dt} = F_{SCC}(K) \tag{II–2}$$

PROST uses several models $F_{SCC}(K)$ from the literature to allow different material and medium conditions in simulations. Important implementations of this crack growth velocity (as it has the unit length per time) are power law-like functions of K with either thresholds or saturation limits, and constant crack growth rates.

Fatigue crack growth rates are governed by a similar differential equation, but the number of load cycles N is the variable for the evolution, and the K-values at minimum and maximum loading are used in the evaluation.

$$\frac{da}{dN} = F_{Fatigue}(K_{min}, K_{max}) \tag{II–3}$$

Implementations of $F_{Fatigue}$ in PROST comprises the classical Paris-Erdogan equation (power law for the K amplitude) and more complex models from the literature, which allows to model individual fatigue behaviours of different relevant materials.

Ductile tearing is based on the comparison of the J-integral with a resistance-curve (r-curve). The ductile crack growth can be stable, such that the crack growth is limited, or unstable, which causes a failure.

II–4. STAGES, FAILURE AND TRANSITIONS

The distinct crack configurations shown in Fig. II–1 represent separate stages of a crack evolution. At a certain point the evolution steps from one stage to the other; usually due to spontaneous failure caused

by continued crack growth up to an instability. A scheme to represent the possible transitions is a discretised structure integrity diagram. While a structure integrity diagram is a two-dimensional scheme with the crack depth and crack length as axes, the discretised version restricts the axis to the discrete values zero, finite, and long. Such a diagram is shown in Fig. II–2; the geometric examples are shown for circumferential cracks, but axial cracks are simulated in the same way.

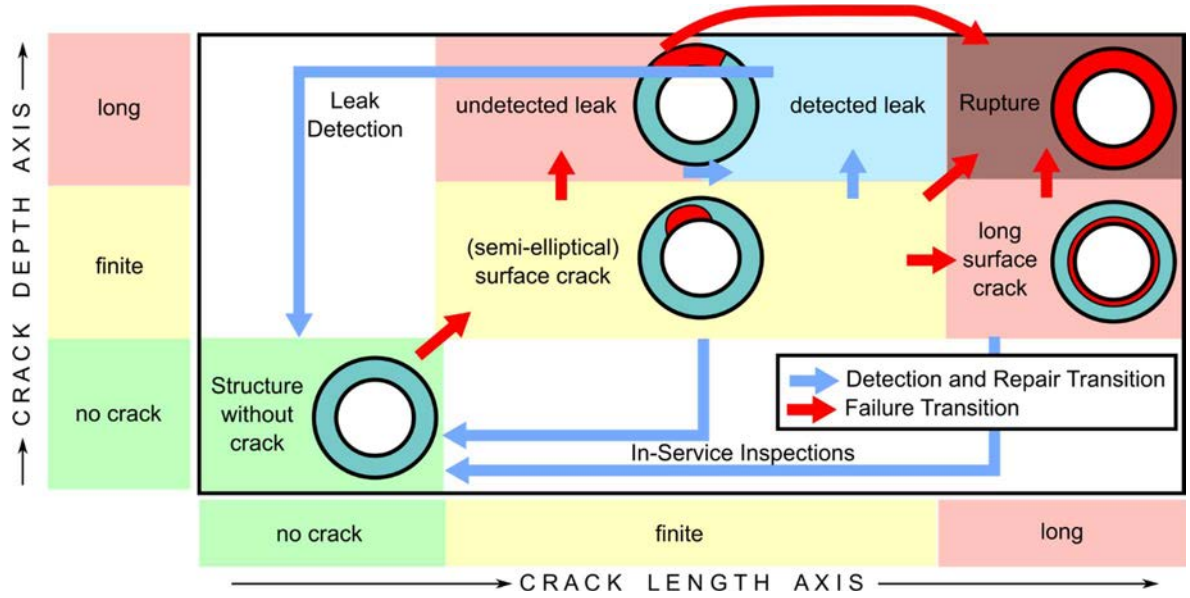

FIG. II−2. Discretised structure integrity diagram with transitions.

In this representation, transitions to a reduced integrity state (failures) are indicated by red arrows. The options in PROST to determine failures can be chosen by the user; standard approaches are geometrical failure criteria (e.g. reaching a certain percentage of wall thickness), failure assessment diagram, and plastic collapse solutions.

Blue arrows in the discretised structure integrity diagram represent detection and repair transitions. PROST is able to simulate ISIs (e.g. ultrasonic testing) by a POD curve; several shapes of POD curves are implemented. Beside this, PROST can also simulate hydrostatic testing: A high pressure load is applied to cause failure in this testing phase instead of operations. Finally, it is possible to compute leak flow rates in the presence of wall penetration cracks, and to simulate the detection of leaks by leak monitoring systems.

II−5. PROBABILISTIC SAMPLING

In a probabilistic simulation, several deterministic computations with different parameters (drawn from distributions) are combined, and a statistical evaluation of the transitions give rise to failure probabilities and failure frequencies. The simplest approach, the Monte Carlo sampling, generates parameter sets from the distribution functions. For highly reliable components such as piping in nuclear power plants, this is a very ineffective approach since only a small fraction of all parameters lead to failures and give valuable information for the computation of failure rate. Therefore, PROST implements a number of efficient algorithms to be able to compute even transition probabilities well below 10^{-10} with relatively few deterministic evaluations. These algorithms include equidistant stratification, Latin Hypercube

Sampling, first-order reliability method, spherical (or radial) sampling, design point-based importance sampling, directional sampling, adaptive directional stratification, and the Vegas algorithm. An overview and application of these sampling strategies is found in [II−6] and [II−7].

REFERENCES TO ANNEX II

[II–1] INTERNATIONAL ATOMIC ENERGY AGENCY (IAEA), “Deterministic Safety Analysis for Nuclear Power Plants.”, IAEA Safety Standards Series No. SSG-2 (Rev.1), 2019.

[II–2] INTERNATIONAL ORGANIZATION FOR STANDARDIZATION (ISO), “Quality management systems – Requirements”, ISO 9001:2015, 2015

[II–3] INTERNATIONAL ORGANIZATION FOR STANDARDIZATION (ISO), “Information security management”, ISO 27001:2017 2017.

[II–4] HECKMANN, K., SIEVERS, J., “Integrity Assessment of Piping with the PROST code”, Enlarged Halden Program Group Meeting, Lillehammer, Norway, 2017.

[II–5] BLÄSIUS, C., HECKMANN, K., SIEVERS, J., “Quality Management, Verification, and Validation of Structure Mechanical Computer Codes at GRS”, Transactions SMiRT-25, Charlotte, NC, USA, August 2019

[II–6] HECKMANN, K. MA, K., SIEVERS, J., „Probabilistic aspects on break preclusion assessment in nuclear piping”, 41st MPA-Seminar, Stuttgart, Germany, October 2015.

[II–7] HECKMAN, K., SIEVERS, J., “Efficient Probabilistic Methods for Leak-Before-Break Analysis,” 2nd Int. Seminar on Probabilistic Methodologies for Nuclear Applications, Ottawa, 25-26 October, 2017.

ANNEX III
METHODOLOGY AND IMPLEMENTATION OF COMPUTER CODES (KAERI)

III−1. INTRODUCTION OF PROFAS-PIPE

KAERI developed the computer code PROFAS-PIPE (PRObability Failure Analysis System – PIPE) Version 1.0 for solving the CRP benchmark problems. The code is written in Python language, which has been gaining popularity recently due to its easiness to learn and abundant open source libraries. Since the developer is not an expert in programming and did not have enough manpower (only one researcher is in charge of the development), Python was chosen rather than C or C++ having much faster speed. The quality assurance on the developed code is not implemented yet, and the code validity was only checked within the CRP activity by sharing the computation results. The code does not have graphic user interface and the code structure is oriented to the developer's convenience, that is, it is not user-friendly. Changing input data and analysis models requires some knowledge about Python language and the code structure. In this Annex, the following subjects of PROFAS-PIPE are described:

- Code architecture;
- Input and setting module;
- Crack initiation module;
- Crack growth module;
- K value calculation module;
- Stability module;
- Inspection module;
- Leak detection module;
- Residual stress module;
- Post processing module.

III−2. CODE ARCHITECTURE

The computer code consists of three modules: 1) input, 2) calculation, and 3) output. The input module is used for the input parameters and computer code run preferences. The analysis data includes material properties, temperature, crack dimensions, etc. The computation parameters include the number of crack case, the CPU number used for parallel computation, parameter boundaries, etc. The second layer is the main part for the calculation and estimation. At the beginning of this layer, a crack instance is generated based on the input and setting parameters. By passing the crack instances into the generation module, initial dimensions of cracks are statistically determined. Then, the assigned dimensions are checked with some criteria, for example, the depth of cracks cannot exceed 80% of the pipe wall thickness and if a crack reach the value, then the crack is flipped from a surface crack to a through-wall crack. The dimension criteria are taken from the input boundaries of the model for the SIF. Being beyond the limits raises error in the SIF module. So, the checking step is always applied after changing crack dimensions in the following process.

Although all cracks are generated and assigned to specific dimensions, the cracks are not activated yet. To include any crack into the following calculation and estimation, their activation is statistically estimated with the activation rule. The rule can be either a simple number or a continuous statistical distribution. Under the rule, a part of the cracks is determined to be activated and then their information

is passed into the next step. The other inactivated cracks are set aside until the assessments on the activated cracks are done. For a set of periods which is defaulted as a month in the CRP benchmarks, the activated crack's evolution and estimation are simulated. Different codes for the calculation of SIF (K) can be applied through the K value calculation module. For an inner surface crack, K values at both bottom (front) and surface points are estimated, and with a through-wall crack, only K at inner surface is calculated. With or without the K values, the growth rate can be determined by the growth model imported from the crack growth module. The dimensions of the activated cracks are updated with the crack growth rate and the inner step time. The inner step time is determined with the period of the outer loop and the calculation interval time. For instance, if the outer loop has a year step, the calculation interval of a month leads to 12 inner iterations with 30 days of inner step time. Each inner iteration includes calculating K values, updating crack dimensions, checking crack dimension, estimating leak rate, and assessing pipe integrity procedures.

Through updating the crack dimension, some cracks are switched from a surface crack to a through-wall crack. They are passed into the leak detection module. In the leak detection module, the crack opening area is estimated, and the crack opening area is passed to the leak rate model. Any models for crack opening area and leak rate can be applied. After determining the leak rates of the through-wall cracks, their detection is checked by the detection limit parameters. If the leak rate of cracks exceeds the detection limit, the cracks are classified as detected crack and they are excluded in the subsequent calculations. The other survived cracks from checking are passed to the stability evaluation step.

In the stability evaluation module, piping integrities are determined for all activated cracks. If the assessed results satisfy the pre-defined criterion, the cracks are passed to the next iteration. If the pipe is determined to be instable, it is considered as failed. The cracks in the failed pipe are eliminated from the subsequent calculation.

The above procedure from the crack initiation to the pipe integrity assessment repeats until the calculation time reaches the total operation years. If ISI is applied during the operation time, the POD module will be called at predefined time or interval, in which the detections of cracks are statistically determined. The detected defects are eliminated from the subsequent calculation.

Any information used before, after, or during the calculation can be extracted and saved. However, changing output data requires some understanding about the code, meaning customizing output demands editing the code directly. The default output data that do not need changes in the code is cumulative failure probability.

There are some functions visualizing the output data in the post processing module, like crack dimension evolution, annual frequencies and cumulative probabilities of leak and rupture, parameter sensitivity analysis, etc. Unfortunately, the module is not well organized and not well-defined. To change some options, the code has to be directly edited.

The above system architecture is schematically illustrated in Fig. III–1. The figure shows the flow of the code and the connection between the main code and the modules. The arrow indicates the data flow and the red circles describe the module connectors that is introduced to facilitate the connection. The concept of the connector is illustrated in Fig. III–2. If several models are embedded in any module, a connector calls one of the models just by editing input parameters without changing the main code.

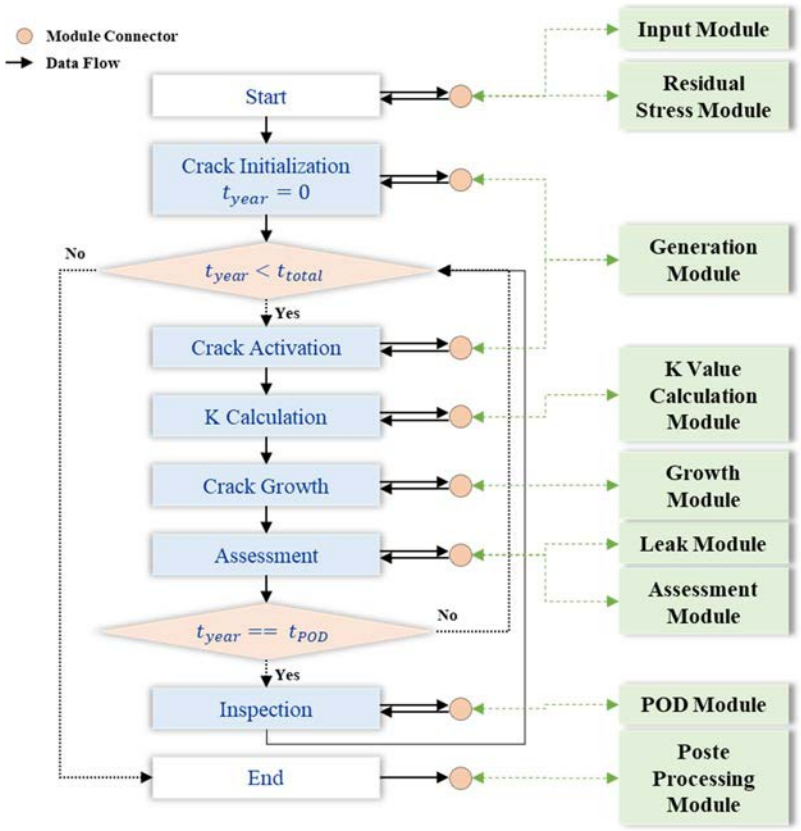

FIG. III–1. Analysis flow of the PROFAS-PIPE code.

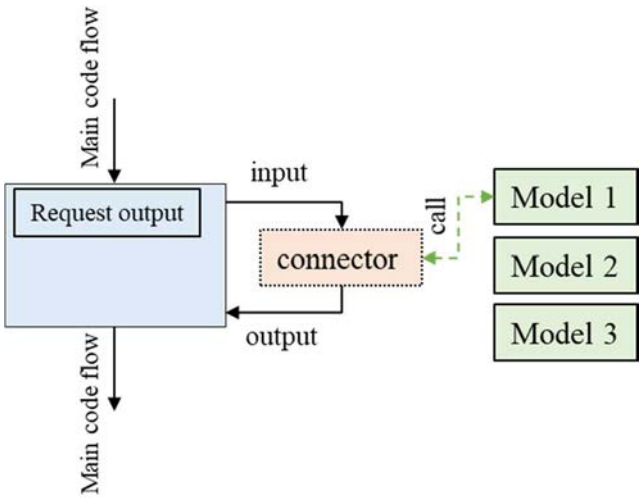

FIG. III–2. Schematic chart of the connector.

III−3. INPUT AND SEETING MODULE

In the module, general information, leak, material, pipe parameters, and the analysis setting parameters can be editable. For readability, the five categories of input file are made, and each file has the related information as ‘dictionary type’ variable. The dictionary variables contain several keywords and Table III−1 lists such keywords in the input module. Basically, all parameters used in the analysis are edited

directly in the information files, in addition any parameter can be modified at the main code layer. For example, parameter sensitivity analysis can be conducted by changing specific parameter value using 'compile' method where one can modify parameter value using parameter keyword.

TABLE III–1. DATA KEYWORDS IN THE INPUT AND SETTING MODULE

Keyword	Type	Description
Material		
'Elastic modulus'	Table data	X: temperature (℃) Y: elastic modulus (GPa)
'Yield strength'	Table data	X: temperature (℃) Y: yield strength (MPa) Y std: standard deviation (MPa)
'Ultimate tensile strength'	Table data	X: temperature (℃) Y: UTS (MPa) Y std: standard deviation (MPa)
'Fracture toughness'	Table	X: temperature (℃) Y: toughness ($MPa \cdot \sqrt{m}$) Y std: standard deviation ($MPa \cdot \sqrt{m}$)
'Poisson ratio'	Constant	Y: poisson ratio
Pipe_		
'Pipe outer radius'	Constant	Y: radius (mm)
'Pipe thickness'	Constant	Y: thickness (mm)
'Pipe inner radius'	Constant	Y: radius (mm)
'Pipe mean radius'	Constant	Y: radius (mm)
'Pipe pressure'	Constant	Y: pressure (MPa)
'Pipe temperature'	Constant	Y: temperature (℃)
'Pipe bending stress'	Constant	Y: stress (MPa)
'Pipe membrane stress'	Constant	Y: stress (MPa)
'Pipe axial load'	Constant	Y: load (N)
'Pipe bending moment'	Constant	Y: moment (N mm)
'Pipe torsion moment'	Constant	Y: moment (N mm)
'Pipe residual stress'	Function	Y: model name ('string' type)
Leak_		
'crack length'	Calculated	This parameter will be updated during the analysis. The specific value can be applied if one needs the calculation result with some specific crack length. (mm)
'hydraulic'	Calculated	Crack opening area. This parameter will be updated during the analysis. (mm^2)
'crack depth'	Constant	Y: depth (mm)
'pressure'	Constant	Y: pressure (MPa)
'temperature'	Constant	Y: temperature (K)
'back pressure'	Constant	Y: pressure (MPa)
'discharge coefficient'	Constant	Y: 0-1
'detectionLimit'	Constant	Y: leak rate (kg/sec)

TABLE III–1. DATA KEYWORDS IN THE INPUT AND SETTING MODULE (Cont.)

Keyword	Type	Description
Material_		
'print on/off'	Constant	'Bool' type variable (True/False). 'True' will print some calculation information when executing the leak module.
Parameter_		
'time step'	Constant	Y: int (#/year). It is the answer to how many steps you want to apply for 1 year calculation.
'time in step'	Constant	Y: sec (s). time per a step.
'crack length model'	Function	Y: model name ('string' type). It is for the model of generating initial crack lengths.
'crack length parameters'	Constant	Y: mu – average (mm) std – standard deviation (mm)
'crack depth model'	Function	Y: model name ('string' type). It is for the model of generating initial crack depths.
'crack depth parameters'	Constant	Y: mu – average (mm) std – standard deviation (mm)
'crack initiation parameters'	Constant	Y: probability (/year)
'crack initiation model'	Function	Y: model name ('string' type)
'material flow model'	Function	Y: model name ('string' type)
'K calculation methods'	Function	Y: model names (list of 'string' type variables)
'crack growth model'	Function	Y: model name ('string' type)
'crack growth parameters'	Constant	Y: model parameters (list of float variables)
'crack opening model'	Function	Y: model name ('string' type)
'leak rate model'	Function	Y: model name ('string' type)
'POD model'	Function	Y: model name ('string' type)
'POD parameters'	Constant	Y: model parameters (list of float variables)
'reference stress model for throughwall crack'	Function	Y: model name ('string' type)
'reference stress model for part-throughwall crack'	Function	Y: model name ('string' type)
'failure model'	Function	Y: model name ('string' type)
Setting_		
'Totalyear'	Constant	Y: int (year)
'crackmodel'	Function	Y: model name ('string' type)
'case number'	Constant	Y: number (#)
'PODyear'	Constant	Y: list of ISI years
'PODapply'	Constant	Y: Ture/False ('bool' type)
'cpunum'	Constant	Y: cpu number (#)

III−4. CRACK INITIATION MODULE

The initiation module has two main functions—generating variables, crack depth or length, etc., and activating crack cases with a predefined distribution or rule. Table III–2 shows the models used in the module.

TABLE III–2. MODELS IN THE GENERATION MODULE

Model	Description	Case
Variable generation		
'normalDistribution'	$p(x) = \frac{1}{\sqrt{2\pi\sigma^2}} e^{\frac{(x-\mu)^2}{2\sigma^2}}$	Benchmark #2
'customFunc1'	Any function, For example, exponential function; $p(x) = \frac{l\lambda e^{-\lambda x}}{2 * (1 - e^{-\lambda})}$	Benchmark #1
'constantVar'	Constant for all case	
Crack initiation		
'constantProbabilityPerYear'	Cracks are activated by a constant probability criterion (p_{year}): $\begin{cases} p_{crack} > p_{year} : \text{active} \\ p_{crack} < p_{year} : \text{nonactive} \end{cases}$	Benchmark #1 and #2
'allInitialActivation'	All crack activates	

III–5. CRACK GROWTH MODULE

For simplicity, we adopted a simple model defined by power law equation having one variable and two constant parameters; the SIF, and exponent 'n' and coefficient 'K', respectively. However, any type of growth model can be implemented by scripting its function into 'models.py' or 'callModel.py' in the crack growth model. Fig. III–3 shows an example of the calculated crack growth rate as a function of SIF.

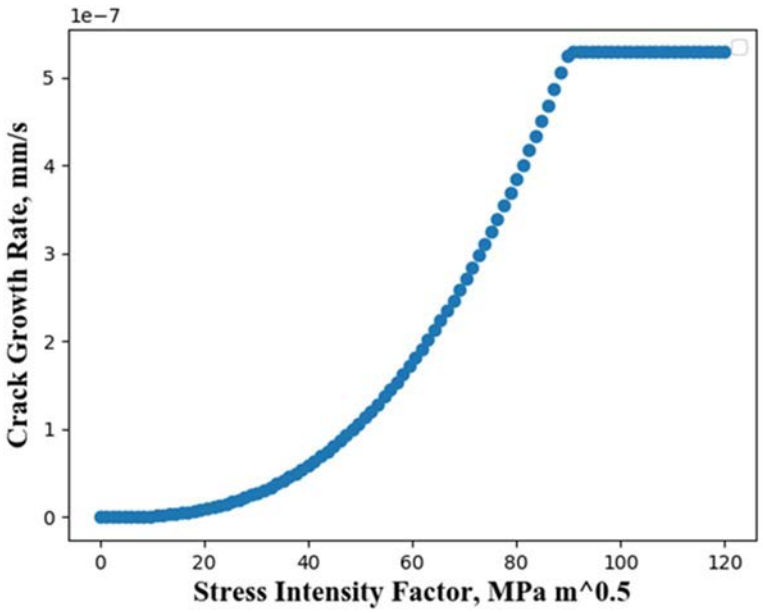

FIG. III–3. Crack growth rate as a function of SIF.

III–6. K VALUE CALCULATION MODULE

In Benchmark #1 and #2, circumferential cracks were chosen as main defect type. There exist a few models or methods for calculating the SIF of the circumferential crack in piping. The equations in RCC

MRx code are adopted. Equations for two crack types—circumferential through-wall and part through-wall defects in RCC-MRx are expressed by,

$$K_{I,\text{through-wall defect}} = \left[\sigma_m F_m + \sigma_b F_b + \sigma_{gb} F_{gb}\right]\sqrt{\pi c} \quad \text{(III–1)}$$

$$K_{I,part\ through-wal\ \ defect} = \left[\sigma_o i_o + \sigma_1 i_1 \left(\frac{a}{h}\right) + \sigma_2 i_2 \left(\frac{a}{h}\right)^2 + \sigma_3 i_3 \left(\frac{a}{h}\right)^3 + \sigma_{gb} F_{gb}\right]\sqrt{\pi a} \quad \text{(III–2)}$$

where:
σ_m: Constant stress through the thickness
σ_b: Linearized stress through the thickness
σ_{gb}: Global bending stress
σ_o: Constant stress through the thickness
σ_1: Linearized stress through the thickness
σ_2: Quadric stress through the thickness
σ_3: Cubic stress through the thickness

Influence coefficients (F_m, F_b, F_{gb}) and (i_{0-3}, F_{gb}) for the through-wall and part through-wall defects are given as table data in RCC MRx code and the values were implanted in the module in binary format. With an assumption that total K factor is determined by linearly adding all K factor calculated from different stress types, the factors are calculated using four functions according to stress types: membrane and bending stresses, non-linearly distributed stress, and pressure.

Table III–3 lists the equations for each K calculation. Fig. III–4 is an example of the calculated SIF as a function of crack depth.

TABLE III–3. K CALCULATION MODEL IN THE K VALUE CALCULATION MODULE

Function name	**Description**	**Equations** ($*$ **p : part through − wall defect,** $*$ **t : through − wall defect**)
'K1membrane_RCCMRx'	Membrane (or axial) stress	$K_p = \sigma_m i_o \sqrt{\pi a}$, $K_t = \sigma_m F_m \sqrt{\pi c}$
'K1bending_RCCMRx'	Bending stress	$K_p = \sigma_b F_{gb} \sqrt{\pi a}$, $K_t = \sigma_b F_{gb} \sqrt{\pi c}$
'K1distributed_RCCMRx'	Distributed (or residual) stress	$K_p = \left[\sigma_o i_o + \sigma_1 i_1 \left(\frac{a}{h}\right) + \sigma_2 i_2 \left(\frac{a}{h}\right)^2 + \sigma_3 i_3 \left(\frac{a}{h}\right)^3\right]\sqrt{\pi a}$, $K_t = 0$
'K1Pressure_RCCMRx'	Pressure	$K_p = Pi_o \sqrt{\pi a} \frac{r_{in}^2}{r_{out}^2 - r_{in}^2} + Pi_o \sqrt{\pi a}$, $K_t = Pi_o \sqrt{\pi a} \frac{r_{in}^2}{r_{out}^2 - r_{in}^2}$

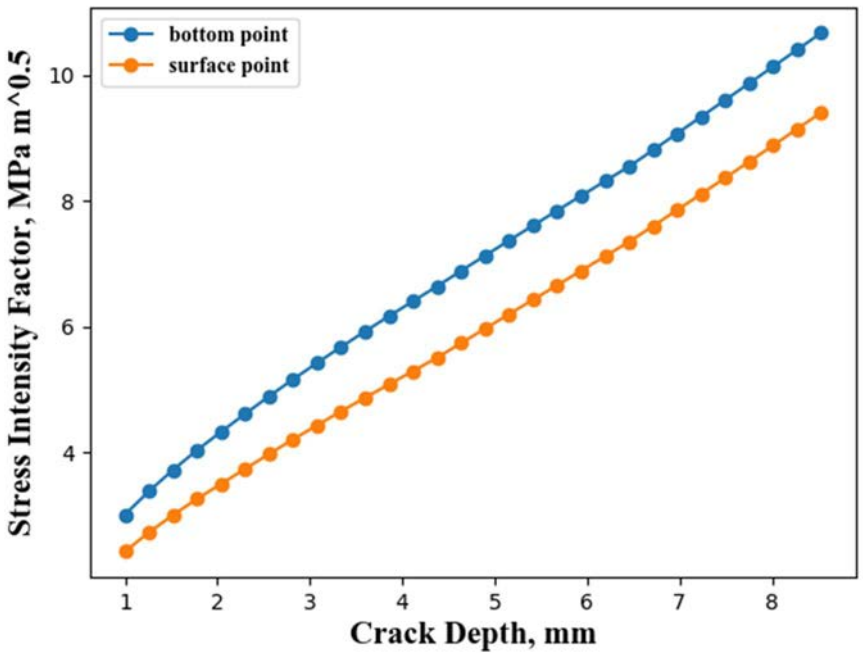

FIG. III–4. SIF as a function of crack depths.

III–7. STABILITY MODULE

To assess the integrity of piping with defects, the criterion defined in R6 code, in which two failure modes (fracture and collapse) are simultaneously considered, was implemented into the assessment module. R6 code suggests three options for the assessment, and the option 1 is the most conservative approach but very simple and does not require much information about the material properties. For this reason, the option 1 criteria are adopted. The following equations are used to establish failure assessment diagram, which defines the boundary between acceptable and not acceptable area:

$$\mathrm{Kr} = (1 - 0.14\mathrm{L_r^2})\left(0.3 + 0.7\mathrm{e}^{-0.65\mathrm{L_r^6}}\right) \tag{III–3}$$

$$\mathrm{L_r} = \frac{\sigma_{\mathrm{ref}}}{\sigma_{\mathrm{y}}} \tag{III–4}$$

To calculate $\mathrm{L_r}$, reference stress (σ_{ref}) is to be computed using the material flow strength and loading conditions. The calculation procedure of the reference stress was taken from RCC-MRx code. The code provides equations for the circumferential defects in an elastic-plastic material:

$$\mathrm{E_{ref}} = \varepsilon_{\mathrm{el}}(\sigma_{\mathrm{eqel}}) + \varepsilon_{\mathrm{pl}}(\sigma_{\mathrm{eqpl}}) \tag{III–5}$$

$$\left[\sigma_{\mathrm{eqel}}\right]^2 = ([s'_{1\mathrm{m}}]^2 + \sigma_{2\mathrm{m}}^2 - s'_{1\mathrm{m}}\sigma_{2\mathrm{m}} + 4\sigma_{12}^2) + \left(\sigma_{1\mathrm{b}}^2 + \sigma_{2\mathrm{b}}^2 - \sigma_{1\mathrm{b}}\sigma_{2\mathrm{b}}\right) + \frac{1}{\sqrt{3}}|s'_{1\mathrm{m}}\sigma_{1\mathrm{b}} + \sigma_{2\mathrm{m}}\sigma_{2\mathrm{b}} - 0.5(s'_{1\mathrm{m}}\sigma_{2\mathrm{b}} + \sigma_{2\mathrm{m}}\sigma_{1\mathrm{b}})| \tag{III–6}$$

$$\left[\sigma_{\mathrm{eqpl}}\right]^2 = (s_{1\mathrm{m}}^2 + \sigma_{2\mathrm{m}}^2 - s_{1\mathrm{m}}\sigma_{2\mathrm{m}} + 4\sigma_{12}^2) + \left(\frac{2}{3}\right)^2\left(\sigma_{1\mathrm{b}}^2 + \sigma_{2\mathrm{b}}^2 - \sigma_{1\mathrm{b}}\sigma_{2\mathrm{b}}\right) + \frac{2}{3\sqrt{3}}|s_{1\mathrm{m}}\sigma_{1\mathrm{b}} + \sigma_{2\mathrm{m}}\sigma_{2\mathrm{b}} - 0.5(s_{1\mathrm{m}}\sigma_{2\mathrm{b}} + \sigma_{2\mathrm{m}}\sigma_{1\mathrm{b}})| \tag{III–7}$$

where:
S_{1m}, S_{1m}': Axial membrane stress through thickness
σ_{1b}: Axial bending stress through the thickness
σ_{2m}: Circumferential membrane stress through the thickness
σ_{2b}: Circumferential bending stress through the thickness
σ_{12}: Shear stress

After obtaining the reference strain, the reference stress can be extracted using stress-strain curve defined by Ramberg-Osgood equation. K_r is defined as $\frac{K_I}{K_{Ic}}$, K_{Ic} and K_I are the fracture toughness of a material and the SIF of a defect, respectively. With K_r and L_r, a point can be drawn in the failure assessment diagram area and its integrity can be assessed by checking whether the point is in or out the failure assessment diagram curve. Fig. III−5 displays the failure assessment diagram curve with the equation of R6 option 1.

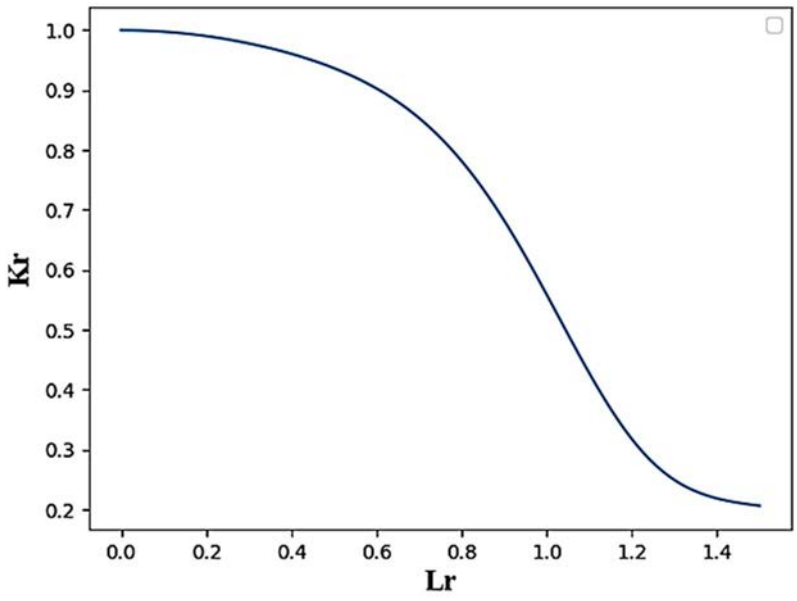

FIG. III−5. Failure assessment diagram.

III−8. INSPECTION MODULE

ISI definitely affects the integrity of components by finding active cracks and eliminating them before they cause the component failure. Since the detection has not a 100% success, their probability of finding is to be included in the inspection. In general, the POD is a function of crack size. In the module, the following equation is considered for the distribution of POD:

$$P = \frac{e^{(\beta_0+\beta_1 \ln a)}}{1+e^{(\beta_0+\beta_1 \ln \ )}} \quad \text{(III−8)}$$

With the POD distribution, cracks can be stochastically eliminated from the analysis. This simple process is shown in Fig. III−6.

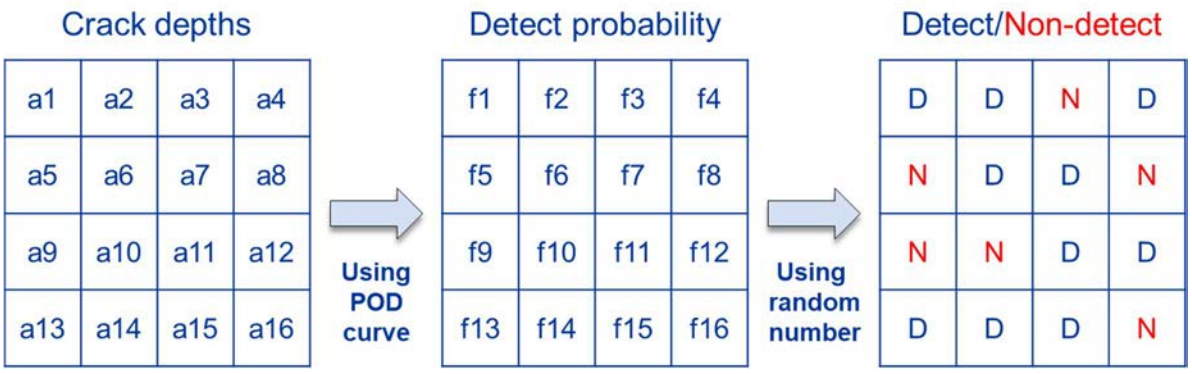

FIG. III–6. Concept of POD effect.

III–9. LEAK DETECTION MODULE

In the leak detection module, crack opening area is calculated first and then leak rate is computed using the calculated crack opening area. To calculate crack opening area, Paris-Tada model for a circumferential through-wall crack is adopted. The following equations describe the Paris-Tada model:

$$A = A_t + A_b \tag{III–9}$$

$$A_b = \sigma_b \left(\frac{\pi R^2}{E}\right) I_b(\theta') \tag{III–10}$$

$$A_t = \sigma_t \left(\frac{\pi R^2}{E}\right) I_t(\theta') \tag{III–11}$$

$$I_t(\theta') = 2\theta'^2 \left[1 + \left(\frac{\theta'}{\pi}\right)^{1.5} \left\{8.6 - 13.3\left(\frac{\theta'}{\pi}\right) + 24\left(\frac{\theta'}{\pi}\right)^2\right\} + \left(\frac{\theta'}{\pi}\right)^3 \left\{22.5 - 75\left(\frac{\theta'}{\pi}\right) + 205.7\left(\frac{\theta'}{\pi}\right)^2 - 247.5\left(\frac{\theta'}{\pi}\right)^3 + 242\left(\frac{\theta'}{\pi}\right)^4\right\}\right] \tag{III–12}$$

$$I_t(\theta') = \frac{(3+\cos\ '\ )I_t(\theta')}{4} \tag{III–13}$$

$$\theta'_{eff} = \theta' + \frac{K'_{eff}}{2\pi R\sigma_f^2}, where\ \sigma_f = \frac{(\sigma_y+\sigma_u)}{2} \tag{III–14}$$

where:
θ: crack angle
KI: SIF 1
R: mean radius of pipe
σ_y: yield strength
σ_u ultimate tensile strength
E: elastic modulus
σ_t: tensile stress
σ_b: bending stress

For calculating the leak rate, two phase Henry-Fauske model and simple Bernoulli equation were implemented into the leak module. In Henry-Fauske model, the leak rate is a function of pressure drops across the thickness, and the pressure drops are a function of the leak rate. This implicit relation indicates that the solution of the leak rate can be obtained through iteration process. The functions in the model have water properties as input variables, like entropy, volume, steam quality, etc. To get these

values the open-source library ‘iapws’ was used, which provides the functions according to IAPWS (The International Association for the Properties of Water and Steam) formulations. IAPWS provides internationally accepted formulations for the properties of light and heavy steam, water, etc. However, ‘iapws’ module is not optimized for massive calculation. The module does not accept vector input but single scalar variable, which leads to loop type coding for a lot of cases; and loop type coding is a weak point of Python language for the computation speed. In the process of Henry-Fauske model, the iteration process significantly slows computational speed, and so makes the analysis impractical.

A simple solution interpolation mapping was adopted to overcome this drawback. Steam properties are determined when two physical properties are fixed. For example, if pressure and temperature are fixed, physical properties like specific volume, specific entropy, etc. for single phase state can be obtained. Based on this feature, we made regular grid interpolator using the pre-calculated data set covering the pipe operation conditions.

Although the interpolation method dramatically improved the computation performance (about 10 times fast) with negligible difference in the results, its use for over 10,000 cases was still impractical. The reason of such difficulty is the implicit relation between the leak rate and the pressure drop, which requires some iterations for solving. As an alternative of Henry-Fauske model, the following simple Bernoulli model was applied.

$$\text{Leak rate}\left(\frac{\text{m}^3}{\text{s}}\right) = \text{KA}\sqrt{\frac{2\Delta\text{P}}{\rho}} \qquad \text{(III−15)}$$

where K, A, ΔP and ρ are discharge coefficient, crack area, pressure drop and liquid density, respectively.

The leak rates from two different leak models, the Henry-Fauske model and the simple Bernoulli equation, were compared using an analysis case in EPRI NP-3596-SR report[8]. Table III–4 lists the predefined crack length and opening displacement, and Table III–5 displays the analysis parameters.

Figure III–7 shows the comparison of the model’s results. The comparison shows very similar leak rates. The computation with Henry-Fauske model for 10 crack cases took relatively long time about 0.2~0.3 sec compared to the Bernoulli case just taking about 1.1~1.5×10^(-5) s. In other words, use of simple Bernoulli equation reduces the computational time by a factor of more than 10,000.

TABLE III–4. CRACK LENGTH AND CRACK OPENING DISPLACEMENT INFORMATION [EPRI NP-3596-SR]

Crack length (mm)	**COD (mm)**
10,16	0.0048514
20.32	0.0105918
30.48	0.0174752
40.64	0.0287782
50.8	0.0499364
60.96	0.0830326
71.12	0.1264666
81.28	0.1814068
91.44	0.2489454
101.6	0.3302254

[8] Original-Pipe Crack Evaluation Program,' 1993, Prepared by EPRI, Palo Alto, Calif., NP-3596-SR.

TABLE III–5. ANALYSIS PARAMETERS [EPRI NP-3596-SR]

Pipe outside diameter (mm)	114.3
Pipe thickness (mm)	8.5598
Crack surface roughness (mm)	0.00508
Number of 45 deg turn	0.315
Number of 90 deg turn	0
Pressure (MPa)	7.89
Temperature (K)	548.7
Loss coefficient	0.61
Friction factor	0.0376
Back pressure (MPa)	0.1

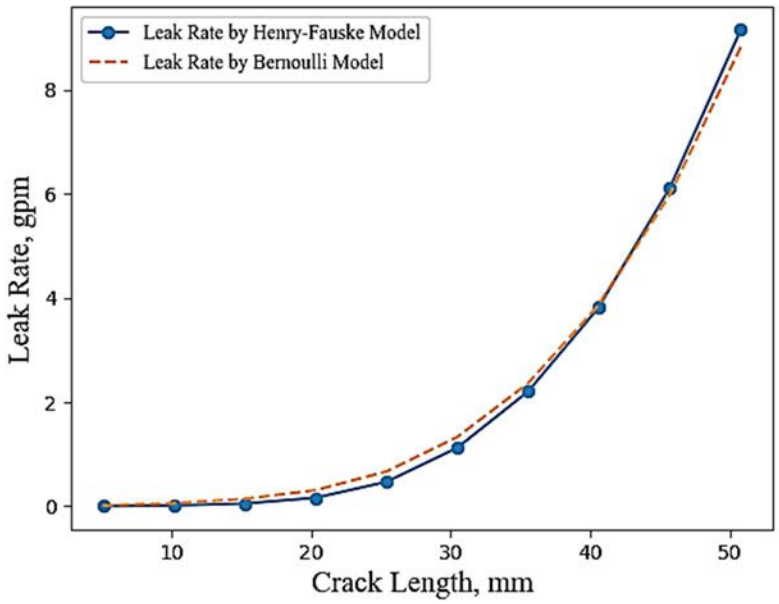

FIG. III–7. Comparison between the leak rates as a function of crack lengths from two leak rate models.

III–10. RESIDUAL STRESS MODULE

Residual stress or any distributed stress through the thickness of pipe is to be determined at the beginning of the analysis. A 3rd polynomial is used to describe the stress as a function of thickness. So, the distributed stress is described by four parameters. One can use only one parameter set to describe one distribution used for all cracks or the distribution set of each parameter to generate different residual stress distribution for all cracks.

III–11. POST PROCESSING MODULE

Any data can be extracted at each iteration using the ‘history’ dictionary type variable. The default extracted parameters are ‘leak probability’, ‘break probability’ and ‘initial crack dimension’. The ‘history’ variable is the final output of main analysis code and it is saved as a binary file. The save file can be used in the next post-processing step, like visualization. Most works in the post processing module are about plotting the final figure using the ‘history’ output.

ANNEX IV
METHODOLOGY AND IMPLEMENTATION OF COMPUTER CODES (LEI)

This annex includes the description of the computer code and methodology used in the benchmarking activities by LEI.

IV−1. INTRODUCTION TO AUTOPIFRAP

AutoPIFRAP is a special program system, which can be used for the risk evaluations, sensitivity analysis, investigation, and comparison of different risk-informed suggestions [IV−1], [IV−2], [IV−3].

A special program denoted AutoPIFRAP has been developed in 2001 year and initially was used for the Risk-Based Inspection Pilot Study of the Ignalina NPP, Unit 2 (IRBIS) project. AutoPIFRAP can perform and manage the risk evaluations and especially it enables quick and clear analysis of different user-defined ISI programs. In the initial data preparation stage, the software for reliability analysis of growing cracks - PIFRAP (PIpe FRActure Probabilities) is used for obtaining the probabilities of leak and rupture per year. Other calculations and analysis parts are performed independently. PIFRAP is a program developed by SAQ Kontroll AB for performing probabilistic fracture assessments of nuclear piping subjected to various crack growth mechanisms, focusing on intergranular SCC and high cycle (vibration fatigue).

PIFRAP is meant for evaluation of the leak and rupture probabilities of a specific cross-section with a certain stress state and possibly containing a circumferential growing crack due to intergranular SCC. Detailed code description is found in the SKI (Swedish Nuclear Power Inspectorate) Report 2000:48 titled “The Use of Risk-Based Methods for Establishing ISI-Priorities for Piping Components at Oskarshamn 1 Nuclear Power Station” and issued by the Swedish Radiation Safety Authority, Stockholm, Sweden in November 2000. This report concerned a study which has been conducted for the Swedish Nuclear Power Inspectorate.

IV−2. AutoPIFRAP

Version and Release Date: AutoPIFRAP 3.10 (update in 2015, LEI), includes PIFRAP solver (started in 1999, SAQ). PIFRAP also includes LBBPIPE (crack grow) and SQUIRT (leak rate). Supported Operating System(s): Windows 64-bit OS (Windows 7 & 10).

The code was not checked against quality assurance standards. It was just verified and validated, for instance, using benchmarking with other computer codes (e. g. WinPRAISE); Comparison with actual leak frequencies and sensitivity studies were also performed. Coding Language(s): Fortran and Visual Basic.

IV−3. MODULES IN AutoPIFRAP

The computer program system AutoPIFRAP is programmed Microsoft® Visual Basic v.6.0, which is used for creating macros in applications of Microsoft Office Package. The macros of AutoPIFRAP consist of more than 1200 lines of programming language commands. The macros are loaded together with the Excel type file IRBISAutoPifrap.xls. No additional installation of Microsoft® Visual Basic is

required, although the same system requirements as for Microsoft® Excel v.97 are to be fulfilled as the basic unit of the user's interface is typical Excel sheets.

One of the main AutoPIFRAP parts is the Subsystem of Integration. It is to ensure that the informational links between the AutoPIFRAP system and the PIFRAP Solver (in case of using Pifrap solver the file Pifrap_solver.exe are in the same directory as IRBISAutoPifrap.xls and Excel is initiated by running the application IRBISAutoPifrap.xls). The Subsystem of Integration can create the input file for each weld, start PIFRAP with this input file and read output file data (for the information flow see the following Figure IV−1).

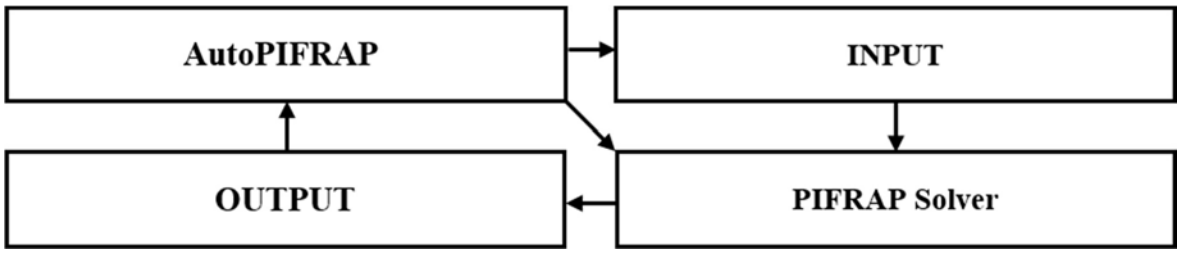

FIG. IV−1. The scheme of information flow between AutoPIFRAP and PIFRAP.

To ensure the interaction with the user, with various data sources and data sheets in AutoPIFRAP, special means of data exchange are created. According to the program functions and information distribution the structure of the program system AutoPIFRAP can be divided into six subsystems and three data libraries (see Fig. IV−2). One of the main parts of AutoPIFRAP is the Subsystem of Integration. It ensures the informational links between the AutoPIFRAP system and the PIFRAP Solver.

The Subsystem of Integration was discussed above. The NPP Data Library includes nine data sheets with NPP-specific information related to welds' grouping, geometry, stresses, material, crack grow, inspection, and system barrier data. The PIFRAP Results Library consists of the PIFRAP output data and calculated estimates of Core Damage Frequency (CDF). All that information is collected in one sheet i. e. "PIFRAP results". The AutoPIFRAP Library (the "Analysis results" sheet) saves the research results after different research cases. The Subsystem of Information Exchange ensures the data flow between different data sheets and other subsystems. The Subsystems of Research Control, Research Interface, and Research Output represent the means used to research risk-based inspection programs, to visualize and analyze the absolute and relative CDF, cumulative inspection amount, and the radiation exposure to the NPP inspection personnel.

The possibilities to investigate various cases of risk-based inspection parameters can be used to perform sensitivity analysis. The Subsystem of Computing performs main AutoPIFRAP calculations. One part of calculations for chart printing and data representation are performed as external Excel formulas directly in datasheets.

Another part of calculations is related to internal macros and functions, which can be activated using various control toolbars.

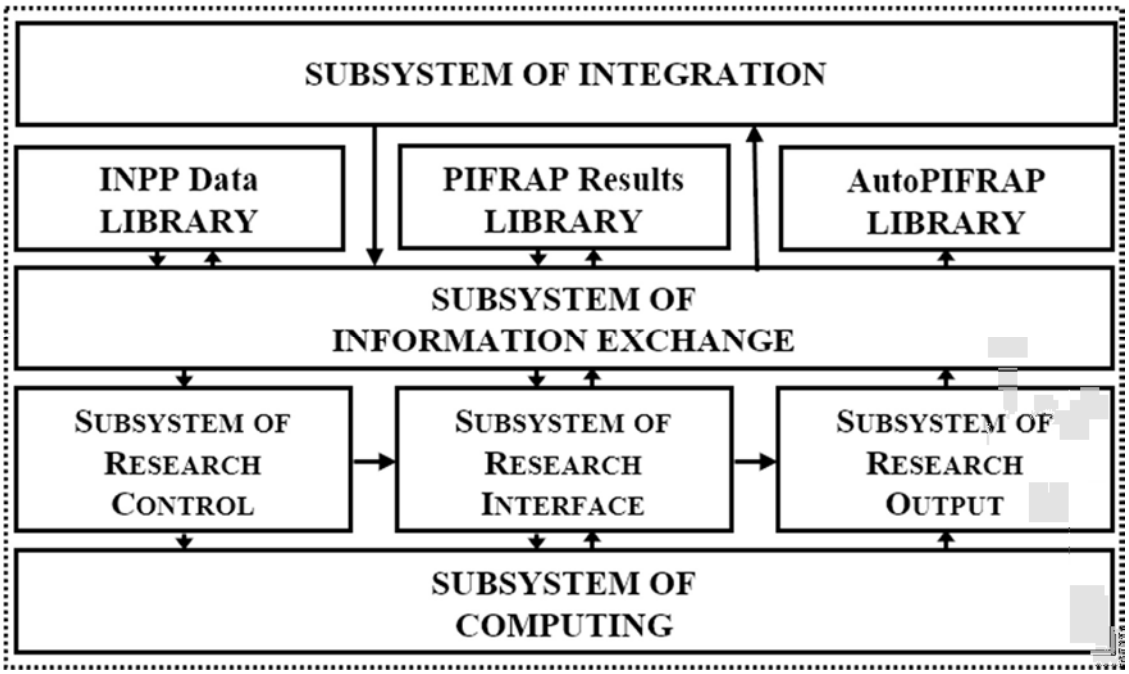

FIG. IV–2. The scheme of the program system AutoPIFRAP.

IV–3.1. Crack growth and transitioning

Supported crack orientation: circumferential. Supported Crack Shape(s): 90 % part-through-wall crack transition to non-idealized through-wall crack, refer to Fig. IV–3. The time step can be adjusted by the user. J-integral is calculated according to R6 procedures.

Crack growth models for SCC are expressed by coefficients or tabular (user-defined) input of *da*/*dt*. General references are [IV–1] and [IV–4].

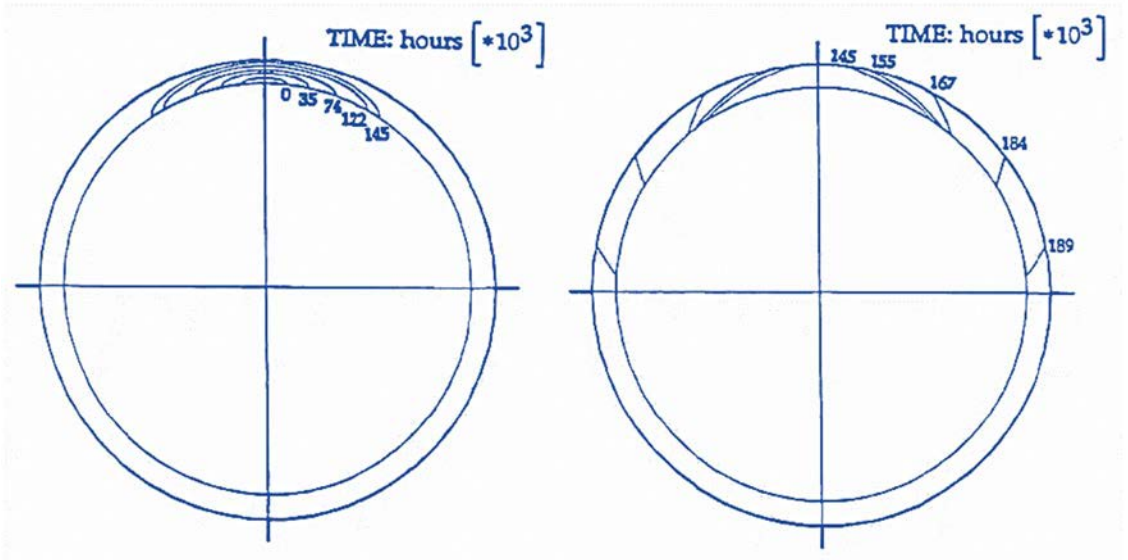

FIG. IV–3. Examples of circumferential cracks grow.

IV–3.2. Degradation and damage mechanisms

Types of degradation mechanisms and damage mechanisms modeled: intergranular SCC, PWSCC, intergranular SCC + high cycle fatigue + water hammer + seismic loads. In the last case crack growth due to high cycle fatigue is treated in a simplified way.

IV–3.3. Stress intensity factors

When the crack depth reaches 90% of the wall thickness, the crack is re-characterized to a through-wall crack, normally having a shorter length at the outside than at the inside of the wall. It might be highlighted that the leak rate is very dependent on the crack shape and crack opening profile that develops for through-wall cracks, and these are in turn very dependent on the residual stress distribution (and crack growth relation).

IV–3.4. Crack opening displacement

Depending on the included LBBPIPE (for crack grow) version the code can be modified in a comparison between the previously released version [IV–1]. Note also that the effect on the leak rate from WRS is accounted for by PIFRAP. This is done by using the standard crack face pressure method. WRS can have a large influence on COD as demonstrated by Rahman et al [IV–5]. Initially, [IV–4] assumed linear elastic behavior for the determination of COD. Finally, the crack opening areas are calculated by separate evaluations using the updated LBBPIPE software. The effects of plastic deformation on the COD and crack opening area for through-wall crack geometries are now accounted for. The plastic collapse parameter used for combined tension and bending is given in the handbook by Andersson et al [IV–6].

IV–3.5. POD for in-service inspection

POD function used in PIFRAP:

$$POD_P\left(\frac{a}{h}\right) = \Phi\left(C_1 + C_2\, ln\frac{a}{h}\right), \tag{IV−1}$$

where: h is a thickness of pipeline, a is the crack depth, and Φ denotes the standard normal distribution. Since

$$C_1 + C_2\, ln\frac{a}{h} = C_1 - C_2\, ln\, h + C_2\, ln\, a, \tag{IV−2}$$

It can be then denoted:

$$\tilde{C}_1 = C_1 - C_2\, ln\, h$$

to obtain:

$$POD_P(a) = \Phi\left(\tilde{C}_1 + C_2 \ln a\right). \quad \text{(IV–3)}$$

In the case if POD function is expressed as follows:

$$POD_R(a) = \frac{e^{\beta_0 + \beta_1 \ln a}}{1 + e^{\beta_0 + \beta_1 \ln a}}. \quad \text{(IV–4)}$$

Since the constants β_0 and β_1 are known, the logistic distribution (Eq. (IV–4)) needs to be fitted to the standard normal distribution (Eq. (IV–3)). This can be done by a nonlinear least-squares method, which is implemented in the excel worksheet. Firstly, these constants

$$\tilde{C}_1 \text{ and } C_2$$

are found with the best fit and then the original constant

$$C_1 = \tilde{C}_1 + C_2 \ln h$$

is obtained. Excel worksheet is programmed in such a way so that only the constants β_0 and β_1 need to be given a priori.

IV–3.6. Leak rate and residual stresses

The leak rate is calculated using the computer code SQUIRT [IV–7].

The WRS profile is provided in a tabular form using deterministic input.

IV–3.7. Outputs

Default: pipe rupture probability per year, pipe leak probability per year, C_plot/P_plot. In debug or additional modes outputs are as follows: the probabilities with various ISI cases, leak rate (kg/s), etc., welds for predefined risk levels, ISI interval, CFD calculations, inspection amount, radiation exposure.

IV–4. MAIN PROCEDURES

An implementation of AutoPIFRAP involves the following steps:

1. To prepare the input file for PIFRAP Solver according to the data (Geometry, Weld stresses, Materials, Crack growth, Leakage limits, Inspection, and Safety barriers), to automatically execute Solver and gather the PIFRAP results.
2. To complete the automatic selection of Safety Barriers, calculate Conditional CDF (CCDF or CDF), C-plot, and P-plot values, and present the charts.
3. To assess the impact of the leak probability reduction factor and to present CCDF and C-P plots and possibly define the limits for risk ranking levels according to the earlier inspection case.

4. To support risk analysis by providing a quick and efficient way to evaluate CCDF, delta-CCDF, amount of inspection sites and amount of accumulated inspections, and radiation exposure for different user-defined inspection alternatives.
5. To ensure automatic generation of combinations of inspection programme parameters and finding the most optimal case for the defined target function.

Each risk analysis case can be examined based on the optionally defined ISI parameters. Different alternatives can be selected where different extents of inspections (100%, 99%, …, 1%, 0%) and/or different future inspection intervals between inspections (1, 2, 4, 6, 10 years) can be selected or the cases with no inspection. It is as well possible to examine and propose improvements based on an integrated risk-informed approach in order to reduce the highest risk concerning the efficiency of inspections and other parameters in the model.

Regardless of the inspection programme alternative, the total risk CCDF for the cases of no inspection, earlier and currently planned inspection programmes can be evaluated and the accumulated radiation exposure to inspection personnel can be calculated. Absolute and relative risk changes of these values are then compared with the equivalent values relevant to the selected future inspection programme. Comparison of inspection costs and radiation exposure includes earlier ISI influence regardless of the selected inspection extent.

Selected inspection risk ranking and other results for each weld group are presented in a separate sheet. The sorted results and the results, related to the optionally selected extent, are also presented in a separate sheet. The main results (Risk research) are presented and added a new row in a separate sheet (Analysis results) to have the ability to compare results of different runs. In the Risk research sheet, it is included the chart, which, in general, represents all results of performed analyses. Furthermore, in the other sheet, the more detailed results and subtotals for each piping system and all weld groups are presented in table form. There is also possible to generate automatically a summary of this information.

To use the corrected Risk data (apply leak probability reduction factor) it is possible to set values of multipliers and automatic Risk data correction or exclusion (0 multipliers) will be performed. For example, to use leak probability reduction factor 100 it is possible to set corresponding Risk data multipliers to 0.01.

Each case of Risk analysis can be investigated concerning the selected and optionally defined ISI parameters (Risk research). Various initial research parameters can be changed. Then to get the results it needs to choose one of two calculation options, which are related to the kind of sorting before and after risk assessment:

- RiskLevelsISI- before risk assessment the sorting according to Risk level + CDF (earlier ISI) is performed. The sorting according to the Systems is performed after the calculations.
- SystemsISI- before risk assessment the sorting according to Risk level + Pipe systems + CDF (earlier ISI) is performed. The selected ISI case assessment and calculations are performed after risk ranking. The subtotals and total sum for some columns are presented according to the Pipe systems.

To perform risk ranking and suggesting a new selection of piping welds concerning risk, it is possible to investigate a lot of alternatives seeking to illuminate the different options and consequences resulting from different suggested RBI selections. The main results of the program are based on the outcome of

the PIFRAP evaluations to be able to perform the evaluations of different RBI alternatives automatically. The risk ranking and suggestion for a new RBI program are based on the CDF for only earlier inspections in the P-plot versus C-plot format.

Then one may choose a different extent of future inspection depending on what risk level the individual weld belongs to. For instance, 50% extent of inspection would conservatively mean that the 50% of the welds with the highest risks in the considered risk interval, in each piping system would be selected for future inspections, whereas the rest of welds in the considered risk interval in each piping system would not be subjected to any further inspection. It is supposed that in each future inspection, the different welds can be selected as welds, which have not been inspected last time, usually have a higher risk. One may also investigate the effect of using different inspection intervals. For instance, one may choose 100% inspections of all welds in all pipe systems but choosing 2-year inspection intervals for the highest risks, 4-year inspection intervals for some medium risks, and 8-year inspection intervals for the lowest risk. In general, the developed software can perform and administrate all the risk evaluations and ensure the possibilities to compare different options and to find the most optimal one.

REFERENCES TO ANNEX IV

[IV−1] BERGMAN, M., BRICKSTAD, B. AND F. NILSSON “A procedure for estimation of pipe break probabilities due to Intergranular SCC”, Int. J. Pres. Ves. & Piping, Vol. 74, pp. 239-248, 1997.

[IV−2] ALZBUTAS R., “Approaches of risk measures minimization and application to inspection”, 13th International Conference on Probabilistic Safety Assessment and Management (PSAM 13) 2-7 October 2016. Sheraton Grande Walkerhill Seoul, Korea. p. 1-14.

[IV−3] DUNDULIS G., ALZBUTAS R., “Pipe rupture and inspection sensitivity analysis”, Proceedings of the 52nd ESReDA Seminar, May 30-31, 2017, Kaunas, Lithuania. ISBN 978-92-79-73870-8. p. 108-116.

[IV−4] BERGMAN, M., PIFRAP user's manual, version 1.0, SAQ FoU-REport 97/07. SAQ Kontroll AB, Stockholm, Sweden, 1997.

[IV−5] RAHMAN, S., GHADIALI, N., WILKOWSKI, G., MOBERG, F. AND BRICKSTAD, B., Crack Opening Area Analyses for Circumferential Through-wall Cracks in Pipes - Part III: Off-center Cracks, Restraint of Bending, Thickness Transition and Weld Residual Stresses, Int. J. Pres. Ves. & Piping, Vol. 75, pp. 397-415, 1998.

[IV−6] ANDERSSON, P., BERGMAN, M., BRICKSTAD, B., DAHLBERG, L., NILSSON, F. AND SATTARI-FAR, I., A Procedure for Safety Assessment of Components with Cracks, SAQ/FoU-Report 96/08, SAQ Kontroll AB, Stockholm, Sweden, 1996.

[IV−7] PAUL, D. D., GHADIALI, N. D., AHMAD J, S. & WILKOWSKI, G., Seepage Quantification of Upsets in Reactor Tubes, SQUIRT User’s manual, version 2.2., Battelle, Columbus, Ohio, USA, 1992.ski, G., SQUIRT.

ANNEX V
METHODOLOGY AND IMPLEMENTATION OF COMPUTER CODES (SPI)

This annex describes the computer implementation of a data-driven methodology as applied by Sigma-Phase Inc. The relevant background information is found in [V−1]–[V−5].

V−1. INTRODUCTION

A data-driven model of piping reliability is implemented in Microsoft® Excel. The model consists of three elements: 1) pipe failure rate λ estimation using Bayesian analysis to update the probability distribution representing the prior state of knowledge with the evidence from a pipe failure event database, 2) the CFP that a failed condition produces a consequence of certain magnitude (e.g. peak through-wall flow rate or exceeding a flow rate threshold value), and 3) an integrated assessment of the frequency of a pipe failure of certain consequence, $\lambda \times CFP$. This analysis scheme is illustrated in Fig. V−1.

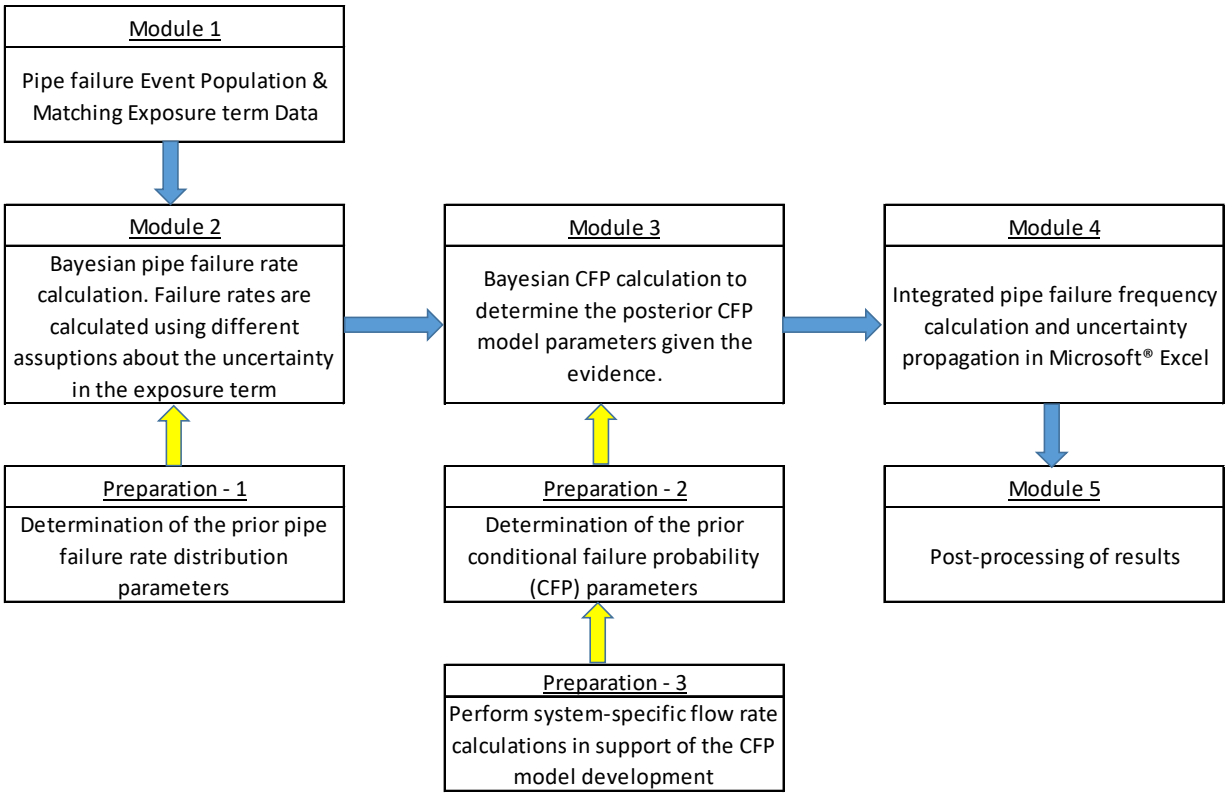

FIG. V−1. Schematic of the analysis process.

The model used for relating failure rates and rupture frequencies uses the following simple model, which is widely used in piping reliability assessment. The pipe failure modes being considered cover all failures requiring repair or replacement, including wall thinning, cracks, leaks, and ruptures of various sizes up to and including complete severance of the pipe.

The reason for expressing piping reliability as a product of failure rate and a conditional failure probability is that in many cases there are insufficient data available to estimate rupture frequencies directly from the service data. There are sufficient data from which to estimate failure rates but not major structural failures. This approach also facilitates the use of different sources of information for the different parameters of interest. The conditional failure probabilities are estimated from a combination of limited data, engineering judgment, expert elicitation and PFM.

V–2. CALCULATION PROCEDURE

The Bayesian analysis procedure is illustrated in Fig. V–2. A potential challenge in calculating pipe failure rates is to correctly address the plant-to-plant variability in piping system design and layout, weld populations, degradation susceptibilities, pipe lengths, etc. The incorporation of the impact of uncertainty in the piping component population is done by using a Bayes weighted posterior approach. A set of three estimates is obtained for the susceptible component population exposure, one for the best estimate, one for an upper bound estimate and one for a lower bound estimate. For each of these three estimates the number of pipe failures and the exposure population estimate is used to perform a Bayes' update of a prior distribution. Next a posterior weighting procedure is applied to synthesize the results of these three Bayes' updates into a single composite uncertainty distribution.

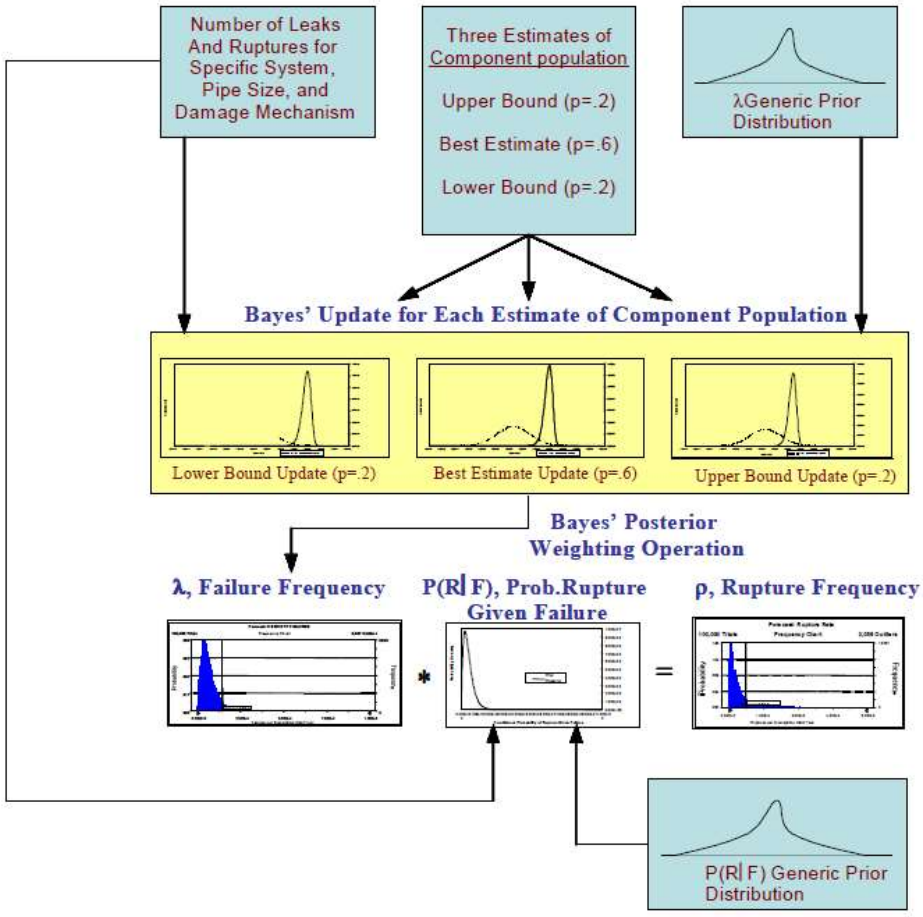

FIG. V–2. Bayesian estimation of pipe failure frequency.

An Excel spreadsheet with the Oracle Crystal Ball add-in program is used to implement the weighted posterior procedure. While there is no "single-format-fits-all" worksheet format, described here are the basic steps. In summary, the calculation procedure consists of the following steps:

- For each calculation case, identify the applicable prior failure rate distribution to be applied together with the event population to be input to the Bayesian update.
- Obtain pipe failure population data, and perform necessary screening to ensure that the input data sets are consistent with the analysis objective.
- Develop the exposure term that produced the event population identified in Step 1, Fig. IV−1. The impact of uncertainties in exposure term is addressed using a weighted posterior procedure.
- The standalone software 'R-DAT Plus' is used to calculate pipe failure rates for each unique combination of pipe size, damage/degradation mechanism and exposure term (low-medium-high).
- In 'R-DAT Plus', define a project with "subsystems." Each subsystem representing a Calculation Case that define the failure rate calculation cases. One set of failure rate parameters per exposure term assumption (low-medium-high). For each case, select an appropriate a priori distribution.
- A CFP posterior distribution is calculated for each of a predefined set of pipe failure consequence categories; e.g. in terms of equivalent break size.

Export the 'R-DAT Plus' results to the Excel workbook to facilitate the posterior weighting procedure for the component-specific "rupture mode" frequency calculations. The 'Export' function creates a *.txt or *csv file for input to the Excel workbook.

The Oracle Crystal Ball add-in software facilitates the posterior weighting process and through Monte Carlo simulation generates a single composite distribution for the pipe failure rate. A Monte Carlo merge technique is used to develop a distribution that has a mean value equal to a weighted average of the three (low – medium – high), while maintaining the full range of values representing the three input distributions.

V−3. INTEGRATED ANALYSIS

The integrated analysis consists of combining the Crystal Ball assumptions about failure rates (FR) and CFP. The pipe failure frequency calculation is performed by multiplying the FR-assumptions with the CFP-assumptions. The products of respective set of FR and CFP are represented by Crystal Ball "forecasts."

V−4. CFP PARAMETER ESTIMATION

The likelihood of a pipe flaw propagating to a significant structural failure is expressed by the conditional failure probability. With no service data available to support a direct statistical estimation of the conditional probability the assessment can be based on PFM, expert elicitation, or a combination of service data insights, expert elicitation and PFM. A practical approach to calculating the CFP is to use a Bayesian approach in which the prior conditional failure probability uncertainty distribution is expressed by a Beta Distribution. The Beta Distribution takes on values between 0 and 1 and is defined

by two parameters *A* and *B* (or "α" and "β" in some texts). However, this approach suggests that an infinite number of combinations of *A* and *B* can lead to one value of CFP.

Another well accepted approach, in which *A* represents a specific consequence of a pipe failure (e.g. an energetic release of process medium) and B represents the overall failure experience. Data do not allow for assessing *A* as very often, $A = 0$. However, *B* can be determined in a robust manner as data is available to quantify *B*. Therefore, an approach consists in setting $A = 0.5$ or 1.0 and determining *B* based on available data. Although this approach has been well accepted, there is no technical justifications on why *A* takes on 0.5 or 1.0, other than being a conservative value.

Three-point approximations are widely used when assessing parameters of distributions because there is usually a good sense of what the median, and two bounds are (for instance 5th, 50th, 95th percentiles, or 2.5th, 50th, 98.5th percentiles). Extensive work has been performed to determine the best approximations of the mean and standard deviation of a beta distribution, based on three percentiles.

Under this assumption, statistical values of percentiles (the Pearson-Tukey approach) can be assessed by fracture mechanics experts and can be used to estimate the values of the parameters *A* and *B* of the Beta distribution. These values represent the prior distribution parameters. Subject matter experts often have a good estimate of the mean of the probability of failure. The prior can later be updated with experience data that are modeled with a binomial likelihood distribution. Whenever the current state-of-knowledge establishes a foundation for assessing the 5th, 50th, 95th percentiles of the conditional probability of failure, the subject matter expert can use the Pearson-Tukey approach to define a defensible set of prior distribution parameters. Figure V−3 illustrates the Pearson-Tukey approach as implemented in the DDM calculation scheme.

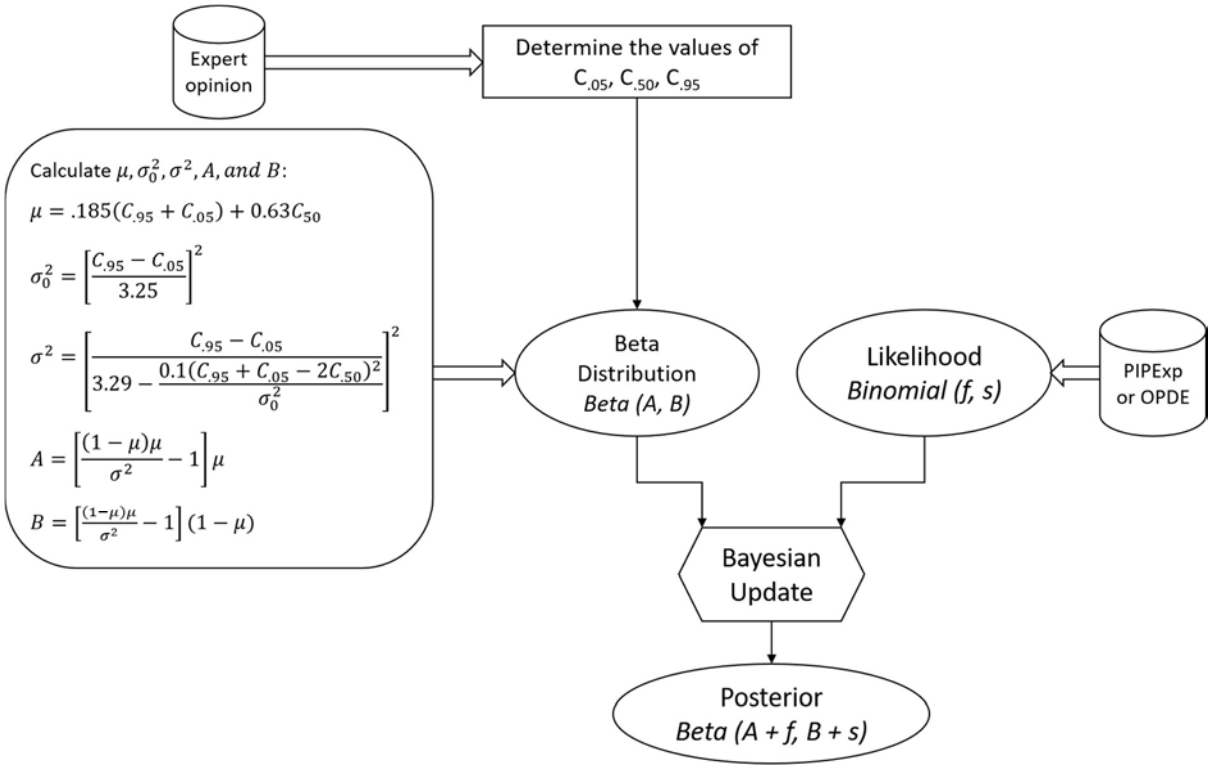

FIG. V−3. CFP parameter estimation.

The $C_{.05}$, $C_{.50}$ and $C_{.95}$ parameters in Fig. V–3 would be derived through PFM in which multiple sensitivity analyses are completed to assess the *A* and *B* parameters given a certain type of degradation mechanism and environmental conditions and loading conditions. As an example, assuming that a weld defect is discovered and confirmed to have been caused by high-cycle fatigue. PFM calculations could then be performed using different assumptions to calculate the probability of a complete through-wall circumferential crack, given certain assumptions about the dimensions and orientation of the crack. These assumption could be: a) the dimensions of the initial weld defect as discovered using non-destructive examination, b) a 50% through-wall circumferential crack, and c) leaking crack with a fixed crack length (e.g. *x* mm measured on the outside pipe diameter). The results could then be interpreted to represent low – medium –high CFP values and converted to the corresponding parameters of a beta distribution.

V–5. THE DDM TOOLSs

The DDM requires access to a pipe failure database that not only generates pipe failure population data, but also the information needed to define the exposure terms that correspond to a given pipe failure population. The determination of exposure terms considers the plant-to-plant variability in the population of pipe locations that are susceptible to material degradation.

Uncertainty propagation is performed through Monte Carlo simulation. There are a number of Monte Carlo simulation add-in tools that are compatible with the Microsoft® Excel software. The Oracle Crystal-Ball software was used in the CRP benchmark.

REFERENCES TO ANNEX V

[V–1] FLEMING, K., LYDELL, B., "Database Development and Uncertainty Treatment for Estimating Pipe Failure Rates and Rupture Frequencies," Reliability Engineering and System Safety, **86**:227-246, 2004.

[V–2] LYDELL, B., "The Probability of Pipe Failure on the Basis of Operating Experience," PVP-26281, Proc. ASME Pressure Vessel & Piping Division Conference, American Society of Mechanical Engineers, New York, NY, 2007.

[V–3] FLEMING, K., LYDELL, B., Pipe Rupture Frequencies for Internal Flooding Probabilistic Risk Assessments, 3002000079, Electric Power Research Institute, Palo Alto, CA, 2013.

[V–4] FLEMING, K., LYDELL, B., "Insights into Location Dependent Loss-of-Coolant-Accident (LOCA) Frequency Assessment for GSI-191 Risk-Informed Applications," Nuclear Engineering and Design, **305**:433-450, 2016.

[V–5] LYDELL, B., "A Review of the Progress with Statistical Models of Passive Component Reliability," Nuclear Engineering and Technology, **49**:349-359, 2017.

ANNEX VI
METHODOLOGY AND IMPLEMENTATION OF COMPUTER CODES (STEG)

The Tunisian Electricity and Gas Company (STEG) team applied the DDM approach. A computer code was developed to calculate the pipe failure rate by using Monte Carlo simulation.

VI–1. METHODOLOGY

The leak frequency is given with:

$$\lambda_L = \frac{n}{f.N.T} \quad \text{(VI–1)}$$

while the break frequency is defined using the following relation:

$$\lambda_B = P(Break|Leak).\lambda_L \quad \text{(VI–2)}$$

where:
λ_L: leak frequency
λ_B: break frequency
n: number of past leak events
N: number of Leak-relevant positions
T: operational time
f: fraction of the component exposure (=1)
P(Break|Leak): conditional rupture probability

In Monte Carlo simulation, some of these variables are considered as random variables following distribution functions shown in Table VI–1 and Fig. VI–1.

TABLE VI–1. RANDOM VARIABLES DISTRIBUTIONS IN PIPE BREAK FREQUENCY SIMULATION

Symbol	Distribution function	Parameters of the Distribution
n	χ^2 *distribution*	(=(7+0.5)/441, =2(7+0.5))
N	*Log-normal distribution*	(=3.65, =0.233)
P (Break|Leak)	β *distribution*	n (p=5.5, q=95.5)

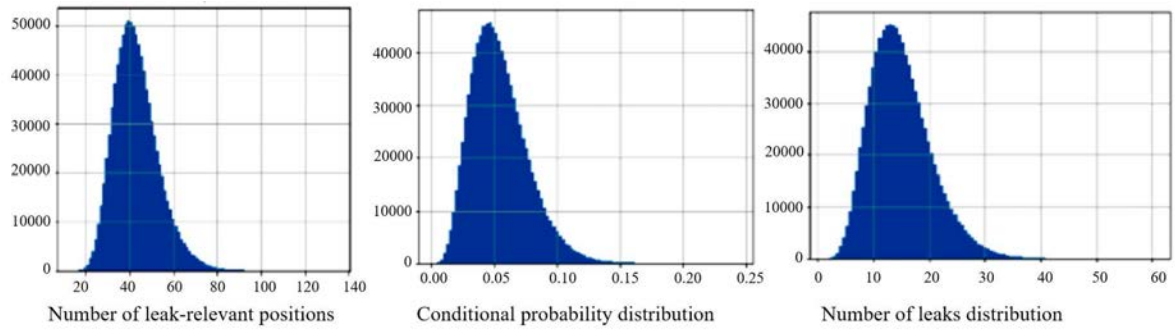

FIG. VI–1. Random variable distribution.

VI–2. RESULTS

The results obtained in the simulation are shown in Table VI–2.

TABLE VI–2. ESTIMATED LEAK AND BREAK FREQUENCIES

Parameter	Leak Frequency	Break Frequency
Expected value	8.341×10^{-4}	4.543×10^{-5}
5%-quantile	3.555×10^{-4}	1.305×10^{-5}
50%-quantile	7.712×10^{-4}	3.877×10^{-5}
95%-quantile	1.527×10^{-3}	1.004×10^{-4}

ANNEX VII
METHODOLOGY AND IMPLEMENTATION OF COMPUTER CODES (UIUC)

VII−1. GENERAL INTRODUCTION OF I-PPOF METHODOLOGY

An Integrated Probabilistic Physics-of-Failure (I-PPoF) methodological framework was developed to obtain probabilistic failure metrics of piping components (such as leak and rupture probabilities) by explicitly simulating the underlying physical degradation processes and maintenance activities [VII–1]–[VII–3]. The I-PPoF consists of four modules including: Renewal Process, Physics-of-Failure (PoF), Maintenance Work Process (MWP), and Interface.

The I-PPoF methodological framework has the following features:

- The PoF module has the capability to model two dominant degradation mechanisms of piping: thermal fatigue and primary PWSCC;
- In the PoF module, results of FEA of thermo-mechanical analysis are coupled with crack initiation and propagation models;
- RIM activities are analyzed explicitly in the MWP module by modeling and quantifying RIM scenarios and human performance using a Human Reliability Analysis (HRA)-based approach;
- The Renewal Process module simulates the interactions between physical degradation processes and RIM activities over time;
- The Interface module is equipped with a comprehensive uncertainty analysis, separating aleatory and epistemic uncertainties. Aleatory uncertainties are quantified by a sampling-based uncertainty propagation technique in the Interface module. Based on the results of the uncertainty propagation, the inputs to the Renewal Process module are estimated. Epistemic uncertainties are quantified by the Probabilistic Validation methodology to construct the uncertainty bounds for the estimations of the probabilistic failure metrics;
- The Interface module includes the capability of conducting Bayesian updating to combine the simulation-based estimation with the OPEX data when any relevant data is available;
- The Interface module also has the capability of conducting global sensitivity analysis to rank the input parameters based on their contribution to the probabilistic failure metrics estimates and the associated epistemic uncertainty.

VII−2. RENEWAL PROCESS MODULE IN I-PPOF

For the Renewal Process module, a multi-phase Markov process (MPMP) model is used to simulate the interactions between physical degradation processes and RIM activities. In the MPMP model, two phases are considered: the operational; and the ISI. During the operation phase, the piping component is subjected to physical degradation, while the leak monitoring is conducted. During the ISI phase, the plant is shut down for an outage, and various RIM activities such as flaw and leak inspections and repair/replacement are conducted. The MPMP model structure includes multiple discrete states representing various degrees of component damage and failure states (S_1,…,S_K in Fig. VII–1), such as flaw, undetectable leak, detectable leak, and rupture. The transition rates and probabilities for the degradation and RIM paths (denoted by $\lambda_{i,j}$ and $\mu_{i,j}$ in Fig. VII–1) are estimated by the outputs of the

uncertainty propagation for the PoF module by and of the MWP module, respectively. Subsections VII–2.1 and VII–2.2 explain the MPMP model for the first and second CRP benchmark case studies, respectively.

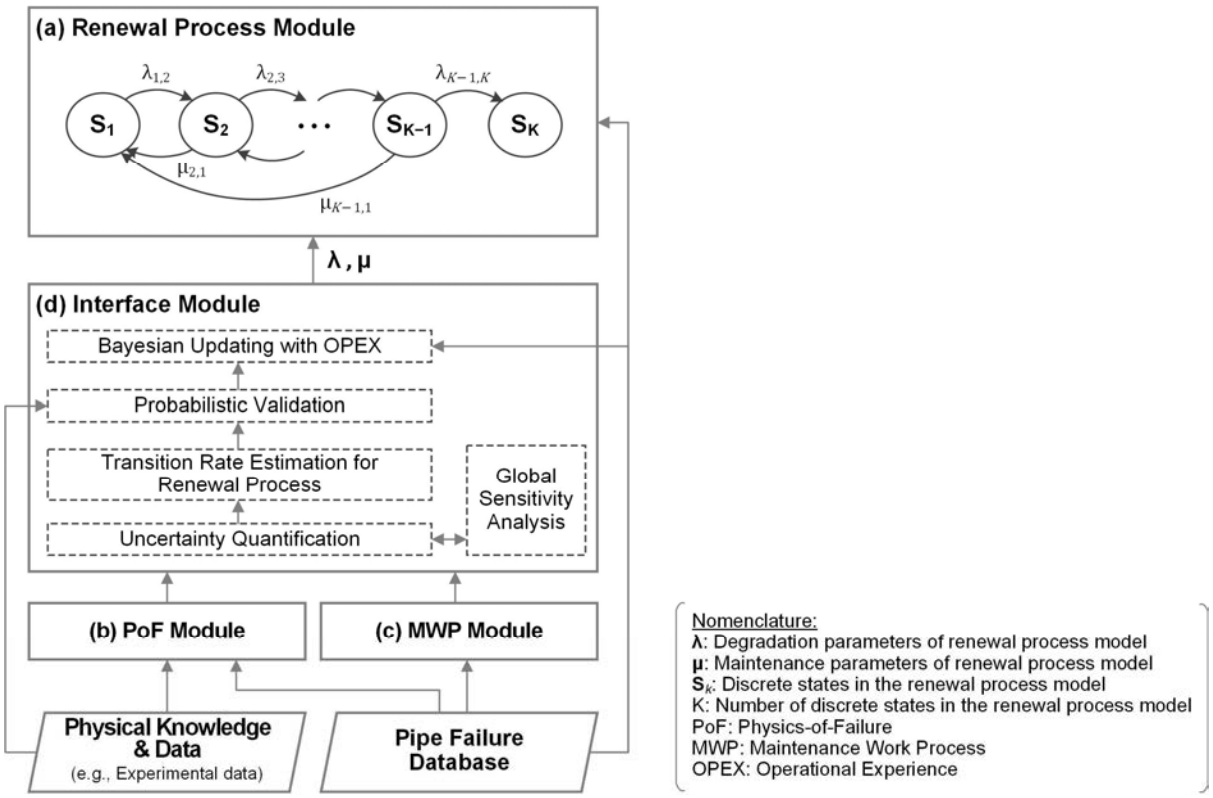

FIG. VII−1: I-PPoF methodological framework [VII−2].

VII−2.1. Renewal process module for the first CRP benchmark case study

Figure VII–2 illustrates the MPMP model developed for the first benchmark study (Section 3.3). Four damage states are defined as follows:

- *New* state: No defect on the inner surface with crack depth greater than 3 mm, which is the threshold for crack initiation [VII−4].
- *Flaw* state: The component has an axial part through-wall crack exceeding 3mm depth before reaching a through-wall crack (<80% wall thickness) [VII−5].
- *Leak* state: The component has an axial through-wall crack.
- *Rupture* state: Rapid, uncontrolled crack propagation to complete failure and separation.

During the operational phase (‘A’ of Fig. VII–2), the piping component is subjected to physical degradation. In the ISI phase (‘B’ of Fig. VII–2), the plant is assumed to be in an outage while flaw and leak inspections are performed. The degradation transition rates (φ and λ) are estimated from the PoF module, while the RIM transition probabilities (P_{FD} and P_{LD}) are estimated from the MWP module. The degradation transition rates for the transition paths to rupture (ρ and γ) are obtained from [VII–6].

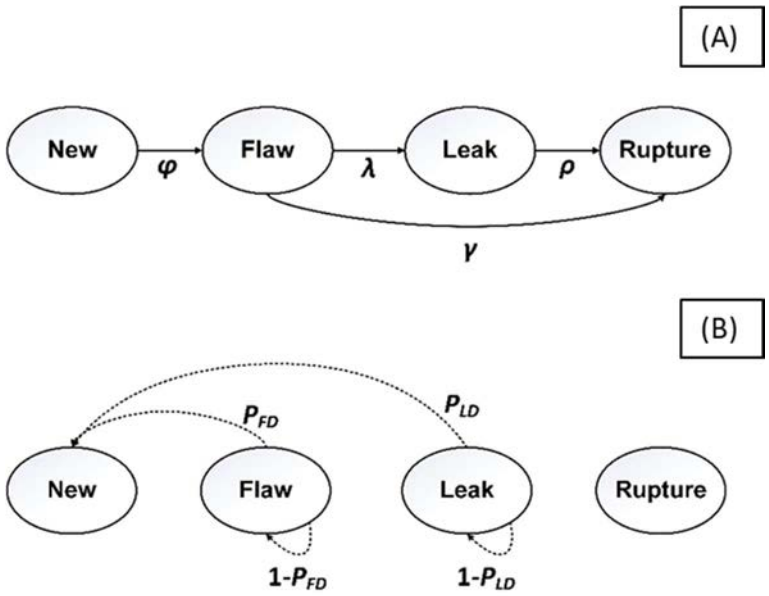

FIG. VII−2: MPMP model structure for the first CRP benchmark study; (A) operational phase and (B) ISI phase.

VII−2.2. Renewal process module for the second CRP benchmark case study

Figure VII–3 illustrates the MPMP model developed for the second benchmark study (Section 3.4.1). Eight damage states are defined as follows:

- *New* state: No defect on the inner surface greater than 15% of the wall thickness, which is the maximum allowable flaw size for DMWs specified in Section IWB-3514.4 of the ASME BPVC Section XI [VII−7].
- *Flaw* state: The component has a circumferential part through-wall crack exceeding 15% of the wall thickness.
- *Leak0* state: A part through-wall crack reaching a through wall crack, with a leak rate lower than the minimum leak detection limit of the Leak Monitoring System (LMS). Based on the Technical Specification of AP1000 [VII−8], a minimum detectable leak rate of 0.05 gpm[9] (~0.032 lps) is selected.
- *Leak1* state: A through wall crack with a leak rate more than 0.05 gpm (~0.032 lps) but less than 0.5 gpm (~0.32 lps). Per the Technical Specification of AP1000, if an unidentified leakage from the RCS exceeds 0.5 gpm (~0.32 lps), the plant needs to be shut down [VII−8].
- *Leak2* state: A through wall crack with a leak rate greater than 0.5 gpm (~0.32 lps).
- *Rupture* state: A part through-wall crack or through wall crack becomes unstable and satisfies the rupture criteria, which will be discussed in Section 4.3.
- Two repair states, *Leak Repair1* and *Leak Repair2*, representing the repair from the *Leak1* and *Leak2* states initiated by the leak detection, respectively.

[9] A gallon per minute (US gallon, gal/m or gmp) is unit of volume flow rate equal to a gallon flow per minute: 1 gallon per minute (US) = 0.0630901964 liters per second (lps).

During the operational phase ('A' of Fig. VII–3), the piping component is subjected to both physical degradation and RIM activities. In the ISI phase ('B' of Fig. VII–3), the plant is in an outage, and the component is subjected to only maintenance in the form of flaw or leak inspections. The degradation transition rates (φ, γ, λ_i, and ρ_i, where i = 0, 1, and 2) are estimated from the PoF module, and the RIM transition probabilities and maintenance transition rates (P_{FD}, P_{LD0}, P_{LD1}, P_{LD2}, μ_1, μ_2, υ_1, and ω_2) are estimated from the MWP module.

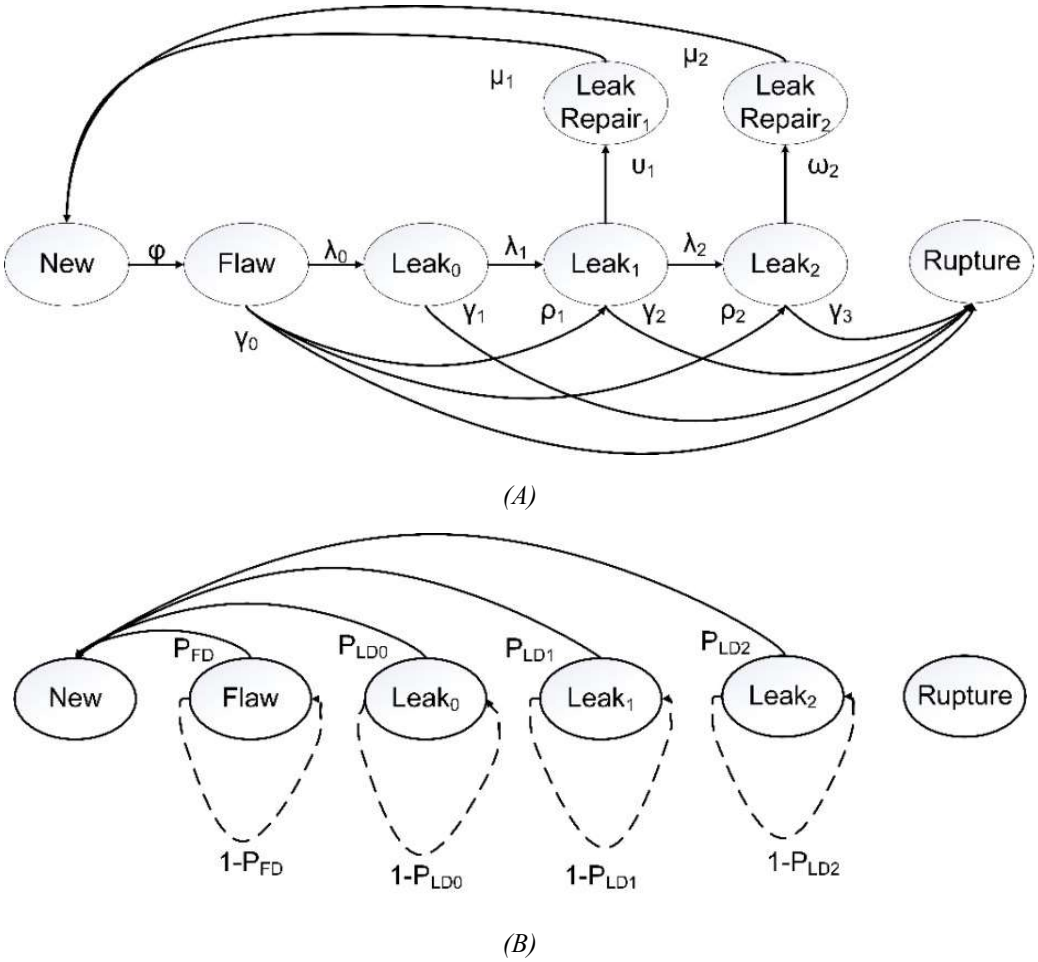

FIG. VII–3: MPMP model structure for the second CRP benchmark case study; (A) operational phase and (B) ISI phase.

VII–3. PHYSICS-OF-FAILURE MODULE IN I-PPOF

The I-PPoF methodological framework is developed with a "modularized design," where different types of models can be plugged in without changing the overall structure of the methodological framework. In the current version, the PoF module was developed for two dominant degradation mechanisms of the RCS piping, i.e. thermal fatigue and PWSCC.

VII–3.1. Physics of failure module for thermal fatigue

The PoF module developed for thermal fatigue in the first benchmark study (Section 3.3) is described. The thermal fatigue submodule covers multiple physical processes underlying damage and failure of

piping: (1) fluid dynamics, (2) thermal-stress analysis, (3) crack initiation, and (4) crack propagation as shown in Fig. VII–4.

The PoF module developed for thermal fatigue uses (i) a correlation-based model for characterizing the fluid temperature distribution, (ii) a mechanistic model for thermal-stress analysis using FEA by treating the fluid temperature distribution as the boundary condition, (iii) correlation-based models (S-N curve) for crack initiation considering spatial and temporal stress distribution from FEA, (iv) a mechanistic model for the SIF estimation considering the spatial and temporal temperature distribution from FEA, and (v) a correlation-based model for crack propagation with consideration of the depth-dependent SIF estimation. Subsections VII–3.1.1to VII–3.1.4.describe each submodule.

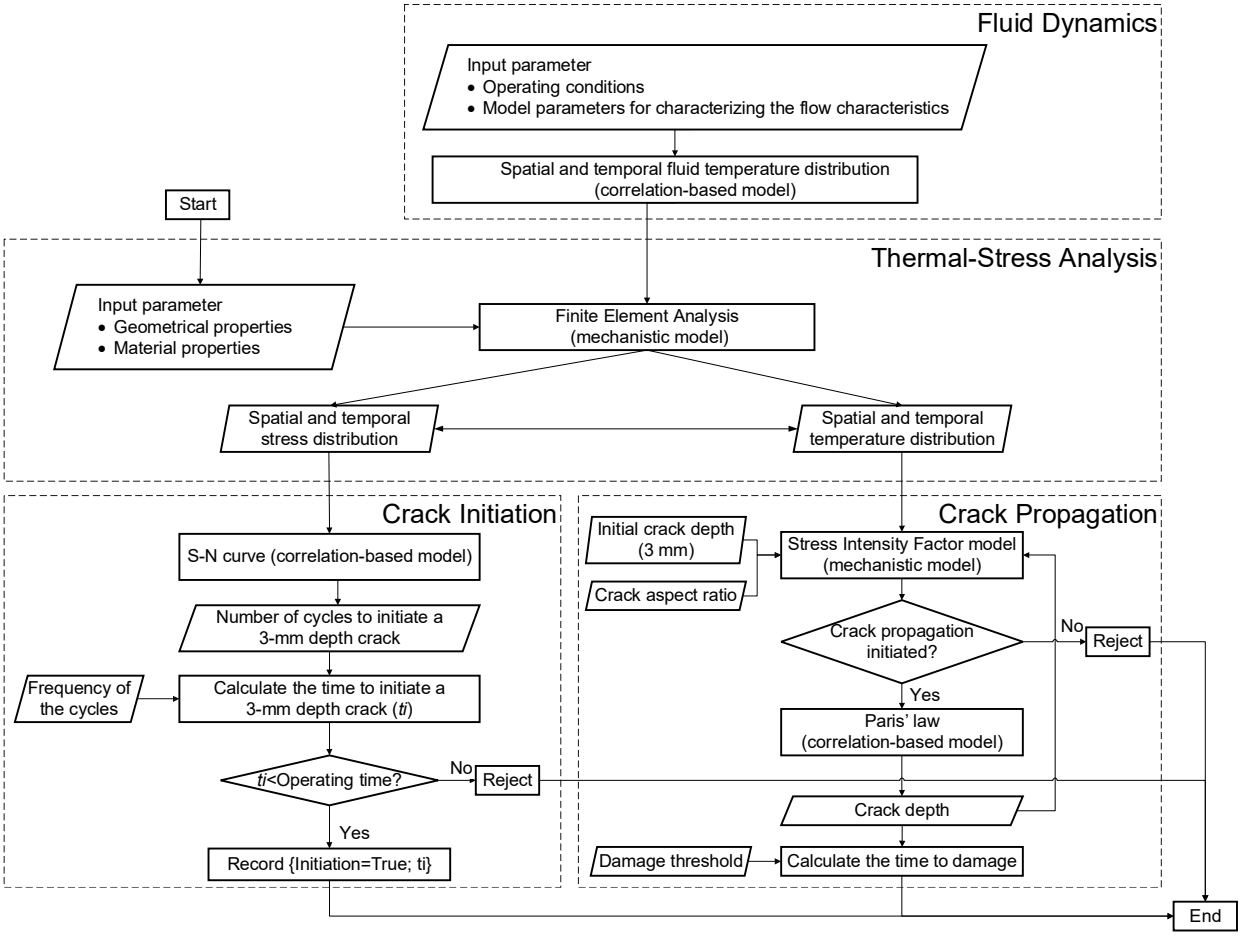

FIG. VII–4: A flow chart for the PoF module used for piping component subjected to thermal fatigue.

VII–3.1.1. Fluid dynamics

For piping containing hot and cold fluid, the initial temperatures of both fluids and temperature fluctuations have a significant impact on the thermal stress distribution. For piping component subjected thermal stratification, the temperature distribution is assumed to follow a hyper-tangent function [VII–9]–[VII–11] as:

$$T_f(z,t) = \frac{T_{f,h}-T_{f,c}}{2} * Tanh\left[c * \left(z - \left(z_1 + \frac{2*d_{SL}}{t_c} * t\right)\right)\right] + \frac{T_{f,h}+T_{f,c}}{2} \quad \text{(VII–1)}$$

where z is the vertical coordinates of the nodes on the pipe in mm and t is the real time in seconds. $T_{f,h}$ is the hot fluid temperature and $T_{f,c}$ is the cold fluid temperature. t_c is the period of the cyclic stratification layer. c is the factor related to the thickness of the stratification layers representing the region that has a temperature gradient when transitioning from the cold layer to the hot layer. d_{SL} is the half displacement of the stratification layer in one cycle. z_1 is the initial centroid position of the stratification layer.

VII–3.1.2. Thermal stress analysis

The spatial and temporal stress and temperature distributions as inputs to the crack initiation and crack propagation models are calculated by FEA. The temperature-dependent material properties and true stress-strain curves are included in FEA. The fluid boundary condition is characterized by Eq. (VII–1). The heat transfer coefficients at the inner and outer surfaces are calculated by a correlation-based model [VII–12] and engineering judgment, respectively. A location with the highest Von Mises stress, which is the most vulnerable place for crack initiation and propagation, is identified from FEA. The maximum hoop stress ranges (ΔS) at this location is calculated by the stress variation occurring within one period of the cycle. Since the crack being analyzed is axial, hoop stress is selected by assuming a Mode I behavior. The hoop stress and wall temperature of the first period of the cycle are sensitive to the initial conditions, therefore, the hoop stress and wall temperature for the second cycle are used as an input to the crack initiation model.

VII–3.1.3. Crack initiation model

The number of cycles required to initiate a 3-mm-depth crack (N_i) is obtained using the fatigue life curves from NUREG-6674 [VII–4] for stainless steel in water:

$$\ln[N_i(x)] = 5.841 + 0.52F^{-1}[x] -$$

$$2.172 * ln\{\varepsilon_a - 0.108 + 0.026F^{-1}[1-x]\} + T^{\Delta}\dot{\varepsilon}^{\Delta}O^{\Delta} - \ln(4) \qquad \text{(VII–2)}$$

where ε_a is the applied strain amplitude, and $T^{\Delta}, \dot{\varepsilon}^{\Delta}, O^{\Delta}$ are defined as follows:

$$T^{\Delta} = \begin{cases} 0 & T < 200^{\circ}C \\ 1 & T \geq 200^{\circ}C \end{cases}$$

$$\dot{\varepsilon}^{\Delta} = \begin{cases} 0 & \dot{\varepsilon} > 0.4\ \left(\frac{\%}{\text{sec}}\right) \\ \ln\left(\frac{\dot{\varepsilon}}{0.4}\right) & 0.0004 \leq \dot{\varepsilon} \leq 0.4\ \left(\frac{\%}{\text{sec}}\right) \\ \ln\left(\frac{0.0004}{0.4}\right) & \dot{\varepsilon} < 0.0004\ \left(\frac{\%}{\text{sec}}\right) \end{cases}$$

$$O^{\Delta} = \begin{cases} 0.260 & DO < 0.05\ ppm \\ 0.172 & DO \geq 0.05\ ppm \end{cases}$$

T, $\dot{\varepsilon}$,, and DO are testing temperature, strain rate, and dissolved oxygen concentration, respectively. $F^{-1}[x]$ is the inverse cumulative distribution function of a standard normal distribution. x in Eq. (VII–2) is the random variable ranging from 0 to 1, representing the family of fatigue life curves. The current PoF module for thermal fatigue utilizes the Ramberg-Osgood type Eq. [VII–13] and Eq. [VII–14] to

construct the relationship between the applied stress amplitude (σ_a) and the applied strain amplitude (ε_a):

$$\varepsilon_a = \frac{\sigma_a}{E} + \alpha\left(\frac{\sigma_a}{\sigma_y}\right)^n \quad \text{(VII–3)}$$

where E, α, and n are the elastic modulus, Ramberg-Osgood parameter, and the Ramberg-Osgood exponent, respectively. As inputs to Eq. (VII–3), the applied stress amplitude and the temperature are obtained from the FEA results.

VII–3.1.4. Crack propagation

A correlation-based model for estimating the fatigue crack propagation rate (CPR) is adopted from the code case N-809 of ASME BPVC.CC.NC.XI [VII–15]. The initiated 3-mm-depth crack starts propagation once the threshold of the SIF (K_{th}) is exceeded:

$$\frac{da}{dN} = C S_T S_R S_{ENV} (\Delta K)^n \quad \text{(VII–4)}$$

where:

$$C = \begin{cases} 9.10E-6 & for\ \Delta K \geq K_{th} \\ 0 & for\ \Delta K < K_{th} \end{cases}, \Delta K = K_{max} - K_{min}$$

$n=2.25$

$$S_T = \begin{cases} e^{-\frac{2516}{T_K}} & for\ 423.15 \leq T_K \leq 616.15 \\ (3.39E-5) * e^{\left[-\frac{2516}{T_K} - 0.0301 T_K\right]} & for\ 293.15 \leq T_K < 423.15 \end{cases}$$

$$S_R = \begin{cases} 1.0 & for\ R < 0 \\ 1 + e^{8.02*[R-0.748]} & for\ 0 \leq R < 1.0 \end{cases}, R = K_{min}/K_{max}$$

$$S_{ENV} = T_R^{0.3}$$

where T_K is the metal temperature obtained from the FEA results. K_{max} and K_{min} are the maximum and minimum SIF at the crack tip, respectively. The SIF solution from ASME FFS-1 [VII–5] is as follows:

$$K_I = \left[\sigma_0 i_0 + \sigma_1 i_1 \left(\frac{a}{t}\right) + \sigma_2 i_2 \left(\frac{a}{t}\right)^2 + \sigma_3 i_3 \left(\frac{a}{t}\right)^3\right] \quad \text{(VII–5)}$$

where:

$$\sigma_0 = 2P\left(\frac{r_e^2}{r_e^2 - r_i^2}\right) + \frac{E\alpha\theta_1}{2(1-\nu)} \frac{2r_i}{3t}\left[\frac{2r_e^2}{r_i(r_e + r_i)} - 1\right]$$

$$\sigma_1 = -2\frac{t}{r_i} P\left(\frac{r_e^2}{r_e^2 - r_i^2}\right) - \frac{E\alpha\theta_1}{2(1-\nu)} \frac{4}{3}\left[\frac{r_e^2}{r_i(r_e + r_i)} + 1\right]$$

$$\sigma_2 = 3\left(\frac{t}{r_i}\right)^2 P\left(\frac{r_e^2}{r_e^2-r_i^2}\right) + \frac{E\alpha\theta_1}{2(1-\nu)}\frac{2t}{r_i}\left[\frac{r_e^2}{r_i(r_e+r_i)}\right]$$

$$\sigma_3 = -4\left(\frac{t}{r_i}\right)^3 P\left(\frac{r_e^2}{r_e^2-r_i^2}\right) + \frac{E\alpha\theta_1}{2(1-\nu)}\frac{8}{3}\left(\frac{t}{r_i}\right)^2\left[\frac{r_e^2}{r_i(r_e+r_i)}\right]$$

where θ_1 , from FEA results, is the temperature difference within one cycle. t is the wall thickness of the pipe with inner radius (r_i) and outer radius (r_e). E is the elastic modulus in the unit of MPa. α is the thermal expansion coefficient in the unit of (mm/mm K). ν is the Poisson ratio. P is the internal pressure of the pipe.

VII–3.2. Physics-of-failure module for PWSCC

The PoF module developed for PWSCC in the second benchmark study (Section 3.4.1) is described. The PWSCC submodule covers multiple physical processes: (1) crack initiation, (2) crack propagation, (3) crack instability, and (4) leak rate calculation. The PoF flow chart to integrate the four physical processes is shown in Fig. VII–5.

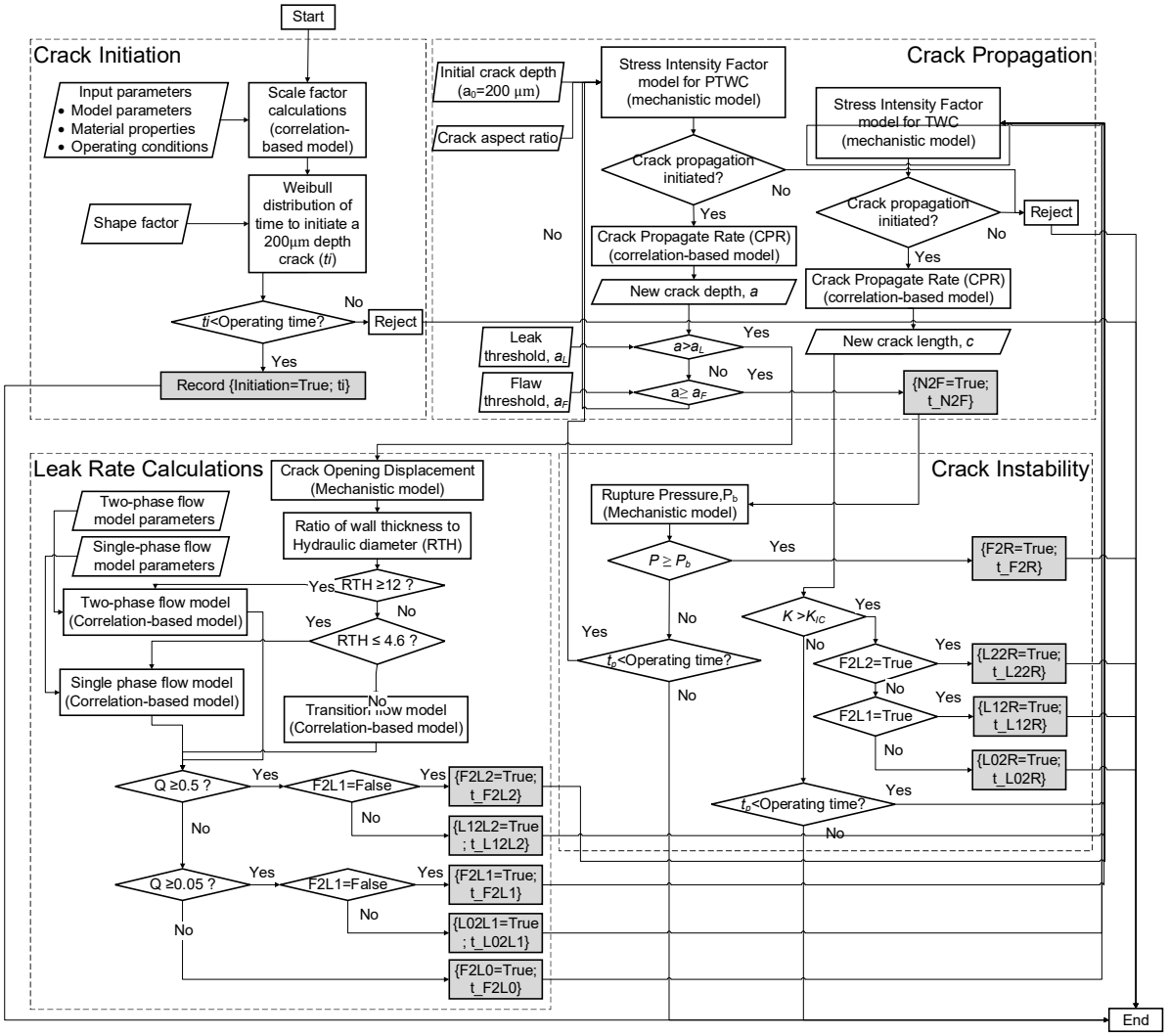

FIG.VII–5. Flow chart for PoF module used for piping component subjected to thermal fatigue.

The time to initiate a 200 μm depth circumferential crack is calculated from the correlation-based crack initiation model. The initiated part through-wall crack can propagate, if the SIF values exceed a threshold value. Once the part through-wall crack reaches the *Flaw* state (i.e., 15% wall thickness), the transition from New to Flaw and the time from *New* to *Flaw* (*t_N2F*) are recorded. Once it reaches the *Flaw* state, the instability of the part through-wall crack would be evaluated based on the crack instability model. The transition from *Flaw* to *Rupture* and the time from *Flaw* to *Rupture* (*t_F2R*) are recorded if the part through-wall crack becomes unstable. The stable part through-wall crack continues to propagate to a through-wall crack if there is an allowable operating time. The transition from *Flaw* to *Leak0, Flaw* to *Leak1, Flaw* to *Leak2* and the time from *Flaw* to *Leak0* (*t_F2L0*), *Flaw* to *Leak1* (*t_F2L1*), and *Flaw* to *Leak2* (*t_F2L2*) are recorded depending on the leakage rates calculated from the leak rate models. The through-wall crack would propagate in circumferential directions from a smaller leak to a larger leak. The transition from *Leak0* to *Leak1, leak1* to *Leak2* and the time from *Leak0* to *Leak1* (*t_L02L1*), *Leak1* to *Leak2* (*t_L12L2*) are recorded. A rupture is reached once a through-wall crack becomes unstable. The crack initiation, crack propagation, crack instability models, and leak rate models for PWSCC are described in Subsections VII–3.2.1 through VII.3.2.4.

VII–3.2.1. Crack initiation

The time to crack initiation for piping component subjected to PWSCC is assumed to follow a Weibull distribution:

$$F(t_i) = 1 - e^{[-(\frac{t_i}{\theta})^b]} \tag{VII–6}$$

where *F(t)* is the cumulative distribution function, and t_i represents the time to initiate a crack with 200 μm depth. The shape factor (b) and the scale factor (θ) are material dependent parameters. For instance, the following correlation-based model shows the scale factor used for alloy 52/152 suggested in MRP-111 [VII–16].

$$\theta_{52/152} = \frac{1}{FOI_i}\eta_{ref}\left(\frac{\sigma_y}{\sigma_p+\sigma_{wrs}}\right)^4 e^{\frac{Q_i}{R}[\frac{1}{T}-\frac{1}{633.15}]} e^{0.0013\,([H_2]-29.2)^2} \tag{VII–7}$$

where FOI_i is the factor of improvement for crack initiation obtained from the experimental data. σ_y is the yield stress of the material. σ_p is the applied stress due to internal pressure while σ_{wrs} is the WRS. Q_i is the activation energy for crack initiation in the unit of kJ/mole. T is the Operating temperature in unit of Kelvin (K). $[H_2]$ is the dissolved hydrogen concentration in the unit of cc/kg STP. The applicable temperature and hydrogen concentration ranges of Eq. (VII–7) are from 593.15 K to 603.15 K and 30 cc/kg to 50 cc/kg STP, respectively.

VII–3.2.2. Crack propagation

The CPRs for component subjected to PWSCC is typically estimated based on the correlation-based models. For example, the CPR for alloy 52/152 recommended by MRP-386 [VII–17] and MRP-115 [VII–18] is estimated based on the following:

$$\left(\frac{da}{dt}\right)_{52/152} = \frac{1}{FOI_p}\varepsilon f_{weld} f_{alloy} f_{orient} {K_I}^{\beta} exp\left[-\frac{Q_g}{R}\left(\frac{1}{T}-\frac{1}{598.15}\right)\right] \quad \text{(VII–8)}$$

where $\left(\frac{da}{dt}\right)_{52/152}$ is CPR in the depth direction for alloy 52/152, and FOI_p is the FOI for crack propagation. The ε is the fitting coefficient based on experimental data. f_{weld} is the weld factor to consider the weld to weld variability. f_{alloy} is the factor associated with the material type. f_{orient} is the factor associated with the orientation of the defect. T is the operating temperature in the unit of K. Q_g is the activation energy for crack propagation in the unit of kJ/mole. β is the exponent of CPR. K_I is the mode I SIF as a function of crack depth, crack length and the applied stress. The SIF solution for a part through-wall crack from Zahoor et al. [VII–19] considering the axial stress due to internal pressure, bending moment and WRS is applied. The SIF solution for through-wall crack is adopted from Anderson's solution [VII–20].

VII–3.2.3. Crack instability

For a component subjected to PWSCC, both the rupture pressure criterion [VII–21] and the net section collapse criterion [VII–22] are used. A part through-wall crack C reaches rupture when the operating pressure exceeds the rupture pressure given a specific crack size. If the rupture pressure criterion is not satisfied, the net section collapse moment (M_c) is calculated for each crack size and compared with the applied bending moment (M_b), as shown in Eq. (VII–9) [VII–22]. If the criterion in Eq. (VII–9) is satisfied, a part through-wall crack immediately becomes a through-wall crack:

$$M_b > M_c = 2\sigma_f {R_m}^2 D_1\left[2\sin\beta - \frac{a_o}{D_1\theta}\sum_{k=0}^{\infty}\frac{(-1)^k}{(2k)!}\frac{\theta^{2k+2}}{2}\frac{\Gamma\left(\frac{2k+1}{k}\right)\Gamma(3/2)}{\Gamma(k+2)}\right] \quad \text{(VII–9)}$$

where, σ_f is the flow stress, R_m is the mean radius of the pipe, and A_c is the crack opening area. D_1 is the pipe wall thickness. The applied bending moment is assumed to be 4.28 MN-m. a_o is the maximum crack depth of a semi-elliptical circumferential crack. θ is the half azimuthal angle of a semi-elliptical circumferential crack. Equation (VII–9) is applicable when $\theta \leq \pi - \beta$, where β is calculated using the following:

$$\beta = \frac{\pi}{2} - \frac{a_o \pi\theta}{8D_1} - \frac{\pi {D_5}^2 P}{4\sigma_f R_m D_1} \quad \text{(VII–10)}$$

The part through-wall crack continues to grow in the depth direction if neither the pressure criterion nor the net section criterion is satisfied. The part through-wall crack becomes a through-wall crack if the net section criterion is met, or the crack depth reaches to 80% wall thickness. If the SIF for the through-wall crack exceeds the fracture toughness of the material or the azimuthal angle reaches the full circumference, through-wall crack is assumed to reach rupture.

VII–3.2.4. Leak rate calculation

The leak rate calculations included in the PoF module have the capability of calculating the leak rate at the exit plane for single-phase, two-phase, and transitional flow. As an input to the leak rate calculation, the COD, represented by δ, is required. The following shows an example for a constant-depth axial through-wall crack, [VII–23]:

$$\frac{\delta}{\delta_e} = \begin{cases} \frac{E\varepsilon_{ref}}{\sigma_{ref}} + \frac{1}{2}\left(\frac{\sigma_{ref}}{\sigma_y}\right)^2 \frac{\sigma_{ref}}{E\varepsilon_{ref}} \\ \left(\frac{E\varepsilon_{ref}}{\sigma_y} + \frac{1}{2}\frac{\sigma_y}{E\varepsilon_{ref}}\right)\left(\frac{\sigma_{ref}}{\sigma_y}\right)^{n_1-1} \end{cases} \quad \text{(VII–11)}$$

where the reference strain (ε_{ref}), reference stress (σ_{ref}), and COD for elastic behavior (δ_e) are calculated as following:

$$\sigma_{ref} = \frac{P\sigma_y}{(\psi(\rho)*P_L)}$$

$$\varepsilon_{ref} = \varepsilon_0 * \left(\frac{\sigma_{ref}}{E} + \alpha\left(\frac{\sigma_{ref}}{\sigma_y}\right)^n\right)$$

$$\delta_e = \frac{4\left(\frac{PR_m}{2t}\right)cV}{E}$$

$$\psi(\rho) = \begin{cases} -0.06\rho^2 + 0.21\rho + 0.82 \; for \; \rho < 1.5 \\ 1 \qquad\qquad\qquad\qquad for \; \rho \geq 1.5 \end{cases}$$

$$P_L = \frac{\sigma_y t}{R_m}\left[\frac{1}{0.614 + 0.87542\rho + 0.386 * e^{(-2.275\rho)}}\right]$$

$$\rho = \frac{c}{\sqrt{R_m t}}$$

P stands for the internal pressure in the piping components. *V* is the shape factor calculated based on the FEA results [VII–23]. Another input that is important in calculating the leak rate is the crack hydraulic diameter. The two-phase flow model based on the Henry and Fauske models [VII–24]–[VII–26] is applied when the ratio of wall thickness to the hydraulic diameter is greater than 30. The single phase flow model from PRAISE is applied when the hydraulic diameter is smaller than 4.6, [VII–27]–[VII–30]. If the hydraulic diameter is between 4.6 and 30, the transition-flow model from PRO-LOCA is applied, [VII–31].

VII−4. MAINTENANCE WORK PROCESS MODULE OF I-PPOF

For the development of the MWP module, an analyst has two options: a DDM [VII–1] [VII–2] and an HRA-based method [VII–31] [VII–32]. The DDM quantifies the RIM transition rates in the Renewal Process module as a function of multiple maintenance parameters estimated from empirical data such as service data and experiments. In contrast, the HRA-based method constructs maintenance scenarios using an Event Tree model, where the RIM process is decomposed into smaller maintenance tasks. The probability of the possible outcome of each task is estimated by existing HRA methods. The overall maintenance performance is then quantified by computing the probability and required time for each maintenance scenario in the Event Tree model. The DDM was used for the first CRP benchmark study (Subsection VII–4.1), while the HRA-based method was used for the second CRP benchmark study (Subsection VII–4.2).

VII−4.1. Maintenance work process module for the first CRP benchmark case study

In the first CRP benchmark case study (Section 3.3), the MWP module is developed using a DDM to analyze the RIM processes for the elbow pipe of CVC system in PWR. Three inspection strategies are

considered: i) Periodic ISI using Ultrasonic Testing, aimed at flaw detection; (ii) Visual inspection (VT-2) during each outage, aimed at leak detection; and (iii) Condition-based ultrasonic testing inspection based on the Usage Factor, aimed at flaw detection. The first of these strategies, ultrasonic testing for flaws, per Article IWB-2411 of the ASME Boiler and Pressure Vessel Code (ASME XI)[10], takes place during a refueling outage after 10 years have passed between inspections. The second of these strategies, VT-2, aimed at detecting leaks during the pressure test, takes place during every outage per Articles IWA-2212 and IWB-5222(a) of ASME XI]. When this type of inspection occurs, only leaks (not flaws) will be detected because the non-destructive examination technique is not used. The third strategy, the condition-based ultrasonic testing inspection based on UF, is performed using non-destructive examination when the computed UF exceeds unity. The calculation of UF is made based on ASME BPVC.III.A-2017, Mandatory Appendix XIII, XIII-3520[11]. At whatever time point the UF exceeds 1.0, the plant is assumed to implement an ultrasonic testing inspection. For the three inspection strategies, the POD of the inspection is computed based on the relationship between POD and crack depth (in mm) shown in Table VII–1, where the POD values for various thicknesses are used to linearly interpolate the estimated POD for the Flaw and Leak states, while the timing of each event is based on either the ASME Section XI standard[10] or the case study definition. The maintenance parameters used for each inspection strategy are summarized in the third column of Table VII–2.

TABLE VII−1. RELATIONSHIP BETWEEN POD AND CRACK DEPTH

Crack Depth (mm)	POD
0.0	0.00
2.8	0.50
4.5	0.80
5.6	0.90
6.7	0.95
9.0	0.98
12.0	1.00

TABLE VII−2. INSPECTION STRATEGIES AND THE ASSOCIATED INPUT PARAMETERS TO THE MULTI-PHASE (MP) MARKOV MODEL

Inspection Strategies	Timing	Transition Probabilities
ASME Section XI: UT	The first planned outage after a ten-year period	$P_{FD} = 0.894$
ASME Section XI: VT-2	Every planned outage (every 18 months)	$P_{LD} = 0.990$
Condition-based Inspection (Usage Factor): UT	Determined based on the fatigue design curve and the period of cyclic stress	$P_{FD} = 0.894$

VII−4.2. Maintenance Work Process Module for the second CRP Benchmark case study

In the second CRP benchmark case study (Section 3.4.1), the MWP module is developed using an HRA-based method to analyze the RIM processes for the DMW in the hot leg of RCS in an AP1000. Two possible RIM strategies for a rejectable flaw or a leak are considered: ISI and leak action as a result of leak detection by LMS. For the RIM scenarios initiated by flaw or leak detection by ISI, maintenance

[10] Following the American Society of Mechanical Engineers, ASME Boiler and Pressure Vessel Code, Section XI, Rules for Inservice Inspection of Nuclear Power Plant Components, New York, NY, 2021N

[11] Following the American Society of Mechanical Engineers, 2017 ASME Boiler and Pressure Vessel Code, Section III, Roles for Construction of Nuclear Power Plant Components, Division 1 – Subsection NB, Class 1 Components, New York, NY, 2017

Event Trees are developed to describe the possible RIM scenarios and the resulting state transition of the component (Figs. VII–6 and VII–7).

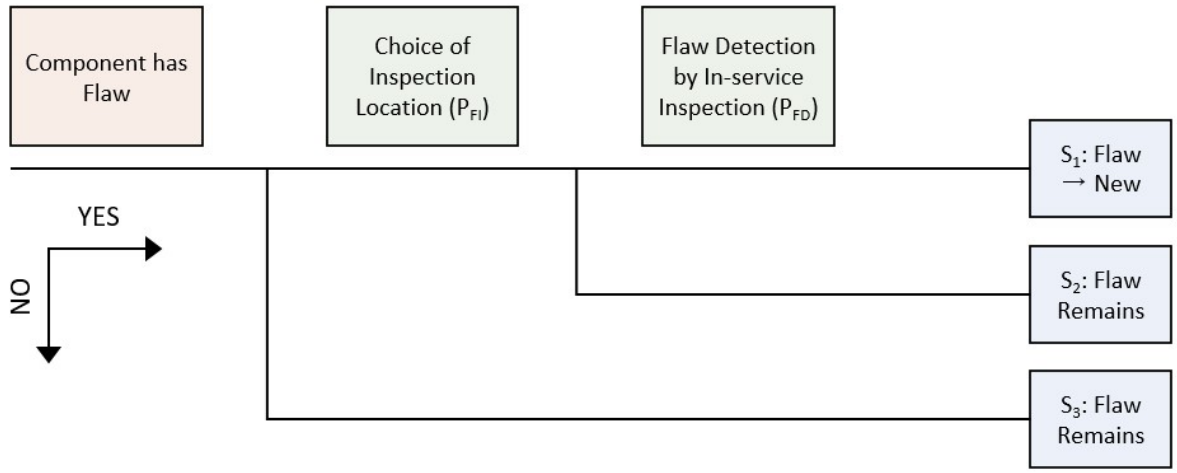

FIG.VII−6: Flaw maintenance Event Tree during ISI.

Maintenance-based Top Events related to the maintenance performance and program selection are colored green while physics-based Top Events related to the progression of physical degradation and associated damage states are orange. In these Event Trees, if the crack depth is between 15%–100% of the wall thickness, the component is considered to have a "Flaw", defined in Subsection VII–2.2. If the crack depth reaches 100% of wall thickness, the component is considered to have a "Leak." Although the size of the leak is explicitly indicated by a variable *x* in Fig. VII–7, this study assumes that the maintenance scenarios initiated by ISI are independent of the leak size. If the crack depth is less than 15% of the wall thickness, the component is considered as "New."

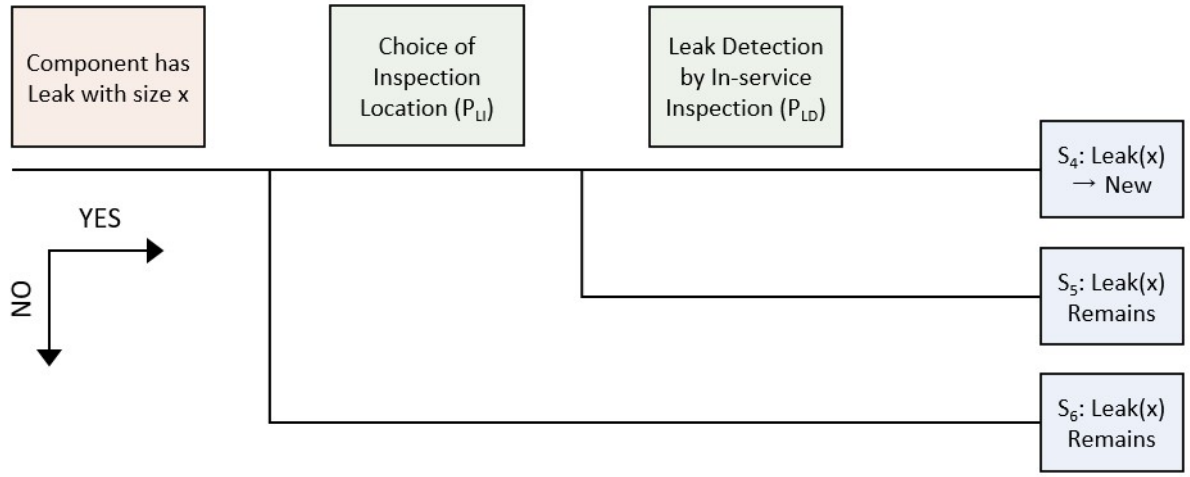

FIG.VII−7: Leak maintenance Event Tree during ISI.

Figure VII–6 is a maintenance Event Tree with the Initiating Event "Component has Flaw". In this case, we assume that a flaw in a component will occur prior to a leak and? can make the component more susceptible to further physical degradation. Two maintenance-based Top Events follow the Initiating Event and involve the selection of the inspection location and the detection of the flaw by ISI. Based

on the success or failure of these maintenance events, the flaw may remain (Scenarios S2 and S3), or the flaw will be repaired to return the component to a new condition (Scenario S1). In Fig. VII–7, the Initiating Event is "Component has an active leak of size *x*", where *x* can refer to the leakage rate of the component under full power operation. Following the Initiating Event, two Top Events, similar to those in Fig. VII–7, involving the choice of inspection location and the detection of the leak by ISI, are present in this Event Tree. The success or failure of these Top Events will either allow the leak of size x to remain (Scenarios S5 and S6) or the leak to be repaired and returned to a new condition (S4).

The quantification of the maintenance Event Trees requires the following input parameters:

- Probability of flaw inspection (P_{FI}): This value gives the probability that the component in the Flaw state will be selected for ISI, given that an inspection is occurring. It is assumed that the DMW being analyzed in this benchmark study is included in the ISI program; thus, $P_{FI} = 1$.
- Probability of flaw detection by ISI (P_{FD}): This value gives the probability that the flaw will be detected for a component in the Flaw state, given that the component is selected for ISI.
- Probability of leak inspection (P_{LI}): This value gives the probability that the component with a leak of size x will be selected for ISI, given that an inspection is occurring. It is assumed that the DMW being analyzed in this benchmark study is included in the ISI program; thus, $P_{LI} = 1$.
- Probability of leak detection by ISI (P_{LD}): This value gives the probability that the leak will be detected for a component with a leak of size x, given that the component is selected for ISI.

S1 in Fig. VII–8 and S4 in Fig. VII–9 results in a change in the state of the component, and the conditional probabilities associated with these end states are calculated as follows:

$$P(Flaw \rightarrow New) = P_{FI}P_{FD}. \tag{VII–12}$$

$$P(Leak \rightarrow New) = P_{LI}P_{LD}. \tag{VII–13}$$

The state transition probabilities in Eqs. (VII–12) and (VII–13) are divided by the mean-time-to-repair for the corresponding transition path to compute the maintenance transition rates for the renewal process model of the I-PPoF methodological framework [VII–32].

For the leak action path, we consider the possibility that the LMS will detect leakage that exceeds the Limiting condition for operation (LCO) for RCS operational leakage. The RIM scenarios due to leak detection by the LMS are shown in Fig. VII–8. Per the Standard Technical Specifications (STS) for AP1000 reactors, there are two primary ways that the leak action path will be initiated [VII–8]. In the first path, unidentified leakage in the form of an imbalance in the RCS water inventory exceeds 0.5 gpm (~0.032 lps) and is not brought below that value within 4 hours. If this LCO is not satisfied, the plant is required to move to lower pressure conditions by entering Mode 3 within 6 hours and Mode 5 within 36 hours (i.e., an unplanned shutdown occurs). This shutdown will prompt an inspection, and the maintenance activities will be initiated as shown in Fig. VII–8. In the second path to the leak action, the unidentified RCS operational leakage does not exceed 0.5 gpm (~0.032 lps), but upon inspection, the leakage is identified as reactor coolant pressure boundary leakage. In this inspection, the sources of leakage are located and evaluated to meet ASME standards. Additionally, an evaluation of the structural integrity of the pressure boundary is performed, [VII–33]. The LCO for reactor coolant pressure boundary leakage requires zero leakage at all times during operation. This path is also shown in Fig. VII–8. In either leak action path, the component will begin the leak repair of size *x* if the LCOs are not satisfied.

The Event Tree in Fig. VII–8 begins with the physics-based Initiating Event "Component has a Leak of size *x*", followed by two physics-based Top Events and two maintenance-based Top Events. In the first Top Event, it is to be determined whether the leak rate is detectable by the LMS or it is to be defined as undetectable leakage. If the leakage is detectable, then the next Top Event specifies whether the leakage exceeds the unidentified leakage limit (0.5 gpm or ~ 0.031 lps). If the leakage rate exceeds this value, then the operators have 4 hours to reduce the leakage amount to one below this threshold; otherwise, an unplanned shutdown will occur. However, if the leakage is identified as reactor coolant pressure boundary leakage, then the component will need to undergo leak repair, regardless of the success or failure of previous Top Events. As a result of the success or failure of each Top Event, the component will either undergo leak repair following an unplanned shutdown (Scenarios S7, S8, S10, and S12) or the leak will remain (Scenarios S9 and S11).

The quantification of the maintenance Event Trees in Fig. VII–8 requires the following input parameters:

- Probability of leak rate exceeding detectability limit (P_{MD}): This value is dependent on the calculated leak rate from the PoF model and its comparison to the minimum detectable leak rate of 0.05 gpm [VII−33]. This probability is addressed as part of the degradation transition rates in the Renewal Process module; thus, it is not considered in the MWP module.
- Probability of unidentified leakage rate exceeding LCO Limit (P_{UL}): This value is dependent on the calculated leak rate from the PoF model and its comparison to the maximum unidentified leakage rate for RCS leakage of 0.5 gpm. This probability is addressed as part of the degradation transition rates in the Renewal Process module; thus, it is not considered in the MWP module.
- Probability of unidentified leakage rate not being reduced below LCO Limit for > 4 hours (P_{LL}): This value is dependent on the feasibility of isolating the leaking component to reduce leakage to an amount under the LCO limit within 4 hours. "reactor coolant pressure boundary leakage" is defined as leakage from a "non-isolable" crack in the RCS piping so, for this benchmark case study, it is assumed that there is no possibility of reducing the leakage within 4 hours such that the value of P_{LL} is 1.
- Probability of identifying leakage as reactor coolant pressure boundary Leakage (P_{RI}): The operators may conduct an inspection to identify the source of unidentified leakage that does not exceed the unidentified leakage LCO limit. Per the STS, this inspection will occur with certainty, so the value of P_{RI} is assumed to be 1 in this publication.

It is theoretically possible for an error in the LMS to report a lower than actual leakage rate which could improperly satisfy the LCO limit for unidentified leakage. However, within the scope of this benchmark case study, LMS are assumed to be 100% reliable in detecting leakage and determining the actual leakage rate. The following relation is used to calculate the conditional probability of the Leak of size *x* undergoing leak repair as in S7, S8, and S10:

$$P(Leak[x] \rightarrow New) = P_{MD}P_{UL}P_{LL} + P_{MD}P_{UL}(1 - P_{LL})P_{RI} + P_{MD}(1 - P_{UL})P_{RI} \quad \text{(VII–14)}$$

The state transition probability obtained from Eq. (VII–14) is divided by the mean-time-to-repair for the corresponding transition path to compute the maintenance transition rates for the Renewal Process module, [VII–32]. The descriptions and the values used for modeling RIM activities are shown in Table VII–3.

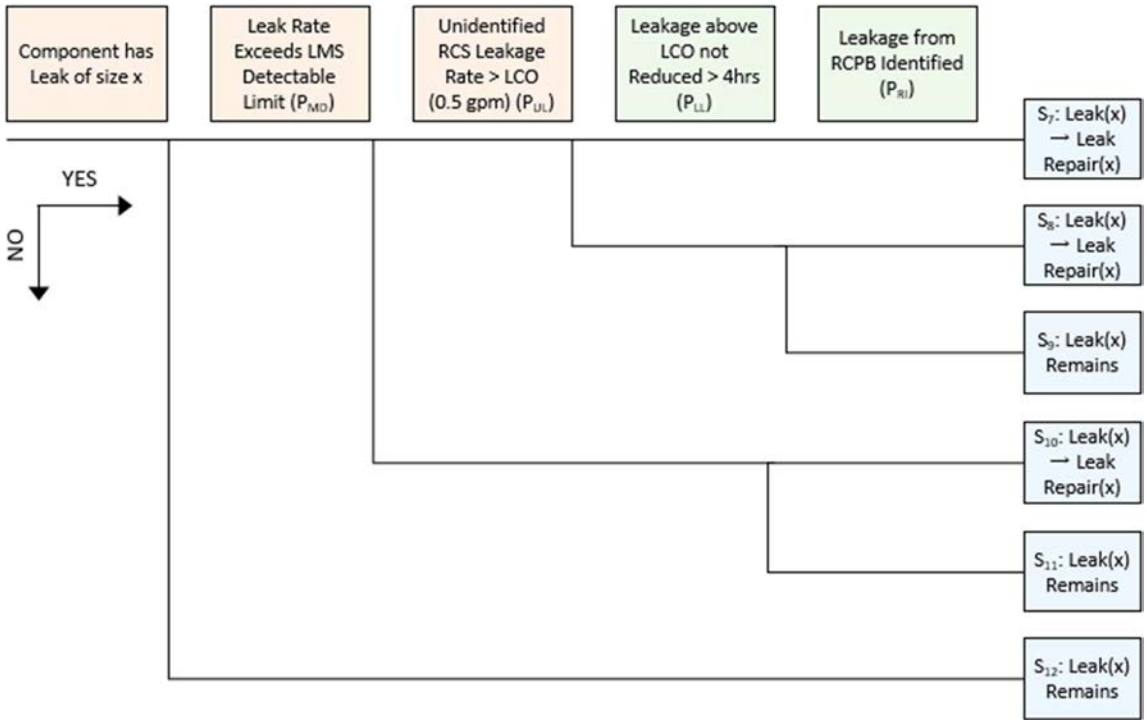

FIG.VII–8: Leak maintenance event tree during operation.

TABLE VII–3. PARAMETERS AND EQUATIONS USED FOR MODELING RIM ACTIVITIES

Parameter	Description	Value
P_{FD}	Probability of detecting component in Flaw state during ISI	0.85
$P_{LD,\,i}$	Probability of detecting component in Leak$_i$ state during ISI	0.99
T_{FI}	Inspection Interval for Flaw Inspection	10 years
T_{LI}	Inspection Interval for Leak Inspection	1.5 years
P_{RI}	Conditional probability that, given a leak less than 0.5 gpm has occurred at the hot leg nozzle and it is detected as unidentified leakage < 0.5 gpm by LMS, it is later identified as reactor coolant pressure boundary leakage by additional inspection	1
MTTLR$_i$	Mean-time-to-repair for component from LR$_i$ state to New state	137.1 hours
MTTS	Mean time to Shutdown reactor following leak detection by LMS	6 hours
ω_i	Transition rate from Leaki state with leak rate > 0.5 gpm to LR$_i$ state	1/MTTS 0.17 hours^{-1}
μ_i	Transition rate from LR$_i$ state to New state	1/MTTLR$_i$ 7.29E-3 hours^{-1}
υ_i	Transition rate from Leak$_i$ state to LR$_i$ state with leak rate between 0.05 gpm and 0.5 gpm	P_{RI}/MTTS 7.29E-3 hours^{-1}

VII–5. INTERFACE MODULE OF I-PPOF

To create a computational interface among the PoF, MWP, and Renewal Process modules, the Interface module performs four functions: (1) uncertainty quantification and transition rates estimation with consideration of aleatory uncertainty, (2) probabilistic validation with consideration of epistemic

uncertainty, (3) Bayesian updating to combine simulation-based estimation with OPEX data (if there is any relevant data available), and (4) global sensitivity analysis to rank input parameters. As part of the Interface Module, the uncertainty analysis is conducted. For the PoF and MWP modules, potential sources of uncertainty are identified based on literature and engineering judgment. Two groups of uncertainty sources are considered: (a) uncertainty associated with the input parameters (e.g., selection of the probability distributions and estimation of the distribution parameters) and (b) uncertainty related to the model structures and assumptions. The identified uncertainty sources are then categorized into two classes: aleatory uncertainty due to natural variability or randomness and epistemic uncertainty due to lack of knowledge.

The separation of aleatory and epistemic uncertainties is critical because, from the viewpoint of the interpretation of the results and further improvements of the models, the epistemic uncertainty can be reduced by adding resolutions to the selected models or collecting additional data, while the aleatory uncertainty cannot be reduced [VII–34]. In the I-PPoF framework, aleatory uncertainties are analyzed in the uncertainty quantification and estimation of the transition rates (Subsection VII–5.1), while epistemic uncertainties are analyzed by the probabilistic validation methodology (Subsection VII–5.2).

VII–5.1. Uncertainty quantification and transition rates estimation with consideration of aleatory uncertainty

In the first CRP benchmark case study, one of the main sources of aleatory uncertainty is the S-N curve for crack initiation. Based on the NUREG-6674, the aleatory uncertainty associated with the S-N curve is characterized by a standard normal distribution, [VII–33]. In the second CRP benchmark case study, three physical input parameters are identified as the most critical sources of aleatory uncertainty: time to crack initiation, initiated crack length, and crack aspect ratio. The aleatory uncertainty associated with the time to crack initiation is characterized by a Weibull distribution as shown in Eq. (VII–6). The aleatory uncertainty associated with the initiated crack length is characterized based on the test data provided in MRP-426, [VII–35] and [VII–36]. The aleatory uncertainty associated with the initiated crack length is characterized by a normal distribution with the 5th percentile equal to 700 μm and the 95th percentile equal to 1200 μm. For the crack aspect ratio, based on the recommended initiated crack depth from Fyfitch and Harrington, [VII–37], 200 μm is assumed to be the minimum initiated crack depth. In addition, the maximum initiated crack depth does not exceed the 15% wall thickness, which is defined as the maximum allowable flaw size. Based on these constraints, the crack aspect ratio is calculated to be between 1/6 and 17. According to ASME BPVC Section XI Article IWA-3300 (a)(3) [VII–7], the crack aspect ratio greater than 0.5 is rarely encountered. Considering all the information, the aleatory uncertainty associated with the crack aspect ratio is characterized by a uniform distribution with the lower limit of 1/6, and the upper limit of 0.5. These sources of aleatory uncertainty are then propagated in the PoF module by conducting the Monte Carlo simulation using simple random sampling. The number of samples that transitioned from one state (D_1) to another state (D_2), denoted by $N_{D_1D_2}$, and the time data for the observed transitions are recorded. The estimation of the degradation transition rates from D_1 to D_2 is based on the right-censored life test and uses the Bayesian inference. A Jeffreys non-informative prior, i.e., a Gamma distribution with $\alpha = 0.5$ and $\beta = 0$, is used. The likelihood function is a Poisson distribution, where the number of events is $N_{D_1D_2}$, while the total exposure time is $T_{D_1D_2}$. For instance, in the second CRP benchmark case study, $T_{D_1D_2}$ for each transition path in Fig. VII–3 is obtained using the following two relations:

$$T_{NF} = t_{int} + (N_S - N_{NF}) * t_o + \sum_{i=1}^{N_{NF}} t_{NF,i} \qquad \text{(VII – 15)}$$

$$T_{FL_j} = \sum_{i=1}^{(N_S - N_{FL_0} - N_{FL_1} - N_{FL_2})} (t_o - t_{NF,i}) + \sum_{i=1}^{N_{FL_0}} t_{FL_0,i} + \sum_{i=1}^{N_{FL_1}} t_{FL_1,i} + \sum_{i=1}^{N_{FL_2}} t_{FL_2,i} \quad , j = 0, 1, 2 \qquad \text{(VII – 16)}$$

where:
N_S: the number of samples
N_{NF}: the number of samples transitioned from New to Flaw within the mission time in the Monte Carlo simulation (t_o years). t_o is set as 60 (years).
N_{FL_0}: the number of samples transitioned from Flaw to Leak0 at t_o years
N_{FL_1}: the number of samples transitioned from Flaw to Leak1 at t_o years
N_{FL_2}: the number of samples transitioned from Flaw to Leak2 at t_o years
$t_{NF,i}$: the time from New to Flaw for the *i*th sample that experienced the New-to-Flaw transition
$t_{FL_0,i}$: the time from Flaw to Leak0 for sample i
$t_{FL_1,i}$: the time from Flaw to Leak1 for sample i
$t_{FL_2,i}$: the time from Flaw to Leak2 for sample i.

Due to the Gamma-Poisson conjugate property, the posterior distribution for each transition rate is a Gamma distribution with updated parameters, α'= α + $N_{D_1D_2}$ and β'= β + $T_{D_1D_2}$ [VII–38].

VII–5.2. Probabilistic validation with consideration of epistemic uncertainty

At the highest level, the probabilistic validation methodology is implemented in the following three steps:

1. Dominant sources of epistemic uncertainties are identified by conducting qualitative analysis (such as engineering judgment based on literature) and quantitative analysis (e.g., sensitivity study for the potential sources of epistemic uncertainty to screen out the non-influential factors);
2. The influential sources of epistemic uncertainties, retained in the first step, are characterized using probability measures. For instance, the epistemic uncertainties associated with the probability distributions representing aleatory uncertainties of the input parameters (e.g., type of the parametric probability distribution and estimation of the distribution parameters) can be characterized by assigning another layer of probability distribution;
3. The epistemic uncertainties characterized in the second step are propagated up to the level of the probabilistic failure metrics, i.e., the outputs from the Renewal Process module. For this purpose, an additional layer of statistical simulation (aside from the uncertainty propagation for aleatory uncertainties) is required. For instance, in the Interface module, a nested Monte Carlo method can be considered, where the outer and inner loops deal with the epistemic and aleatory uncertainties, respectively.

Subsections VII–5.2.1 and VII–5.2.2 describe the implementation of the probabilistic validation methodology for the two CRP benchmark case studies.

VII–5.2.1. Probabilistic validation for the first CRP benchmark case study

The epistemic uncertainties associated with the thermal stratification layer modeling in FEA are identified as major sources of uncertainty in the PoF module. Five FEA input parameters, including the HTC on the inside and outside surfaces, fluid temperature difference across the stratification layer,

displacement of the thermal stratification layer, and the period of the cycles, are identified as factors that can have significant impacts on the stress distribution in FEA. For each combination of the five key parameters (Table VII–4), the hoop stress range predicted by FEA, as well as the physical degradation transition rates estimated based on the uncertainty qualification outputs, are shown in Table VII–5.

TABLE VII−4. CHARACTERIZATION OF EPISTEMIC UNCERTAINTY FOR KEY INPUT PARAMETERS OF FEA

Parameter	h_i	h_o	ΔT	t_f	d_{SL}	**Probability weight**
Unit	W/m^2 K	W/m^2 K	K	sec	mm	
1	25,000	10	244.44	100	8	0.158
2	2500	10	244.44	100	8	0.294
3	1920	10	244.44	120	8	0.317
4	1920	10	244.44	300	8	0.181
5	1920	10	244.44	360	8	0.181
6	1920	10	244.44	300	66.65	0.034
7	100	10	244.44	100	8	0.113
8	100	10	244.44	300	8	0.065
9	1784	10	244.44	100	8	0.294
10	1784	10	116.67	100	8	0.317
11	1784	10	116.67	100	66.65	0.059

TABLE VII−5. DEGRADATION TRANSITION RATES OBTAINED BASED ON HOOP STRESS RANGES AND MAXIMUM AND MINIMUM WALL TEMPERATURE FROM FEA

Case Inner diameter	**Probability weight**	**S_h (MPa)**	**φ (per year)**	**λ (per year)**
1	0.158	471	5.542E-2	5.213E+2
2	0.294	403	1.841E-2	1.434E+2
3	0.317	368	1.025E-2	1.027E+2
4	0.181	374	9.937E-3	7.994E+1
5	0.181	373	9.482E-3	7.417E+1
6	0.034	431	2.385E-2	1.515E+2
7	0.113	44	1.750E-6	5.130E+0
8	0.065	88	8.604E-6	3.617E+0
9	0.294	331	5.610E-3	9.782E+1
10	0.317	156	9.811E-5	4.821E+1
11	0.059	184	2.214E-4	4.320E+1

The epistemic uncertainty associated with the degradation transition rates, provided in Table VII–5, is then propagated up to the level of the probabilistic failure metrics, including the annual and cumulative probabilities of leak and rupture. Considering the probability weight for each option, the mean and the 5th and 95th percentiles of the probabilistic failure metrics are estimated.

Table VII–6 shows the point estimates and uncertainty bounds for the annual probabilities of leak and rupture at 60 years.

TABLE VII−6. POINT ESTIMATES AND UNCERTAINTY BOUNDS OF ANNUAL PROBABILITIES OF LEAK AND RUPTURE (AT 60 YEARS)

Annual Probability @ 60 Years	**Point Estimate (Mean)**	**Uncertainty Bounds (5th and 95th percentiles)**
Leak	1.01×10^{-4}	$(1.53\times10^{-6}, 3.41\times10^{-2})$
Rupture	5.33×10^{-6}	$(1.51\times10^{-8}, 3.43\times10^{-4})$

VII–5.2.2. Probabilistic validation for the second CRP benchmark case study

The epistemic uncertainty associated with FOI for crack propagation phase (FOI_p) in Eq. (VII – 8) is considered to be the major source of epidemic uncertainty in the PoF module. To characterize the epistemic uncertainty associated with the FOI for crack propagation, 109 alloy 52/152 data points in MRP-386 are reanalyzed as shown in Fig. VII–9.

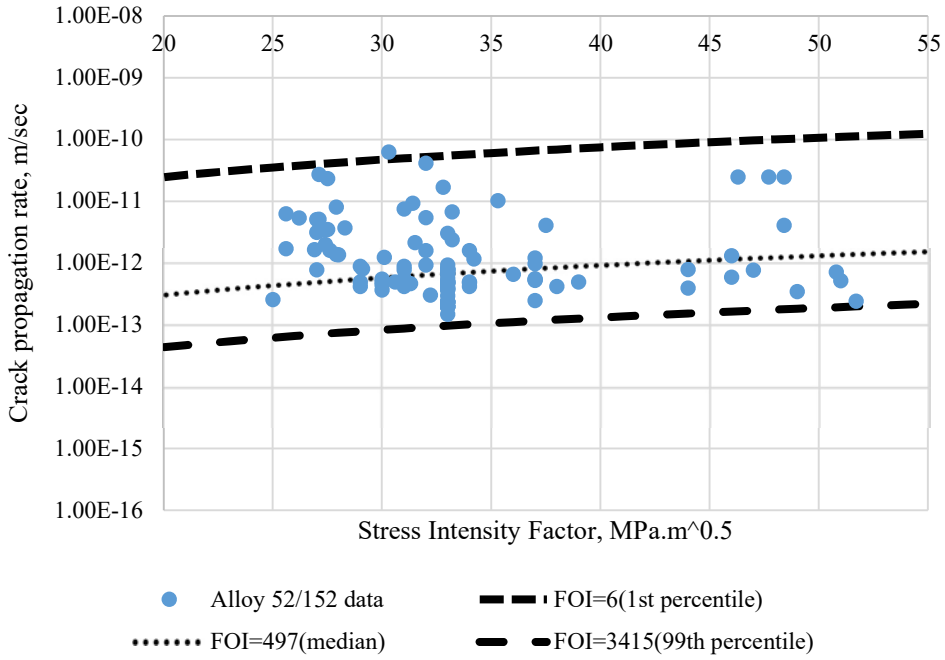

FIG.VII–9. Crack propagation rates with respect to SIF for alloy 52/152 data and the Gamma distribution characterizing epistemic uncertainty of FOI_p.

The Kolmogorov–Smirnov goodness-of-fit test shows that the Gamma distribution[12] is not rejected with a significance level of 5%; thus, the epistemic uncertainty associated with FOI_p is characterized by a Gamma distribution whose median is 497, the 1st percentile is 6, and the 99th percentile is 3415. The epistemic uncertainty for FOI_p, characterized by the Gamma distribution, is propagated up to the probabilistic failure metrics estimations. Table VII–7 shows the results of flaw, leak and rupture frequency (per year) for different FOI

TABLE VII–7. FLAW AND LEAK FREQUENCY AT 60 YEARS OF OPERATION

FOIp		Flaw Frequency (per year)	Leak Frequency (per year)	Rupture Frequency (per year)
6	5th percentile	5.96×10^{-2}	4.89×10^{-3}	5.48×10^{-8}
	50th percentile	5.99×10^{-2}	4.95×10^{-3}	1.07×10^{-7}
	95th percentile	6.04×10^{-2}	5.04×10^{-3}	2.58×10^{-7}
497	5th percentile	6.43×10^{-10}	1.70×10^{-18}	5.65×10^{-19}
	50th percentile	1.63×10^{-7}	1.09×10^{-13}	3.63×10^{-14}
	95th percentile	6.28×10^{-7}	1.62×10^{-12}	5.39×10^{-13}
3415	5th percentile	6.43×10^{-10}	1.70×10^{-18}	5.65×10^{-19}
	50th percentile	1.63×10^{-7}	1.09×10^{-13}	3.63×10^{-14}
	95th percentile	6.28×10^{-7}	1.62×10^{-12}	5.39×10^{-13}

[12] $G(\lambda|\alpha,\beta)=\frac{\beta^{\alpha}}{\Gamma(\alpha)}\lambda^{\alpha-1}\exp(-\beta\lambda)$ for $\lambda>0$

REFERENCES TO ANNEX VII

[VII–1] SAKURAHARA, T., O'SHEA, N., CHENG, W.C., ZHANG, S., REIHANI, S., KEE, E., MOHAGHEGH, Z., "Integrating renewal process modeling with Probabilistic Physics-of-Failure: Application to Loss of Coolant Accident (LOCA) frequency estimations in nuclear power plants," Reliability Engineering & System Safety, vol. 190, 2019.

[VII–2] CHENG, W.C., BEAL, J., SAKURAHARA, T., REIHANI, S., KEE, E., MOHAGHEGH, Z., "Integrated Probabilistic Physics of Failure Methodology to Estimate Pipe Failure Rates for Risk-Informed Analysis of Advanced Reactors," at 2020 Winter Meeting and Nuclear Technology Expo, Chicago, IL, 2020.

[VII–3] BEAL, J., SAKURAHARA, T., KEE, E., REIHANI, S., MOHAGHEGH, Z., "An algorithm for risk-informed analysis of advanced reactors with a case study of pipe failure rate estimation," at 30th European Safety and Reliability Conference (ESREL) and the 15th Probabilistic Safety Assessment and Management (PSAM) Conference, Venice, Italy, 2020.

[VII–4] KHALEEL, M.A., SIMONEN, F.A., PHAN, H.K., HARRIS, D.O., DEDHIA, D., "Fatigue Analysis of Components for 60-Year Plant Life," Pacific Northwest National Laboratory (PNNL), Richland, WA, NUREG/CR-6674 (PNNL-13227), 2000.

[VII–5] AMERICAN PETROLEUM INSTITUTE & AMERICAN SOCIETY OF MECHANICAL ENGINEERS, "API 579-1/ASME FFS-1 2016 Fitness-For-Service," Washington, DC, 2016.

[VII–6] FLEMING, K.N., "Markov Models for Evaluating Risk-Informed In-Service Inspection Strategies for Nuclear Power Plant Piping Systems," Reliability Engineering & System Safety, vol. 83, no. 1, pp. 27-45, 2004.

[VII–7] AMERICAN SOCIETY OF MECHANICAL ENGINEERS, "ASME BPVC.XI.1 2019, Section XI, Rules for Inservice Inspection of Nuclear Power Plant Components, Division 1, Rules for Inspection and Testing of Components of Light-Water-Cooled Plants," New York, NY: American Society of Mechanical Engineers (ASME), 2019.

[VII–8] US NUCLEAR REGULATORY COMMISSION, "Standard Technical Specifications; Westinghouse Advanced Passive 1000 (AP1000) Plants," NUREG-2194, Washington, DC, 2016.

[VII–9] KAMAYA, M., "Assessment of Thermal Fatigue Damage Caused by Local Fluid Temperature Fluctuation (Part I: Characteristics of Constraint and Stress Caused by Thermal Striation and Stratification)," Nuclear Engineering and Design, vol. 268, pp. 121-138, 2014.

[VII–10] BOROS, I., PETOEFI, G., ASZODY, A., "CFD Analysis of Thermal Stratification in the Primary Circuit," in Fifteenth Symposium of Atomic Energy Research, Hungary, 2005.

[VII–11] LU, T., LI, H., ZHU, X., "Numerical Simulation of Thermal Stratification in an Elbow Branch Pipe of a Tee Junction with and without Leakage," Annals of Nuclear Energy, vol. 60, pp. 432-438, 2013.

[VII–12] ELECTRIC POWER RESEARCH INSTITUTE, "Thermal Stratification, Cycling, and Striping (TASCS)," 1994.

[VII–13] RAMBERG, W., OSGOOD, W.R., "Description of Stress-Strain Curves by Three Parameters," TN 902, National Advisory Committee for Aeronautics, Washington, DC, 1943.

[VII–14] HILL, H., "Determination of stress-strain relations from" offset" yield strength values," Aluminium Co. of America, Pittsburgh, PA, 1944.

[VII–15] AMERICAN SOCIETY OF MECHANICAL ENGINEERS, "ASME BPVC.CC.NC.XI 2019 — Section XI, Rules for In-service Inspection of Nuclear Power Plant Components," New York, NY, 2019.

[VII–16] XU, H., FYFITCH, S., SCOTT, P., FOUCAULT, M., KILIAN, R., WINTERS, M., "Materials Reliability Program Resistance to Primary Water Stress Corrosion Cracking of Alloys 690, 52, and 152 in Pressurized Water Reactors (MRP-111)," U.S. Department of Energy, Washington, DC, EPRI, Palo Alto, CA, 2004.

[VII–17] CROOKER, P., "Materials Reliability Program: Recommended Factors of Improvement for Evaluating Primary Water Stress Corrosion Cracking Growth Rates of Thick-Wall Alloy 690 Materials and Alloy 52, 152, and Variants Welds (MRP 386)," EPRI, Palo Alto, CA, 2017.

[VII–18] WHITE, G., GORMAN, J., NORDMANN, N., JONES, P., KREIDER, M., "Materials Reliability Program Crack Growth Rates for Evaluating Primary Water Stress Corrosion Cracking of Alloy 82, 182, and 132 Welds (MRP-115)," Electric Power Research Institute, Palo Alto, CA, 2004.

[VII–19] ZAHOOR, A., Ductile Fracture Handbook, Research Project 1757-69, Electric Power Research Institute, Palo Alto, CA, 1989.

[VII–20] ANDERSON, T.L., THORWALD, G.V., REVELLE, D.J., LANAUD, C., "Stress Intensity Solutions for Surface Cracks and Buried Cracks in Cylinders, Spheres, and Flat Plates," Service Experience and Fitness-For-Service in Power and Petroleum Processing, vol. 411, pp. 105-120, 2000.

[VII–21] LEIS, B., STEPHENS, D., "An Alternative Approach to Assessing the Integrity of Corroded Pipeline, Part I: Current Status," in The Seventh International Offshore and Polar Engineering Conference, 1997: International Society of Offshore and Polar Engineers.

[VII–22] ERICKSON, M., AMMIRATO, F., BRUST, B., DEDHIA, D., FOCHT, E., KIRK,M., LANGE, C., OLSEN, R., SCOTT, P., SHIM, D.,"Models and Inputs Selected for Use in the xLPR Pilot Study," Electric Power Research Institute (EPRI), Palo Alto, CA, MRP-302 1022528, 2011.

[VII–23] KIM, Y.J., HUH, N.S., PARK, Y.J., KIM, Y.J., "Elastic–plastic J and COD estimates for axial through-wall cracked pipes," International Journal of Pressure Vessels and Piping, vol. 79, no. 6, pp. 451-464, 2002.

[VII–24] HENRY, R.E., "The two-phase critical discharge of initially saturated or subcooled liquid," Nuclear Science and Engineering, vol. 41, no. 3, pp. 336-342, 1970.

[VII–25] HENRY, R.E., FAUSKE, H.K., MCCOMAS, S.T., "Two-phase critical flow at low qualities Part I: Experimental," Nuclear Science and Engineering, vol. 41, no. 1, pp. 79-91, 1970.

[VII–26] HENRY, R.E., FAUSKE, H.K., MCCOMAS, S.T., "Two-phase critical flow at low qualities Part II: Analysis," Nuclear Science and Engineering, Vol. 41, No. 1, pp. 92-98, 1970.

[VII–27] PRIYA, C., RAO, K.B., ANOOP, M.B., LAKSHMANAN, N., GOPIKA, V., KUSHWAHA, H.S., SARAF, R.K., "Probabilistic Failure Analysis of Austenitic Nuclear Pipelines Against Stress Corrosion Cracking," (in English), Proceedings of the Institution of Mechanical Engineers Part C: Journal of Mechanical Engineering Science, vol. 219, no. 7, pp. 607-626, 2005.

[VII–28] GUEDRI, A., "Reliability Analysis of Stainless Steel Piping Using A Single Stress Corrosion Cracking Damage Parameter," International Journal of Pressure Vessels and Piping, vol. 111-112, pp. 1-11, 2013.

[VII–29] GUEDRI, A., "Effects of Remedial Actions on Small Piping Reliability," Journal of Risk and Reliability, vol. 227, no. 2, pp. 144-161, 2013.

[VII–30] DATTA D., JANG, C., "Failure Probability Assessment of A PWR Primary System Piping Subcomponents under Different Loading Conditions," in IAEA Second International Symposium on Nuclear Power Plant Life Management, Shanghai, China, 2007.

[VII–31] SCOTT, P., KURTH, R., COX, A., OLSON, R., RUDLAND, D., "Development of the PRO-LOCA Probabilistic Fracture Mechanics Code," Swedish Radiation Safety Authority (SSM), Stockholm, Sweden, MERIT Final Report 2010:46, 2010.

[VII–32] BEAL, J., SAKURAHARA, T., PENCE, J., FARSHADMANESH, P., REIHANI, S., KEE, E., MOHAGHEGH, Z., "Coupling Degradation and Maintenance to Model Safety Risk and Financial Risk under an Integrated Enterprise Risk Management Methodology for Nuclear Power Plants," in 25th International Conference on Structural Mechanics in Reactor Technology (SMiRT 25), Charlotte, North Carolina, 2019.

[VII–33] US NUCLEAR REGULATORY COMMISSION, Regulatory Guide 1.45: Guidance on Monitoring and Responding to Reactor Coolant System Leakage, Revision 1. (May 2008)

[VII–34] RAYNAUD, P., KIRK, P.M., BENSON, M., HOMIACK, M., "Important Aspects of Probabilistic Fracture Mechanics Analyses," US Nuclear Regulatory Commission, Washington, DC, Technical Letter Report TLR-RES/DE/CIB-2018-01, 2018.

[VII–35] CROOKER, P., "Materials Reliability Program: Stress Corrosion Crack (SCC) Initiation Testing of Ni-Base Alloys for PWR Applications –Part 1 (MRP-426)," 2017.

[VII–36] CROOKER, P., FOCHT, E., TOLOCZKO, M., ZHAI, Z., JENKS, A., "EPRI-NRC Cooperative Research Project: PWSCC Crack Initiation Characterization of Alloys 600/182 and 690/52/152," presented at the Alloy 690/52/152 PWSCC Research Collaboration Meeting, Tampa, FL December 3-6, 2019.

[VII–37] FYFITCH, S., HARRINGTON, C., "PWSCC Initiation Modeling for the Extremely Low Probability of Rupture (xLPR) Code," in 16th International Conference on Environmental Degradation of Materials in Nuclear Power Systems--Water Reactors, Asheville, NC, 2013.

[VII–38] MODARRES, M., KAMINSKIY, M.P., KRIVTSOV, V., Reliability Engineering and Risk Analysis: A Practical Guide, Third Edition. Boca Raton, FL: CRC Press, 2016.

GLOSSARY

ADVANCED WATER COOLED REACTOR

This term encompasses Gen-III) and Gen-III+ evolutionary water cooled reactors. Additional details are available: https://aris.iaea.org/Publications/IAEA_WRC_Booklet.pdf

ALEATORY UNCERTAINTY

This form of uncertainty is associated with the randomness of events such as component failures, initiating events and hazard events. This is addressed by modeling these events using probability models e.g., these are typically Poisson and binomial distributions for initiating events and component failures. These probability models represent initiating event frequencies and component failure probabilities or failure rates.

ASME SECTION XI

The ASME Code Section XI (Rules for Inservice Inspection of Nuclear Power Plant Components) provides standards for the examination, in-service testing and inspection, and repair and replacement of nuclear power plant components, pressure vessels and piping. The code details if a flaw found within a component is acceptable for continued operation, or if the component instead requires repair or replacement. The first edition of ASME Section XI was published on January 1, 1971.

ASME SECTION XI, DIVISION 2

Issued in July 2019, Division 2 provides the requirements for the creation of a RIM Programme for advanced nuclear reactor designs. A RIM Programme addresses the entire life cycle for all types of nuclear power plants, it requires a combination of monitoring, examination, tests, operation, and maintenance requirements that ensures each Structure, System, and Component (SSC) meets plant risk and reliability goals that are selected for the RIM Programme.

BAYESIAN RELIABILITY ANALYSIS

In the Bayesian approach a subject matter expert develops a well-informed estimate of the probability of failure distribution; the prior state of knowledge. This probability distribution is then updated as more information is collected about the structural integrity of a certain piping system component.

BUTTERING

The adding process of material in welding. Weld metal is deposited on one or more surfaces to provide a metallurgically compatible weld metal for the subsequent completion of the weld.

CALIBRATION

Calibration is an analytical process that is used to adjust a set of parameters associated with a computational science and engineering code so that the model agreement is maximized with respect to a set of experimental data or OPEX data.

CRITICAL CRACK LENGTH

The length of a crack (either axial or circumferential) for which the crack will propagate unstably for a given set of loading conditions.

COMPONENT BOUNDARY

Defines the physical boundary of a component required for system operation. A component boundary definition is expected to be consistent with the parameter database supporting PSA model quantification. For piping components, the component boundary is established through degradation mechanism evaluations (see below).

DEGRADATION MECHANISM

Phenomena or processes that attack (wear, erode, crack, etc.) the pressure-retaining material over time and might result in a reduction of component pressure boundary integrity. The damage mechanisms and degradation mechanisms could interact to cause major, catastrophic passive component failures.

DISPLACEMENT-CONTROLLED STRESSES

Stresses that result from the application of displacements, such as those due to thermal expansion or seismic anchor motion.

DOUBLE-ENDED GUILLOTINE BREAK

A condition for which a circumferential through-wall crack propagates around the entire circumference of the pipe such that the cracked pipe section severs into two pieces and the two ends are displaced relative to their pipe axes to allow for full flow from each end.

DUCTILE CRACK GROWTH

With ductile fracture a crack moves slowly and is accompanied by a large amount of plastic deformation around the crack tip. A ductile crack will usually not propagate unless an increased stress is applied and generally cease propagating when loading is removed.

EPISTEMIC UNCERTAINTY

The uncertainty that comes from the lack of knowledge. This lack of knowledge comes from many sources. Inadequate understanding of the underlying processes, incomplete knowledge of the phenomena, or imprecise evaluation of the related characteristics. For rare event the failure parameters may be derived from extrapolation using statistical models and sparse historical data.

EQUIVALENT BREAK SIZE

The calculated size of a hole in a pipe given a certain through-wall flow rate and for a given pressure.

FACTOR OF IMPROVEMENT

Also referred to as "relative improvement factor", the FOI is an estimate of the crack growth rate in one type of material relative to another material type. It is an indication of the estimated improvement in material performance as a function material chemical composition, mechanical properties, local stresses, degradation mitigation techniques, etc. The FOI can be determined on the basis of testing in laboratory environments, analytical work, expert elicitation, and or OPEX data.

FAILURE

A condition for which a component or system is no longer capable of performing its design function. Depending on the context, failure can be defined as either the condition for which the piping system is no longer capable of maintaining internal pressure, or when the pipe experiences a DEGB. National codes and standards (e.g. the ASME Boiler and Pressure Vessel Code, Section XI, Rules for Inservice Inspection of Nuclear Power Plant Components) give specific details on what constitutes a failure.

FLAW

An imperfection or unintentional discontinuity that is detectable by nondestructive examination.

FLAW ASPECT RATIO

Ratio of length of deepest crack to depth of deepest crack.

FULL STRUCTURAL WELD OVERLAY

A structural reinforcement and SCC mitigation technique through application of a SCC resistant material layer around the entire circumference of the treated weldment. The minimum acceptable full structural weld overlay thickness is 1/3 the original pipe wall thickness. The minimum length is $0.75\sqrt{(R \times t)}$ on either side of the DMW to be treated, where R is the outer radius of the item and t is the nominal thickness of the item.

HEAT AFFECTED ZONE[13]

The heat affected zone refers to a non-melted area of metal that has experienced changes in its material properties as a result of exposure to high temperatures. The alterations in material properties are usually a result of welding or high heat cutting procedures. The heat affected zone is identified as the area between the weld or cut and the base metal. These areas can vary in size and severity depending on the properties of the materials involved, the intensity and concentration of

[13] inspectioneering.comF

heat, and the process employed. During welding operations, the heat affected zone may range from small to large depending on the rate of heat input. Welding processes with high rates of heat input (i.e. fast heating) have faster cooler rates compared to welding processes with low rates of heat input (i.e. slow heating) and thus, have smaller heat affected zones. Conversely, a process with low rates of heat input will result in a larger heat affected zone. The size of a heat affected zone also increases as the speed of the welding process decreases. heat affected zone problems can be mitigated by performing a pre- and/or post-weld heat treatment. Weld geometry also plays a role in the size of the heat affected zone. During high temperature cutting operations, the depth of the heat affected zone is associated with the cutting process, cutting speed, material properties, and material thickness. Similar to the results of welding processes, cutting processes that operate at high temperatures and slow speeds tend to lead to large heat affected zones. Furthermore, cutting processes that operate at high speeds tend to reduce the width of the heat affected zone. Because the heat affected zone experiences sufficient heat for a long enough period of time, the layer undergoes microstructure and property changes that differ from the parent metal. These property changes are usually undesirable and ultimately serve as the weakest part of the component. For example, the microstructural changes can lead to high residual stresses, reduced material strength, increased brittleness, and decreased resistance to corrosion and/or cracking. As a result, many failures occur in the heat affected zone.

LEAK-BEFORE-BREAK

Generally referred to as a methodology whereby one shows that a crack can be detected by leakage under normal operating conditions and that that crack would be stable at normal plus safe shut-down earthquake loads. Sometimes also referred to as a condition whereby a surface crack breaks through the pipe thickness and remains stable even if the break-through occurs at emergency or faulted loads.

LOSS OF COOLANT ACCIDENT

Those postulated accidents that result in a loss of reactor coolant at a rate in excess of the capability of the reactor makeup system from breaks in the reactor coolant pressure boundary, up to and including a break equivalent in size to the double-ended rupture of the largest pipe of the RCS.

NOMINAL PIPE SIZE

A North American set of standard sizes for pipes used for high or low pressures and temperatures. "Nominal" refers to pipe in non-specific terms and identifies the diameter of the hole with a non-dimensional number (for example, 2 inch nominal steel pipe consists of many varieties of steel pipe with the only criterion being a 2.375 inch (60.3 mm) outside diameter). Specific pipe is identified by pipe diameter and another non-dimensional number for wall thickness referred to as the Schedule (Sched. or Sch., for example, 2 inch diameter pipe, Schedule 40). The European and international designation equivalent to NPS is DN, in which sizes are measured in millimeters.

PROBABILITY OF DETECTION

The probability that a flaw of a certain size will be detected, and it is conditional on factors such as wall thickness, non-destructive examination personnel qualifications, and flaw orientation.

RELIABILITY AND INTEGRITY MANAGEMENT

Those aspects of the plant design and operational phase that are applied to provide an appropriate level of reliability of SSCs and a continuing assurance over the life of the plant that such reliability is maintained. The most recent edition of the ASME Boiler and Pressure Vessel Code Section XI was issued in 2019. Division 2 of the 2019 Edition provides the requirements for the creation of the RIM programme for advanced nuclear reactor designs. The RIM Programme addresses the entire life cycle for all types of nuclear power plants. It requires a combination of monitoring, examination, tests, operation, and maintenance requirements that ensures each Structure, System, and Component (SSC) meets plant risk and reliability goals that are selected for the RIM Programme.

REPAIR WELD

A weld subjected to high residual stresses as a result of extensive repairs; e.g. during original construction. Such regions may be subjected to premature SCC.

RESIDUAL STRESSES

Residual stresses are those stresses that remain in an object (in particular, in a welded component) even in the absence of external loading or thermal gradients. In some cases, residual stresses result in significant plastic deformation, leading to warping and distortion of an object. In others, they affect susceptibility to fracture and fatigue.

ROUND-ROBIN TEST

An analysis or experiment performed independently several times and by different teams. This can involve multiple teams performing analyses using a common set of data with the use of a variety of methods. A round-robin test may be conducted to determine the reproducibility of an analysis; from input parameters to results interpretation.

SAFE SHUTDOWN EARTHQUAKE

The maximum earthquake potential for which certain systems, structure, and components, important to safety, are designed to sustain and remain functional,

STRESS CORROSION CRACKING

SCC is a localized non-ductile failure which occurs only under the combination of three factors: 1) tensile stress, 2) aggressive environment, and 3) susceptible material. The SCC failure mode can be intergranular SCC or transgranular SCC.

THERMAL STRATIFICATION

Hot water can flow above cold water in horizontal runs of piping when the flow (hot water into a cold pipe or cold water into a hot pipe) does not have enough velocity to flush the fluid in the pipe. The temperature profiles in the pipe where the top of the pipe is hotter than the bottom causes the pipe to bow along with the normal expansion at the average temperature.

THERMAL STRIPING

Incomplete mixing of high temperature and low temperature fluids near the surface of structures with subsequent fluid temperature fluctuations give rise to thermal fatigue damage to wall structures.

THROUGH-WALL CRACK INSTABILITY

A condition where a through-wall crack grows around the pipe circumference in a rapid manner.

VEGAS ALGORITHM

A method for reducing error in Monte Carlo simulations by using a known or approximate probability distribution function to concentrate the search in those areas of the integrand that make the greatest contribution to the final integral. The Vegas algorithm is based on importance sampling.

ABBREVIATIONS

ASME	American Society of Mechanical Engineers
CEI	CANDU Energy Inc.
CFP	Conditional Failure Probability
COD	Crack Opening Displacement
CRP	Coordinated Research Project
CVC	Chemical and Volume Control
DEGB	Double Ended Guillotine Break
DDM	Data-Driven Method
DMW	Dissimilar Metal Weld
DN	Nominal Diameter
FFS	Fitness for Service
FEA	Finite Element Analysis
FOI	Factor of Improvement
GRS	Global Research for Safety (formerly the Gesellschaft für Anlagen und Reaktorsicherheit)
HRA	Human Reliability Analysis
IAEA	International Atomic Energy Agency
ID	Inside Diameter
I-PPoF	Integrated Probabilistic Physics-of-Failure
ISI	In-Service Inspection
KAERI	Korea Atomic Energy Research Institute
LEI	Lithuanian Energy Institute
LMS	Leak Monitoring System
LCO	Limiting Condition for Operation
LOCA	Loss of Coolant Accident
MWP	Maintenance Work Process
PFM	Probabilistic Fracture Mechanics
POD	Probability of Detection
PSA	Probabilistic Safety Assessment
PWR	Pressurized Water Reactor
PWSCC	Primary Water SCC
RCC-MRx	Regles de Conception et de Construction des Materels Mechaniques des Ilots Nucleaires PWR (Design and Construction Rules for the Mechanical Components of PWR Nuclear Islands)
RCS	Reactor Coolant System
RIM	Reliability and Integrity Management
ROY	Reactor Operating Year
SCC	Stress Corrosion Cracking
SIF	Stress Intensity Factor
STEG	Société Tunisienne de l'Electricité et Gaz (Tunisian Electricity and Gas Company)
UIUC	University of Illinois at Urbana-Champaign
VVER	Water Cooled and Water Moderated Energy Reactor
WCR	Water Cooled Reactor
WRS	Weld Residual Stresses

CONTRIBUTORS TO DRAFTING AND REVIEW

Ahn, D.-H.	Korea Atomic Energy Research Institute, Republic of Korea
Alzbutas, R.	Lithuanian Energy Institute, Lithuania
Carroll, B.	Canadian Nuclear Safety Commission, Canada
Duan, X.	Candu Energy Inc., Canada
Hechmann, K.	Global Research for Safety, Germany
Jevremovic, T.	International Atomic Energy Agency
Liang, D.	International Atomic Energy Agency
Lydell, B.	Sigma-Phase Inc., United States of America
Mohaghegh, Z.	University of Illinois Urbana-Champaign, United States of America
Riznic, J.	Canadian Nuclear Safety Commission, Canada
Sakurahara, T.	University of Illinois Urbana-Champaign, United States of America
Wang, M.	Candu Energy Inc., Canada
Zammali, C.	Tunisian Electricity and Gas Company, Tunisia

RESEARCH COORDINATION MEETINGS

1st RCM: Vienna, Austria, 12–14 June 2018

2nd RCM: Vienna, Austria, 18–21 June 2019

3rd RCM: Vienna, Austria, 9–10 June 2020

4th RCM: Vienna, Austria 16–18 June 2021

IAEA
International Atomic Energy Agency

No. 26

ORDERING LOCALLY

IAEA priced publications may be purchased from the sources listed below or from major local booksellers.

Orders for unpriced publications should be made directly to the IAEA. The contact details are given at the end of this list.

NORTH AMERICA

Bernan / Rowman & Littlefield

15250 NBN Way, Blue Ridge Summit, PA 17214, USA
Telephone: +1 800 462 6420 • Fax: +1 800 338 4550

Email: orders@rowman.com • Web site: www.rowman.com/bernan

REST OF WORLD

Please contact your preferred local supplier, or our lead distributor:

Eurospan Group

Gray's Inn House
127 Clerkenwell Road
London EC1R 5DB
United Kingdom

Trade orders and enquiries:

Telephone: +44 (0)176 760 4972 • Fax: +44 (0)176 760 1640
Email: eurospan@turpin-distribution.com

Individual orders:

www.eurospanbookstore.com/iaea

For further information:

Telephone: +44 (0)207 240 0856 • Fax: +44 (0)207 379 0609
Email: info@eurospangroup.com • Web site: www.eurospangroup.com

Orders for both priced and unpriced publications may be addressed directly to:

Marketing and Sales Unit
International Atomic Energy Agency
Vienna International Centre, PO Box 100, 1400 Vienna, Austria
Telephone: +43 1 2600 22529 or 22530 • Fax: +43 1 26007 22529
Email: sales.publications@iaea.org • Web site: www.iaea.org/publications

21-03960E

International Atomic Energy Agency
Vienna